Analysis of Advanced Diversity Receivers for Fading Channels

Sudhanshu Gaur

Thesis submitted to the Faculty of the
Virginia Polytechnic Institute and State University
in partial fulfillment of the requirements for the degree of

Master of Science
in
Electrical Engineering

A. Annamalai, Chair
R. Michael Buehrer
Jeffrey H. Reed

September 19, 2003
Blacksburg, Virginia

Keywords: Wireless Communications, Antenna Diversity, General Selection Combining, UWB, EGC, Marcum Q-function

Analysis of Advanced Diversity Receivers for Fading Channels

by

Sudhanshu Gaur

Committee Chair: A. Annamalai

Electrical Engineering

Abstract

Proliferation of new wireless technologies has rekindled the interest on the design, analysis and implementation of suboptimal receiver structures that provide good error probability performance with reduced power consumption and complexity particularly when the order of diversity is large. This thesis presents a unified analytical framework to perform a trade-off study for a class of hybrid generalized selection combining technique for ultra-wideband, spread-spectrum and millimeter-wave communication receiver designs.

The thesis also develops an exact mathematical framework to analyze the performance of a dual-diversity equal gain combining (EGC) receiver in correlated Nakagami-m channels, which had defied a simple solution in the past. The framework facilitates efficient evaluation of the mean and variance of coherent EGC output signal-to-noise ratio, outage probability and average symbol error probability for a broad range of digital modulation schemes. A comprehensive study of various dual-diversity techniques with non-independent and non-identical fading statistics is also presented.

Finally, the thesis develops some closed-form solutions for a few integrals involving the generalized Marcum Q-function. Integrals of these types often arise in the analysis of multichannel diversity reception of differentially coherent and noncoherent digital communications over Nakagami-m channels. Several other applications are also discussed.

Acknowledgements

I would like to thank Dr. Annamalai for providing an opportunity to work with him. His knowledge, expertise, and unending enthusiasm helped immensely in the completion of this research. I would also like to thank Dr. Buehrer and Dr. Reed for serving on my advisory committee and their helpful comments and suggestions.

It has been a pleasure to work alongside the motivated research team of MPRG students who were all fantastic colleagues. I wish to specially thank fellow MPRGers Sarfraz, Ram, Vivek, Ramesh, Nishant, and Sameer for all their help and support. I would also like to thank my friends Bhupi and Kamesh for making my stay in Blacksburg a pleasant and memorable one.

And foremost, I offer my heartfelt thanks to my parents and my brothers Abhishek, Nalinaksh and Himanshu, who although far away, were always close to me in their thoughts and hearts, for their everlasting encouragement, faith, support and love. Thank you for everything. To you, I dedicate this work.

List of Acronyms

ABER	Average Bit Error Rate
ASER	Average Symbol Error Rate
ASEP	Average Symbol Error Probability
AWGN	Additive White Gaussian Noise
BER	Bit Error Rate
BFSK	Binary Frequency Shift Keying
BPSK	Binary Phase Shift Keying
CDF	Cumulative Distribution Function
CDMA	Code Division Multiple Access
CEP	Conditional Error Probability
DPSK	Differential Phase Shift Keying
DQPSK	Differential Quadrature Phase Shift Keying
EGC	Equal Gain Combining
FCC	Federal Communications Commission
FDMA	Frequency Division Multiple Access
FSK	Frequency Shift Keying
GSC	Generalized Selection Combining
IID	Independent and Identically Distributed
IND	Independent and Non-identically Distributed
MGF	Moment Generating Function
MRC	Maximal Ratio Combining
***M*-DPSK**	*M*-ary Differential Phase Shift Keying

***M*-PSK**	*M*-ary Coherent Phase Shift Keying
MRC	Maximum Ratio Combining
OFDM	Orthogonal Frequency Division Multiplexing
PDF	Probability Density Function
PSK	Phase Shift Keying
QPSK	Quadrature Phase Shift Keying
SC	Selection Combining
SNR	Signal to Noise Ratio
TDMA	Time Division Multiplexing Access
UMTS	Universal Mobile Telephone Service
UWB	Ultra-WideBand
WCDMA	Wideband CDMA

CONTENTS

LIST OF FIGURES

LIST OF TABLES

Chapter 1

Introduction

The wireless communications industry has been experiencing phenomenal annual growth rates exceeding 50% over the past several years. This degree of growth reflects the tremendous demand for commercial "untethered" communications services such as paging, analog and digital cellular telephony, and emerging Personal Communications Services (PCS) including high speed data, full motion video, Internet access, on-demand medical imaging, real-time road maps, and anytime, anywhere video conferencing. By 2007, the total worldwide wireless population will exceed 2 billion subscribers [1]. Of these subscribers, it is expected that by 2005 half will have data-capable handsets, creating an even greater demand for wireless data services [2]. Since wired broadband services such as Digital Subscriber Loop (DSL) and cable modems have been slow to market, this will drive even more customers to wireless alternatives. In many applications, wireless telecommunications can eliminate the high costs of installing and maintaining traditional wired systems. Wireless services make even the most rural community accessible through communications.

The wireless revolution was triggered and is being sustained by several important factors: advances in microelectronics, high-speed intelligent networks, positive user response and an encouraging regulatory climate worldwide [3]-[4]. Current spectrum allocations for cellular and PCS systems are concentrated at frequency bands around 900 MHz and 1.8 GHz; future allocations for PCS systems are expected around 2.4 GHz and 5.8 GHz. Beyond the arena of mobile communications, there are numerous wireless applications including satellite communications, Local Multipoint Distribution Systems (LMDS), Local Area Networks (LAN), and radio frequency identification (RFID) operating at frequencies extending into the millimeter-wave regime (>30 GHz). The move to higher (millimeter-wave) frequencies has been motivated by the need for more and more bandwidth for multimedia applications such as wireless "cable" TV and high-speed internet access, and by increased overcrowding of lower frequency bands. While some

additional frequency bands will be allocated towards wireless applications, this alone will not provide the capacity to meet the growing demand for untethered communications services via pocket-sized terminals at an affordable price. To meet this increasing demand, new wireless techniques and architectures must be developed to maximize capacity and quality of service (QoS) without a large penalty in the implementation complexity or cost. This provides many new challenges to engineers involved with system design, one of which is ensuring the integrity of the data is maintained during transmission.

The largest obstacle facing designers of wireless communications systems is the nature of the propagation channel. The wireless channel is non-stationary and typically very noisy due to fading and interference. The sources of interference could be natural (e.g., thermal noise in the receiver) or man-made (e.g., hostile jammer, overlay communication), while the most common type of fading is caused by multipath effects, in which multiple copies of a signal arrive out of phase at the receiver and destructively interfere with the desired signal. Another problem imposed by multipath effects is a delay spread, in which the multiple copies of a signal arriving at different times spread out each data symbol in time. The stretched out data symbols will interfere with the symbols that follow, causing inter-symbol interference. All of these effects can significantly degrade the performance and QoS of a wireless system. Another critical issue in wireless system development is channel capacity. Shannon's channel capacity may be conveniently expressed in terms of the channel characteristics as where is the signal-to-noise ratio (SNR), denotes the channel bandwidth, and is the normalized channel power transfer characteristic. The ratio is called spectral efficiency, which is the information rate per Hertz, is directly related to the modulation of a signal. To illustrate this, the analog AMPS cellular telephone system has a spectral efficiency of 0.33 bps/Hz while the digital GSM system has a spectral efficiency of 1.35 bps/Hz and the IS-54 system has 1.6 bps/Hz.

1.1 Motivation

Motivation behind this research effort is to investigate one of the powerful techniques for improving the spectral efficiency and the reliability of data transmission over wireless

links, viz., diversity methods. Specifically, this thesis contributes the development of novel mathematical techniques and tools for the design and analysis of next generation wireless communication systems.

Diversity methods (implemented either at the receiver, or at the transmitter, or both) are known to be very effective for combating the effects of multipath fading at a relatively low cost. Since the goals for performance and implementation complexity are more or less conflicting, there could be numerous options for implementing these wireless link improvement techniques. For instance, consider the design of an antenna array receiver for millimeter-wave communications. Since the wavelength is less than 1 cm, several tens of array elements can be placed on the surface of a portable receiver. Classical signal combining techniques such as maximal-ratio combining (MRC), equal-gain combining (EGC), selection combining (SC), or switched diversity are not easily adaptable to diversity reception for a large number of antenna elements because the required complexity of their combiners tend to outweigh the benefits obtained from the additional diversity. Thus, there is a need for new combining techniques designed to be used effectively with large antenna arrays. The suboptimal receiver structures may exploit order statistics or consider a partitioned diversity combining scheme [5] to achieve the performance comparable to the optimal receiver but with considerably fewer electronics (hardware) and power consumption. In light of this, it would be highly desirable to be able to assess the efficacy of different receiver design options so as to determine the most appropriate choice in the face of complexity and implementation constraints. To undertake this task, one may resort to many runs of computationally intensive Monte Carlo simulations or consider developing an analytical framework for the communication receiver design. The analytical approach has three obvious advantages over the Monte Carlo simulation methodology:

- Facilitates rapid computation of the system performance.
- Provides insight as to how different design parameters affect the overall system performance
- Easier to optimize the design parameters.

Nevertheless, the analytical solutions are usually governed by a set of assumptions which are needed for analytical tractability. This is not a serious concern in most cases, however, because the framework allows one to quickly narrow down the viable design options to only a few before an extensive computer simulation effort is undertaken. Hence, it is ideal for use in the first-step of the design process of a communication system.

1.2 Contributions

Some of the major contributions of the thesis are listed below:

- The trade-off between the error performance and receiver complexity of a partitioned diversity combining technique in generalized fading channels including the effects of signal correlation.
- Develops exact analytical expressions for computing the statistics of signal-to-noise ratio (SNR) at the output of a dual-branch EGC combiner in correlated Nakagami-m fading channels with a realistic assumption of unequal average branch SNRs. This has not been reported in the literature previously. A comparative study of different dual-branch diversity receivers is also performed.
- Closed-form formulas for two generic integrals involving generalized Marcum Q-function. The new framework allows for a more general solution to some of the fading and noise analysis problems in statistical communication theory that in the past defied a simple closed-form solution.
- The trade-off between UWB receiver complexity and required throughput performance at a specified coverage range. A realistic operating environment is considered by taking into account of multipath correlation effects.

1.3 Thesis Outline

Chapter 2 discusses the small scale wireless fading channel models. The moment generating function, cumulative density function and the probability density function are the main statistics of interest for the small scale fading.

Chapter 3 is devoted to the development of the mathematical framework; expressions have been derived for bit or symbol error probabilities, outage probabilities and mean output SNRs for coherent and noncoherent partitioned diversity combining (PGSC) receivers in generalized fading channels. A trade-off study is performed between the receiver complexity and error performance. The bit and symbol error rate performances for many modulation schemes in correlated fading channels are presented for the first time.

Chapter 4 deals with the development of exact analytical expressions for computing the statistics of SNR at the output of a two-branch equal gain diversity combiner in correlated Nakagami-m channels. The new framework facilitates efficient evaluation of mean and variance of coherent equal-gain combining (EGC) output SNR, outage probability and average bit or symbol error rate for a wide range of digital modulation schemes. A comparative performance study of different dual-branch diversity combining schemes is also presented.

Integrals involving the generalized Marcum Q-function with linear arguments often arise in the analysis of multichannel diversity reception of differentially coherent and noncoherent digital communications in Rayleigh and Nakagami-m channels. Chapter 5 presents different methods to derive closed-form formulas for two generic integrals and discuss their application to problems of diversity reception in Rayleigh and Nakagami-m fading channels.

In Chapter 6, we utilize the expressions derived in Chapter 3 to investigate the possibility of increasing the range of UWB transmissions using rake receivers (instead of a matched filter correlator receiver). A trade-off study between receiver complexity and required throughput performance at a specified coverage range is presented by taking into account of multipath fading effects. An approximate formula for predicting the performance of generalized selection combining (GSC) receiver with identical but non-independent multipaths is also presented.

Finally, Chapter 7 concludes the thesis and summarizes the important results. Potential

and interesting problems that can be carried out in future research are also listed in Chapter 7.

Chapter 2

Wireless Channel Models

The mobile channel places fundamental limitations on the performance of wireless communication systems. The radio link between the transmitter and the receiver varies from simple line-of-sight to one that is severely obstructed by buildings, mountains, and hence suffers from severe multipath fading. Mobile channels are very different from stationary and predictable wired channels, because of their randomness. There are several factors which determine the behavior of such a channel. For example: terrain features between the transmitter and receiver, the speed of transmitter and receiver, weather conditions etc. Over the years several studies and measurements have been undertaken in different locations for such channels. Various models have been proposed for both indoor and outdoor environments.

The instantaneous signal strength at a receiver can be predicted using the traditional large-scale and small-scale models, wherein the large-scale models predict the average received signal strength depending on the transmitter-receiver distance and the small-scale channel models represent local variations about the average signal strengths. The lognormal model, in which the measured signal levels have a normal distribution about the mean received signal, are suitable for emulating the large scale fading effects for mobile channels models. The normal deviation about the mean captures the random shadowing effects that occur because of the variation in the clutter surrounding a moving vehicle, though the mean signal strength at the vehicular receiver remains the same. Frameworks for modeling and simulating the satellite channel along with the time variations have been extensively reported in the literature. It is widely accepted that, while the lognormal-Rayleigh model accurately depicts the shadowed channel, a Rician channel model is more appropriate for the unshadowed channel.

The organization of the rest of this chapter is as follows. Section 2.1 discusses the small scale fading phenomenon while section 2.2 discusses the statistical parameters used to characterize the fading channels followed by a brief discussion on common small scale fading models.

2.1 Different Types of Fading

Small-scale fading can be classified into different types depending on multipath delay spread and Doppler spread as shown in Figure 2.1. In the following, we describe these categories.

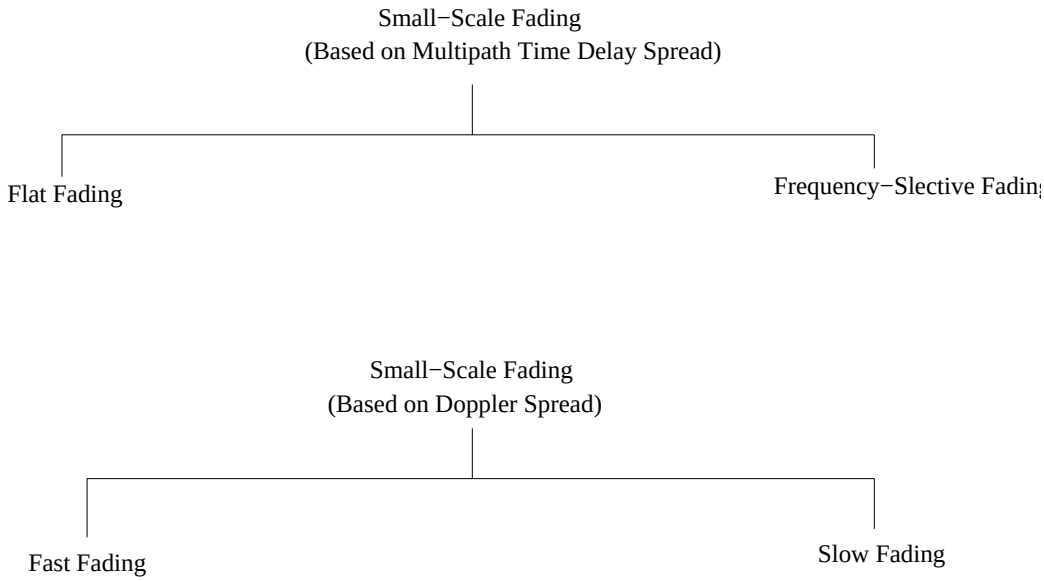

Figure 2.1 Types of fading

2.1.1 Flat Fading

If the channel frequency response is flat and linear in phase over whole signal bandwidth, the signal is said to undergo flat fading and the channel impulse response can be modeled as an impulse. But, if the mobile moves with time or the objects close by move (thus changing the channel), then the channel response can be seen as an impulse function but with time-varying gain. Another way to look at flat fading is that it occurs when the rms delay spread of the channel is much less compared to the time duration of a modulated symbol. In this case it can be assumed that all multipath components arrive almost at the same time at the beginning of a symbol, thus preserving the spectral characteristics of the signal. In other words, flat fading occurs when $B_S \ll B_C$ (or $T_S > \sigma_\tau$) where T_S denotes the symbol duration and B_S is the signal bandwidth. B_C and σ_τ are respectively the coherence bandwidth and the rms delay spread. Figure 2.2 shows flat fading.

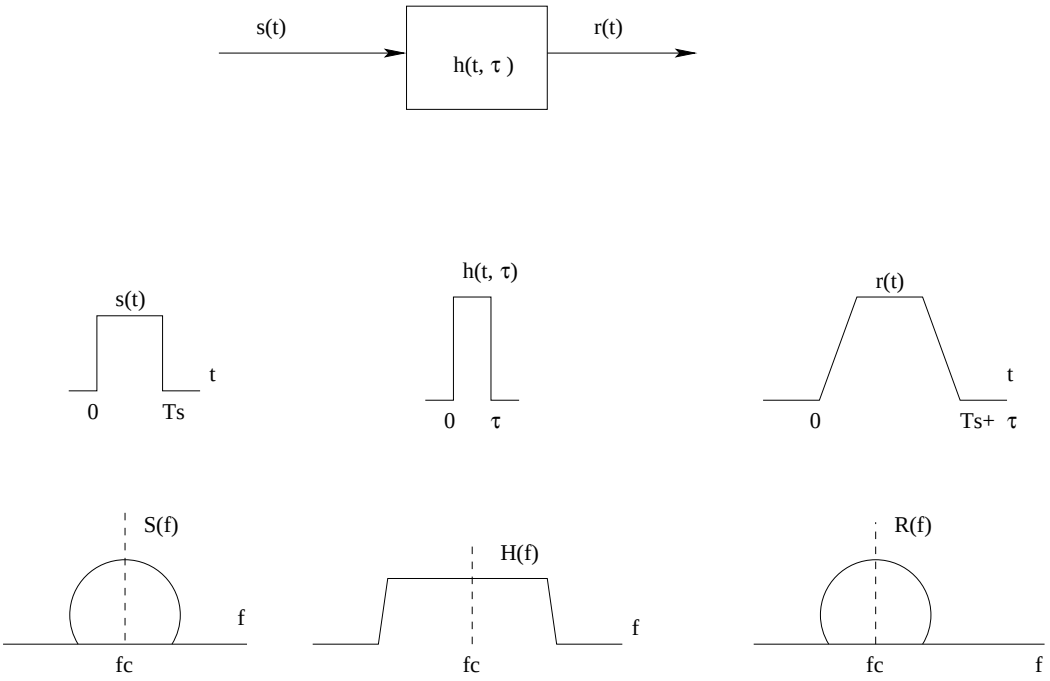

Figure 2.2 Flat fading in time and frequency domain

2.1.2 Frequency Selective Fading

When the transmitted signal has a bandwidth greater than the band in which the channel offers constant gain and linear phase, the signal is said to undergo frequency selective fading. In this case, the received signal contains several multipath replicas of the transmitted signal which are faded and delayed in time. The delay spread exceeds the symbol duration causing inter-symbol interference or ISI. Figure 2.3 demonstrates a pictorial representation of frequency selective fading. Viewed in the frequency domain, frequency selective fading is said to occur when the transmitted signal's bandwidth is more than the coherence bandwidth of the channel, i.e., when different frequency components have different gains. It is a common practice to describe the channel as flat fading when $T_S > 10\sigma_\tau$ or frequency selective when $T_S < 10\sigma_\tau$.

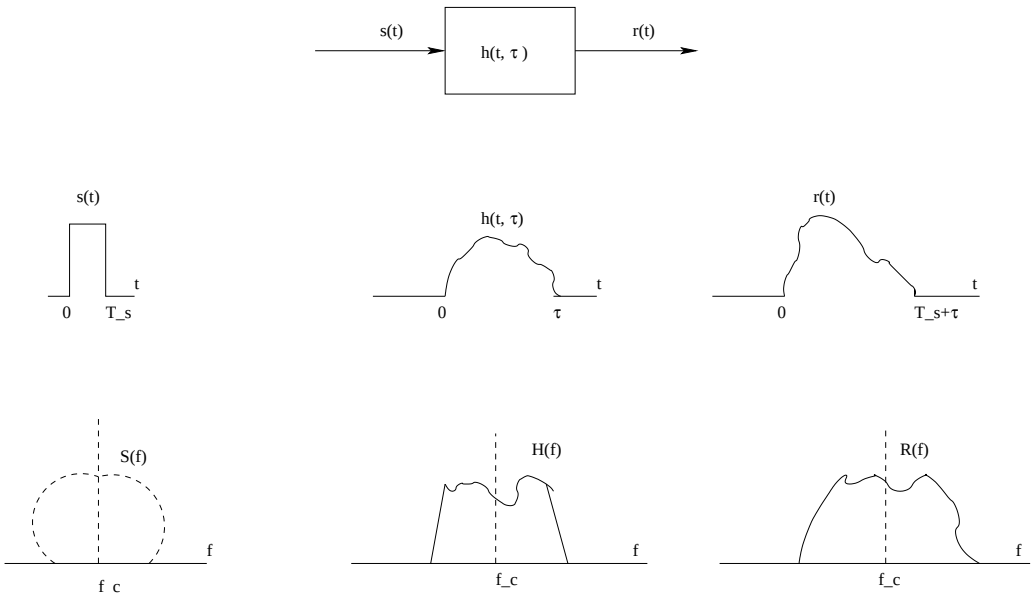

Figure 2.3 Frequency selective fading in time and frequency domain

2.1.3 Fast Fading

Fast fading occurs when the characteristics of the channel change faster than the symbol duration of the transmitted signal, i.e. the coherence time of the channel is less than the transmitted symbol duration. The coherence time of the channel refers to the time during which the characteristics of the channel remains almost the same. This kind of time-selective fading introduces frequency dispersion due to Doppler dispersion. Fast fading generally occurs at very low data rates. Fast fading can occur jointly with flat fading or frequency selective fading.

2.1.4 Slow Fading

When the characteristics of the channel change slowly compared to the symbol duration of the transmitted signal, the transmitted signal is said to undergo slow fading. The channel can be assumed to be static for several symbol durations. Thus for several symbol durations the channel response will stay the same. In the frequency domain, slow fading means smaller Doppler spread compared to the baseband signal bandwidth. As in case of fast fading, slow fading can be flat fading or frequency selective fading.

2.2 Statistical Representation of Fading Channels

The Probability Density Function (PDF), Cumulative Density Function (CDF) and Moment Generating Function (MGF) are the three most important statistics that are used to represent a channel model. The relation between the three is listed below.

The CDF of random variable X evaluated at any fixed value of x is defined as

$$F_X(x) = \text{Prob}[X < x] \tag{0.1}$$

The PDF of X is given as

$$p_X(x) = \frac{d}{dx} F_X(x) \tag{0.2}$$

Finally, the MGF is defined as

$$\phi_X(s) = \int_0^\infty e^{-sx} p_X(x) dx \tag{0.3}$$

As will be seen in Chapter 3, the marginal MGF $\phi_X(s,x)$ is needed for simplistic representation of many expressions and is given as

$$\phi_X(s,x) = \int_x^\infty e^{-st} p_X(t) dt \tag{0.4}$$

It is trivial to note that $\phi_X(s)$ is a special case of $\phi_X(s,x)$ with $x = 0$. In the following, we will describe the channel models for small scale mobile radio propagation. The PDF $p_X(x)$ and the marginal MGF $\phi_X(s,x)$ needed to represent different multipath fading environments are summarized in Table 2-1.

2.2.1 Rayleigh Distribution

The Rayleigh distribution is the most widely used distribution to describe the received envelope value. The Rayleigh flat fading channel model assumes that all the components that make up the resultant received signal are reflected or scattered and there is no direct path from the transmitter to the receiver. The Rayleigh distributed envelope of a received signal is given by

$$p_X(x) = \begin{cases} \dfrac{x}{\sigma^2} \exp\left(-\dfrac{x^2}{2\sigma^2}\right), & 0 \le x < \infty \\ 0, & x < 0 \end{cases} \tag{0.5}$$

where σ is the received root-mean-square (rms) envelope level and σ^2 is the average power of the received signal.

2.2.2 Rician Distribution

In micro-cellular environments, there usually exists a dominant line of sight (LOS) path in addition to numerous diffused multipath components between the transmitter and receiver. In such a case, the other faded signal components are superimposed on the dominant component and the resultant signal amplitude follows Rician distribution with the ratio between the LOS and diffused components denoted by the Rice factor *K*. The complex envelope of the received signal following a Rayleigh distribution is given by

$$p_X(x) = \begin{cases} \dfrac{x}{\sigma^2}\exp\left(-\dfrac{x^2+A^2}{2\sigma^2}\right) I_0\left(\dfrac{Ax}{\sigma^2}\right), & x \geq 0, A \geq 0 \\ 0 & , \quad x < 0 \end{cases} \tag{0.6}$$

where A is the peak amplitude of the dominant component, and $I_0(.)$ denotes the modified Bessel function of the first kind. The distribution can also be expressed in terms of the Rice factor $K = A^2/(2\sigma^2)$ which is the ratio of the dominant component's power and the variance of the combined power of all the multipath components. As the power in the dominant component decreases to zero, the Rician distribution can be shown to approach the Rayleigh distribution.

2.2.3 Nakagami-m Distribution

The Nakagami-m distribution is a versatile statistical model because it can model fading amplitudes that experience either less or severe fading than that of Rayleigh variates. It sometimes fits experimental data much better than a Rayleigh or Rician distribution [6]-[7]. The Nakagami-m distribution of envelope of the received signal is given by [8]

$$p_X(x) = \begin{cases} \dfrac{2m^m x^{2m-1}}{\Gamma(m)\sigma^{2m}} e^{-mx^2/\sigma^2}, & x \geq 0, m \geq 1/2 \\ 0 & , \quad x < 0 \end{cases} \tag{0.7}$$

where σ is the received rms envelope level, m is the fading severity index and $\Gamma(.)$ denotes the Gamma function. When m = 1, Nakagami distribution degenerates to a

Rayleigh distribution and closely approximates the Rician distribution via relationship $m = (K+1)^2/(2K+1)$ [8].

Table 2-1 PDF and the marginal MGF of SNR for a single diversity branch

Channel Model	**PDF *p*(x) and the marginal MGF $\phi(s,x)$ of SNR for a single diversity branch**
Rayleigh	$p(x) = \frac{1}{\Omega}\exp(-x/\Omega),\ x \geq 0$ $\phi(s,x) = \frac{\exp[-x(s+1/\Omega)]}{1+s\Omega}$ where $\Omega = E[x]$ = average SNR/symbol/path
Rician	$p(x) = \frac{1+K}{\Omega}\exp\left[-K - \frac{(1+K)x}{\Omega}\right] I_o\left[2\sqrt{\frac{K(K+1)x}{\Omega}}\right],\ x \geq 0$ $\phi(s,x) = \frac{1+K}{s\Omega+K+1}\exp\left[\frac{-sK\Omega}{s\Omega+K+1}\right] Q\left(\sqrt{\frac{2K(K+1)}{s\Omega+K+1}}, \sqrt{\frac{2(s\Omega+K+1)x}{\Omega}}\right)$ where $K \geq 0$ is the Rice factor and $Q(.,.)$ denotes the first-order Marcum Q-function.
Nakagami-m	$p(x) = \frac{1}{\Gamma(m)}\left(\frac{m}{\Omega}\right)^m x^{m-1}\exp\left(-\frac{mx}{\Omega}\right),\ x \geq 0$ $\phi(s,x) = \frac{1}{\Gamma(m)}\left(\frac{m}{m+s\Omega}\right)^m \Gamma(m, sx + mx/\Omega)$ where $m \geq 0.5$ is the fading severity index and $\Gamma(a,x)$ denotes the complementary incomplete Gamma function.

Chapter 3

Error Probability Analysis of Partitioned General Selection Combining Technique

In this chapter, we present Partitioned General Selection Combining, PGSC(*M*, *L*, *D*), technique that adaptively combines *M* "strongest paths" each from *D* partitions where each partition consists of *L* diversity branches. Bit error rate performance of various digital modulation schemes in conjunction with coherent and non-coherent PGSC receivers are analyzed in i.i.d fading as well as mixed fading environment. A comparison is also drawn between the bit error performance of various diversity combining schemes, namely, selection combining (SC), PGSC, generalized selection combining (GSC) and maximal ratio combining (MRC). We show that a trade-off between the receiver circuit complexity and required level of performance can be achieved using PGSC. It is observed that for large number of received signal paths, PGSC offers comparable performance to GSC receiver but at reduced selection circuit complexity. Also, coherent and non-coherent PGSC receivers offer similar performances with the former having slight diversity gain over the latter.

3.1 Introduction

Recent studies have focused on the low-complexity receiver design for wideband CDMA, millimeter-wave and ultra-wideband communication systems. High spreading bandwidth employed by these systems results in large number of multipath signals each carrying a small fraction of the transmitted energy. A Rake-type receiver can be employed to avoid deep fades by tapping the dispersed energy. However, large number of diversity paths at the input of maximal-ratio-combiner (MRC) circuit will increase the complexity of the combiner circuit enormously. To circumvent this problem, a selective Rake (SRake) receiver has been proposed in [9]-[11] that feeds only a selected subset of diversity branches to the MRC circuit. Previous work [12]-[22] has largely focused on generalized selection combining, GSC(*M*, *L*), technique for SRake receiver that adaptively combines a subset of *M* signals with the best SNR out of *L* available paths. GSC receiver requires

ranking of M best diversity branches among a group of L available diversity branches. However, the high spreading bandwidth limits the time available to rank the M signals.

A design trade-off is possible between the complexity of the selection-circuit and the complexity of the combiner-circuit to achieve a required level of performance. In [23] authors proposed a less-complex selection combining technique that divides the available signals into D groups, each having L signals, and then combines the "strongest" signal from each group. Their study of this model was limited to indoor wireless systems operating in mm-wave frequency band with the assumption of very slow frequency nonselective Rayleigh fading environment. However, in practical situations such an assumption rarely holds good.

Motivated by this, we propose a coherent and non-coherent Partitioned General Selection Combining (PGSC) scheme that can be easily employed by SRake receivers. Figure 3.1 gives a schematic diagram of PGSC(M, L, D) combining technique consisting of D partitions, each having L diversity branches, with each partition contributing M "strongest paths". Thus a total of $M \times D$ diversity branches are selected from a group of $L \times D$ available branches. Though the performance of PGSC(M, L, D) is slightly inferior to that of equivalent GSC($M \times D, L \times D$), the selection circuit complexity is greatly reduced as it involves the ranking of M strongest diversity branches out of L in each group, unlike $M \times D$ out of $L \times D$ required for an equivalent GSC receiver.

In this chapter, we evaluate the performance of PGSC scheme in i.i.d channels as well as mixed fading channels and draw a comparison vis-à-vis conventional MRC and GSC receiver structures for numerous digital modulation schemes. Bit error rate performance of various digital modulation schemes in conjunction with coherent and non-coherent PGSC receivers are also analyzed. The organization of the rest of the chapter is as follows. In Section 3.2 we derive the moment generating function (MGF), probability density function (PDF) and the cumulative distribution function (CDF) of PGSC(M, L, D) output SNR for i.i.d as well as mixed fading environment. In Section 3.3, we investigate the performance of PGSC receiver for varying combination of M, L and D in generalized

fading environment. Section 3.4 briefly talks about Graphical-User-Interface (GUI) developed to integrate the comprehensive analytical framework developed for PGSC receiver. Finally, the major contributions are summarized in Section 3.5.

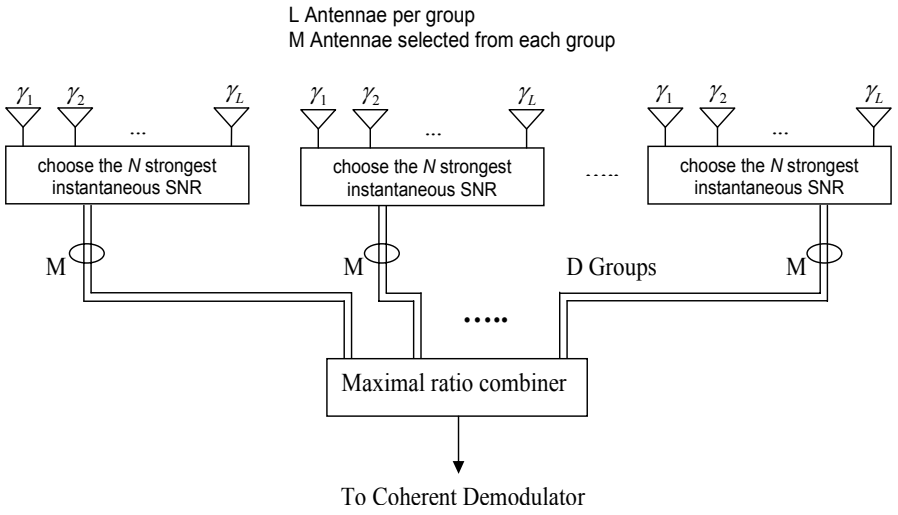

Figure 3.1 Coherent PGSC(*M*, *L*, *D*) combiner employing predetection combining with groups of received signals.

3.2 PGSC COMBINER OUTPUT STATISTICS

In this section, we will derive analytical expressions for the PGSC(*M, L, D*) combiner output statistics. These expressions can be applied directly for computing the average bit error rate (ABER) or the average symbol error rate (ASER), and outage probability for different modulation schemes. To analyze the bit error performance of PGSC over realistic fading environment, we model the branch amplitudes as (a) independent and identically distributed (i.i.d) random variables (b) independent but non-identical (i.n.d) random variables. It is assumed that there are a total of $L \times D$ received signals which are divided into D groups each consisting of L diversity branches. The D selection combiners select M signals from each group having best SNRs in their respective groups. Thus a total of $M \times D$ input signals are applied to the maximal-ratio-combiner (MRC) circuit. The output of MRC circuit is then fed to a coherent demodulator. In case of non-coherent PGSC receiver, selection combiner circuit outputs are fed to a differential detector. The differential detector outputs, which are all co-phased, are then combined by a maximal ratio combiner. If $M = L$, all the received signals ($L \times D$) are combined and conventional

MRC is considered. For $M = D = 1$, there is no combining and conventional SC is considered. For $D = 1$, PGSC(M, L, D) degenerates to GSC(M, L).

3.2.1 MGF of PGSC output SNR

Let us consider a partition consisting of L diversity paths where γ_k denotes the instantaneous SNR/symbol of the k-th diversity branch. Let $f_k(.)$, $F_k(.)$ and $\phi_k(s,x) = \int_x^\infty e^{-st} p(t)dt$ denote the PDF, CDF and the marginal MGF of γ_k. From [22], we know that when M strongest diversity branches are selected from a group of L available diversity branches in a generalized fading channel, the MGF of the group output SNR, γ_{group}, is given by

$$\phi_{\gamma_{group}}(s) = \sum_{\sigma \in T_{L,M}} \int_0^\infty e^{-sx} f_{\sigma(L-M+1)}(x) \left[\prod_{t=1}^{L-M} F_{\sigma(t)}(x) \right] \left[\prod_{k=L-M+2}^{L} \phi_{\sigma(k)}(s,x) \right] dx, \quad 1 \le M \le L \qquad (1.1)$$

where $\sum_{\sigma \in T_{L,N}} = \sum_{\substack{\sigma \in S_L, \sigma(1)<\sigma(2)<\ldots<\sigma(L-N) \\ \sigma(L-N+2)<\ldots<\sigma(L)}}$, S_L is the set of all permutations of integers $[1,2,...,L]$ and $\sigma \in S_L$ denotes the specific function $\sigma = [\sigma(1), \sigma(2), ..., \sigma(L)]$ which permutes the integers $[1,2,...,L]$. Since the SNR of all diversity branches are statistically independent variables, the MGF of the PGSC output SNR, $\phi_{\gamma_{pgsc}}(.)$, is simply the product of the MGFs of all group's output SNRs, viz.,

$$\phi_{\gamma_{pgsc}}(s) = \prod_{i=1}^{D} \phi_{\gamma_{group(i)}}(s) \qquad (1.2)$$

For the special case of i.i.d fading, the MGF of the group output SNR, γ_{group}, is given by [18]

$$\phi_{\gamma_{group}}(s) = M \binom{L}{M} \int_0^\infty e^{-sx} f(x) [F(x)]^{L-M} [\phi(s,x)]^{M-1} dx \qquad (1.3)$$

Since the SNR of all diversity branches are statistically independent and identically distributed variables, the MGF of the PGSC output SNR, $\phi_{\gamma_{pgsc}}(.)$, may be computed as

$$\phi_{\gamma_{pgsc}}(s) = [\phi_{\gamma_{group}}(s)]^D \qquad (1.4)$$

3.2.2 Mean Combined SNR

The mean combined SNR is another useful performance measure of diversity systems. The mean combined group output SNR, $\overline{\gamma}_{group}$, can be found by computing the sum of the expected value of the individual ordered SNRs as

$$\overline{\gamma}_{group} = \sum_{k=L-M+1}^{L} \overline{\gamma}_k \tag{1.5}$$

From [22], the marginal density of the k^{th} order statistic, $\gamma_{k:L}$, at x is given by

$$f_{\gamma_{k:L}}(x) = \sum_{\sigma \in T_{L,L-k+1}} f_{\sigma(k)}(x) \left[\prod_{t=1}^{k-1} F_{\sigma(t)}(x) \right] \left[\prod_{j=k+1}^{L} [1 - F_{\sigma(j)}(x)] \right] \tag{1.6}$$

where *f(x)* and *F(x)* are the PDF and CDF of the random variable *x*. Substituting (1.6) in (1.5) we obtain the desired expression

$$\overline{\gamma}_{group} = \sum_{k=L-M+1}^{L} \sum_{\sigma \in T_{L,\ L-k+1}} \int_0^{\infty} x f_{\sigma(k)}(x) \left[\prod_{t=1}^{k-1} F_{\sigma(t)}(x) \right] \left[\prod_{j=k+1}^{L} \phi_{\sigma(j)}(0,x) \right] dx \tag{1.7}$$

Since the SNR of all diversity branches across the *D* groups are statistically independent variables, this implies that the mean combined PGSC output SNR, $\overline{\gamma}_{pgsc}$, can be found by adding together the mean combined output SNR, $\overline{\gamma}_{group}$, of each group as

$$\overline{\gamma}_{pgsc} = \sum_{i=1}^{D} \overline{\gamma}_{group(i)} \tag{1.8}$$

For the special case of i.i.d fading, the mean combined output SNR, $\overline{\gamma}_{group}$, can be computed as

$$\overline{\gamma}_{group} = \sum_{k=L-M+1}^{L} k \binom{L}{k} \int_0^{\infty} x f(x) [F(x)]^{k-1} [1 - F(x)]^{L-k} dx \tag{1.9}$$

Since the SNR of all diversity branches across the *D* groups are statistically independent and identically distributed variables, this implies that the mean combined PGSC output SNR, $\overline{\gamma}_{pgsc}$, can be found by multiplying the mean combined group output SNR in (1.9) by *D*

$$\overline{\gamma}_{pgsc} = D \sum_{k=1}^{M} k \binom{L}{k} \int_0^{\infty} x f(x) [F(x)]^{L-k} [1 - F(x)]^{k-1} dx \tag{1.10}$$

3.2.3 CDF of PGSC output SNR

Since outage probability P_{out} is defined as the probability that the instantaneous symbol error rate of the system will exceed a specified value, say P_e^*, it can be expressed in terms of the CDF of γ_{pgsc} as

$$P_{out} = P_r[0 \le \gamma_{pgsc} \le \gamma^*] = F_{\gamma_{pgsc}}(\gamma^*) \tag{1.11}$$

where γ^* is the threshold SNR. Given a digital modulation scheme with conditional error probability $P_s(\gamma)$, γ^* is obtained by solving $P_s(\gamma^*) = P_e^*$. For instance, if $P_e^* = 10^{-4}$ is specified, $P_{out} = F_{\gamma_{pgsc}}(6.92)$ because $\gamma^* = [erfc(2\times10^{-4})]^2 = 6.92$ for BPSK modulation scheme. Similarly for coherent $\pi/4$-DQPSK, $P_{out} = F_{\gamma_{pgsc}}(11.97)$.

The CDF of PGSC output SNR can be computed using the Laplace inversion method suggested in [24] as

$$F_{\gamma_{pgsc}}(x) \cong 2^{1-C} e^{A/2} \sum_{c=0}^{C} \binom{C}{c} \sum_{b=0}^{c+B} (-1)^b \alpha_b \text{Real}\left[\phi_{\gamma_{pgsc}}\left(\frac{A + j2\pi b}{2x} \right) / (A + j2\pi b) \right] \tag{1.12}$$

where , $a_0 = 0.5$, $a_1 = 1$ for any $b \ge 1$and the constants A, B and C are arbitrarily chosen to be 30, 18 and 24 respectively, yield an accuracy of at least 10^{-13}.

3.3 PERFORMANCE ANALYSIS OF PGSC

3.3.1 Mean Combined SNR at PGSC output

Figure 3.2 illustrates the normalized mean combined SNR, $\bar{\gamma}_{pgsc}/\Omega$, at the PGSC($M$, L, 2) output as a function of total number of combined paths ($M\times D$) for varying diversity order ($L\times D$) over a Nakagami-m fading channel (m = 1.4) for two different values of multipath intensity profile (MIP). We observe that mean combined SNR increases as more paths/partition are combined. However, the rate of increase of mean combined SNR diminishes as M increases for a given diversity order. It is also apparent that a maximum value of 1 is achieved when $M = L$ i.e. MRC($2\times L$) as expected. To be more general, the performance is lower and upper bounded by PGSC(1, L, 2) and PGSC(L, L, 2). Furthermore, the performance is better when the received power is evenly distributed among all the multipaths i.e. when fading is i.i.d.

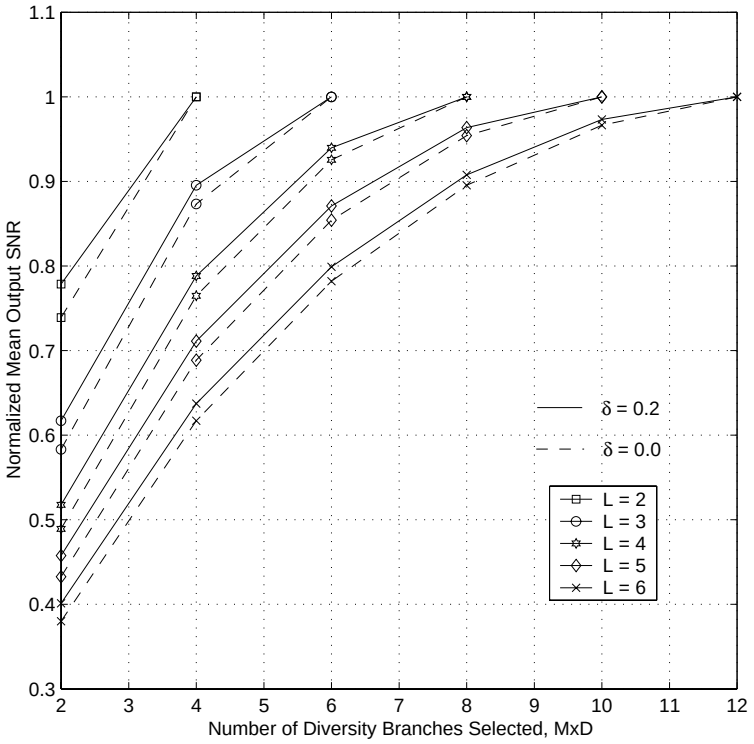

Figure 3.2 Normalized mean combined output SNR, $\overline{\gamma}_{pgsc}/\Omega$, versus number of diversity branches combined ($M\times D$) for PGSC(M, L, 2) receiver over a Nakagami-m channel (m = 1.4).

3.3.2 Outage Probability

Figure 3.3 depicts the CDF curves as a function of normalized mean SNR/symbol/branch Ω/γ^* for various PGSC schemes with $L\times D = 8$ diversity branches in a i.i.d Nakagami-m fading channel with fading severity index m = 0.5. These curves can be used to determine the mean SNR/symbol/branch to satisfy an outage requirement for given PGSC receiver structure. For example, to achieve an outage probability $P_{out} = 10^{-4}$, $\pi/4$-DQPSK modulation requires approximately 2.38 dB higher mean SNR/symbol/branch compared to BPSK for a given PGSC(*M, L, D*) scheme. Thus, while higher order alphabets allow higher data transmission rates, the increased bandwidth efficiency is attained at the expense of increasing the mean SNR/symbol/branch requirement (to compensate for denser signaling constellation). It is also apparent from Figure 3.3 that the

relative diversity gain attained diminishes as numbers of diversity paths per group are increased.

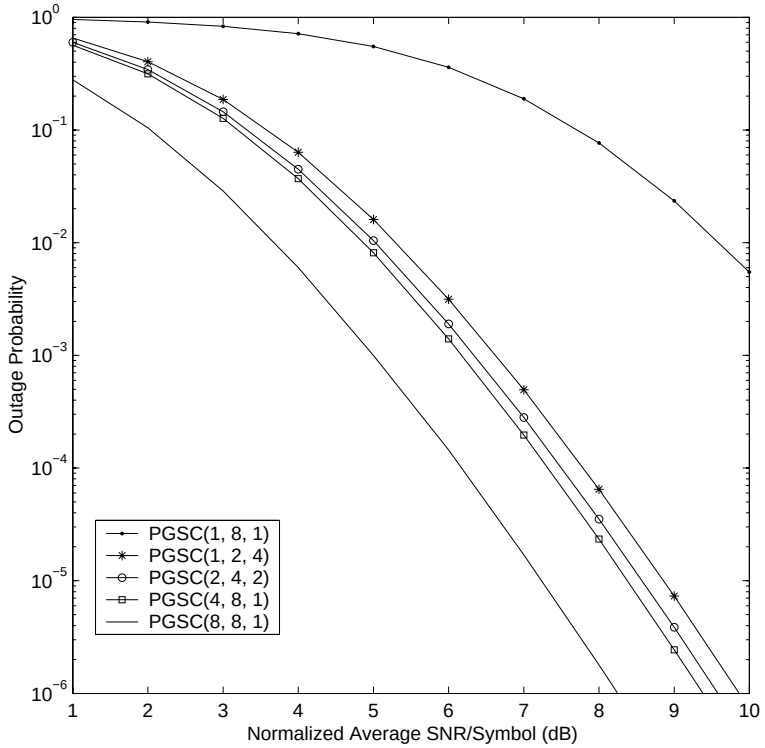

Figure 3.3 Outage probability $F_{pgsc}(\gamma^*)$ versus the normalized average SNR (Ω/γ^*) for PGSC receiver with a total of $L \times D = 8$ antennas in i.id Nakagami-m channel with $m = 0.5$.

3.3.3 ASER ANALYSIS

The error probability analysis for various digital modulation schemes in conjunction with coherent and non-coherent PGSC receiver structures can be easily rendered using the MGF of the PGSC output SNR derived in (1.2) or (1.4). Several examples are considered below.

3.3.3.1 Coherent PGSC Receiver

Using (1.2) or (1.4), the ASER of M_c-ary PSK with PGSC can be evaluated as

$$\overline{P_s} = \frac{1}{\pi}\int_0^{\pi-\pi/Mc} \phi_{\gamma_{pgsc}}\left(\frac{\sin^2(\pi/M_c)}{\sin^2\theta}\right)d\theta \qquad (1.13)$$

where M_c denotes the alphabet size. For the special case of binary PSK ($M_c = 2$), (1.13) simplifies to

$$\overline{P}_s = \frac{1}{\pi}\int_0^{\pi/2} \phi_{\gamma_{pgsc}}(\text{cosec}^2\theta)d\theta \tag{1.14}$$

Similarly, the ASER performance of M-ary QAM with coherent PGSC receiver is given by

$$\overline{P}_s = \frac{4}{\pi}(1-1/\sqrt{M_c})\int_0^{\pi/2} \phi_{\gamma_{pgsc}}\left[\frac{1.5/(M_c-1)}{\sin^2\theta}\right]d\theta$$
$$-\frac{4}{\pi}(1-1/\sqrt{M_c})^2\int_0^{\pi/4} \phi_{\gamma_{pgsc}}\left[\frac{1.5/(M_c-1)}{\sin^2\theta}\right]d\theta \tag{1.15}$$

Using the procedure above, it is possible to write down the ASER expressions for various other modulation schemes. Figure 3.4 shows the bit error curves for BPSK in conjunction with a PGSC receiver of fixed diversity order, $L\times D$ = 12, in a mixed[1] fading environment. As one would expect, all the performance curves are upper and lower bounded by PGSC(1, 12, 1) and PGSC(12, 12, 1) respectively, which correspond to selection diversity, SC(12), and the maximal-ratio combining, MRC(12) schemes respectively. It is apparent that at very low values of mean SNR/bit/branch, all PGSC schemes with equal number of total combined paths offer similar ABER performances. It may be noted that as multipath intensity profile[2] (MIP), δ, is small the, transmitted energy is symmetrically distributed across all the groups; hence resulting in almost identical performances of PGSC(*M, L, D*) with equal number of combined paths.

[1] In this chapter, all simulation results for mixed fading environment implicitly assume the fading parameters of the resolvable multipaths to be distributed as [$K_1 = 2.5$, $m_2 = 1$, $m_3 = 0.75$, $K_4 = 1$, $m_5 = 1.5$, $K_6 = 2$] with the pattern repeating itself in the given order.

[2] The average SNR of the n-th diversity path is $\overline{\gamma_n} = \Theta e^{-n\delta}\overline{\gamma_b}$ where $\overline{\gamma_b}$ denotes the average SNR/bit and the parameter Θ is chosen such that the constraint $\sum_{n=1}^{L}\overline{\gamma_n} = \overline{\gamma_b}$ is satisfied, solving for Θ yields $\overline{\gamma_n} = \frac{(1-e^{-\delta})e^{-\delta(n-1)}}{1-e^{-L\delta}}\overline{\gamma_b}$.

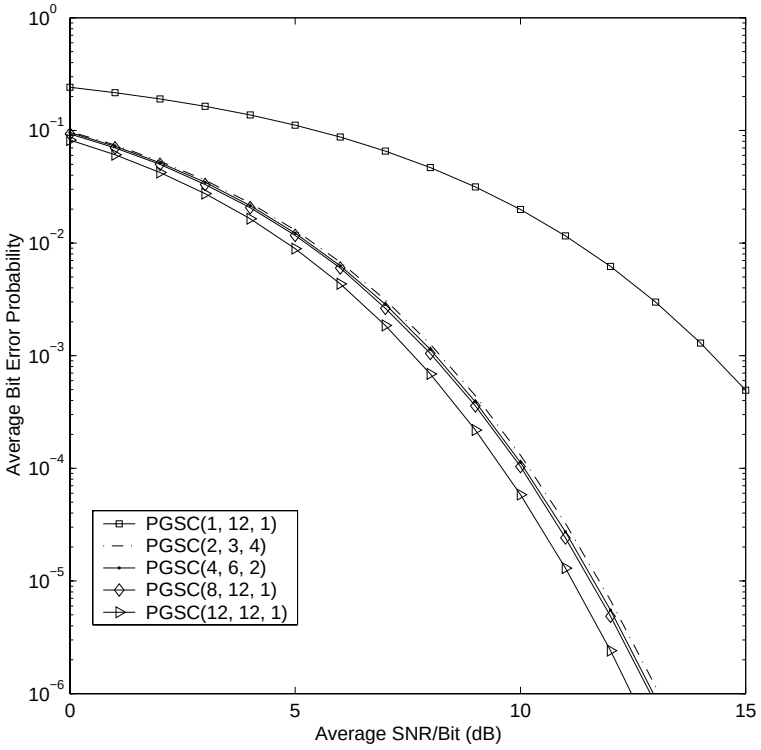

Figure 3.4 ABEP performance of BPSK with a coherent PGSC receiver in a mixed fading channel and exponentially decaying MIP ($\delta = 0.1$) for fixed diversity order ($L \times D$).

Figure 3.5 illustrates the comparative diversity gain achieved as number of diversity paths combined in each group are increased for a coherent BPSK PGSC(M, 5, 2) receiver. In accordance with the law of diminishing returns , the diversity gain diminishes with an increase in M and PGSC(3, 5, 2) offers performance almost identical to PGSC(5, 5, 2) i.e. MRC(25).

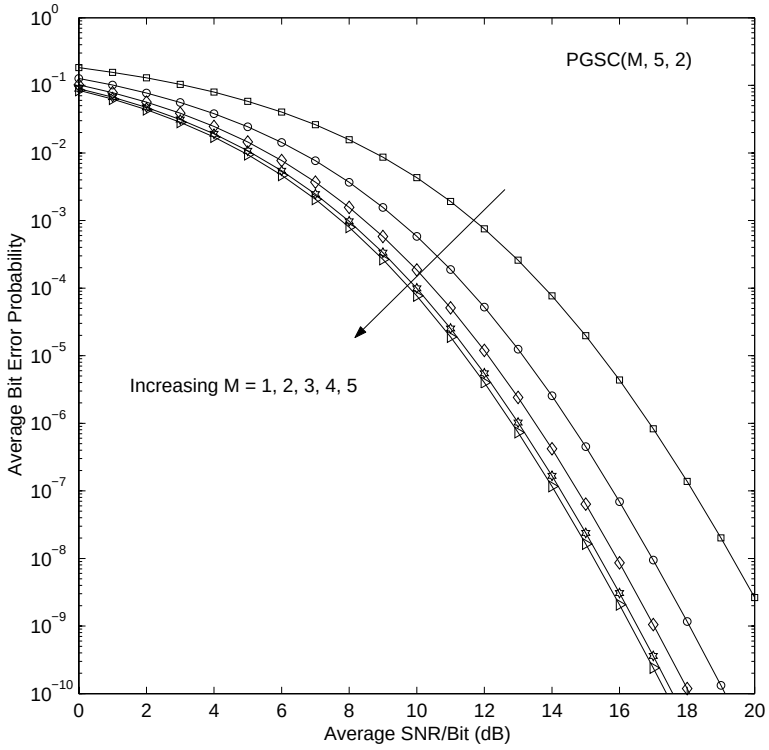

Figure 3.5 ABEP performance of BPSK with a coherent PGSC(*M*, 5, 2) receiver in a mixed fading channel and exponentially decaying MIP ($\delta = 10^{-4}$) environment for different values of *M*.

Figure 3.6 investigates the effect of number of partitions used on the performance of PGSC receiver for different values of δ. It is apparent that for large values of δ, transmitted energy is contained in first partition, and increasing the number of groups doesn't have any significant impact on the ABER performance. However, when the energy is distributed less asymmetrically across the group, i.e. δ is close to zero, an increase in the number of partitions used results in significant diversity gain.

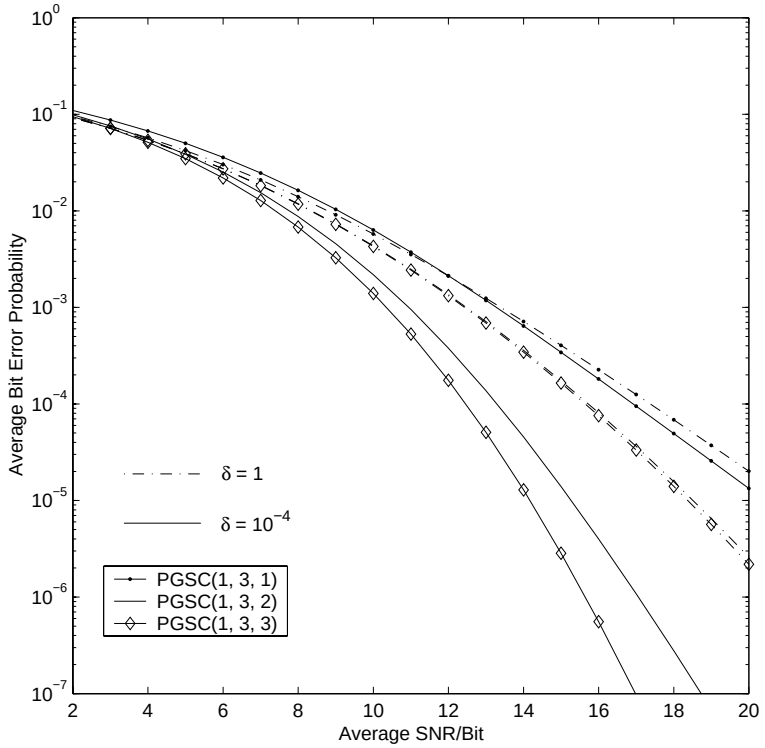

Figure 3.6 ABEP performance of BPSK with a coherent PGSC(1, 3, *D*) receiver in a mixed fading channel for different values of *D*.

Effect of varying exponential multipath intensity profile (MIP) on the performance of noncoherent DQPSK receiver structure is illustrated in Figure 3.7. For large values of MIP (greater than 0.5) the energy is mainly concentrated in the first partition, hence the criteria of choosing equal number of multipath components from each group doesn't serve well as depicted in the figure. However, for smaller values of MIP energy is equally distributed across the groups; hence an improvement in performance is observed as total number of partitions is increased.

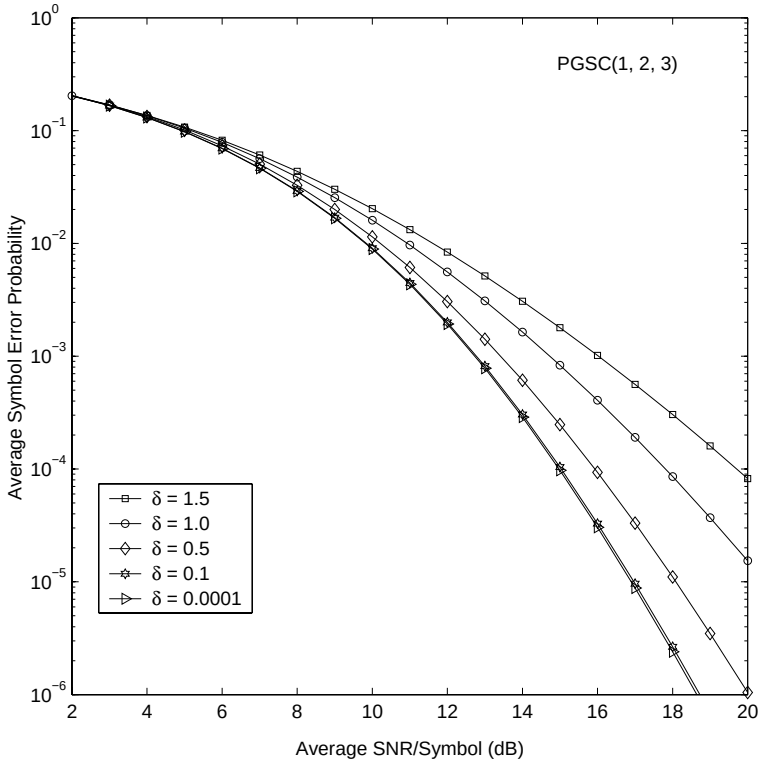

Figure 3.7 ASER performance of π/4-DQPSK with a noncoherent PGSC(1, 2, 3) receiver in different multipath intensity profiles.

3.3.3.2 Non-Coherent PGSC Receiver

The ABER performance of DPSK, BFSK and π/4-DQPSK in conjunction with a noncoherent PGSC(*M, L, D*) receiver may be computed as [25]

$$\overline{P}_b = \frac{1}{2\pi(1+\eta)^{2N-1}} \int_0^{2\pi} \frac{g(\theta)}{1-2\beta\cos\theta+\beta^2} \phi_{\gamma_{pgsc}} \left[\frac{b^2}{2}(1-2\beta\cos\theta+\beta^2) \right] d\theta \qquad (1.16)$$

where $0^+ < \beta = a/b < 1$, $N = M \times D$,

$$g(\theta) = \sum_{k=0}^{2N-1} \binom{2N-1}{k} \beta^{k+1-N} \eta^k \left(\cos\{(k-N+1)\theta\} - \beta\cos\{(k-N)\theta\} \right) \qquad (1.17)$$

and the values for constants *a, b,* and η for various modulation schemes are summarized in Table 3-1. It may be noted that as $a \to 0$, (1.16) assumes an indeterminate form but its limit converges smoothly to the exact ABER. Thus, the ABER of DPSK and BFSK can be computed using (1.16) with good accuracy by setting $a = 10^{-3}$ instead of zero. Alternatively, one may utilize the characteristic function method discussed in [25] to yield an infinite series expression for the ABER.

In Figure 3.8, we compare the ASER performances of coherent and noncoherent PGSC receiver structures in conjunction with π/4-DQPSK modulation scheme in a mixed fading channel. The ASER of π/4-DQPSK with coherent PGSC receiver may be computed as [21]

$$\overline{P}_s = \frac{1}{2\pi}\int_0^{\pi} \phi_{\gamma_{pgsc}}\left(\frac{2}{2-\sqrt{2}\cos\theta}\right)d\theta \tag{1.18}$$

It is apparent that coherent PGSC performs only slightly better than noncoherent PGSC receiver. Further the improvement offered by coherent PGSC diminishes at higher values of average SNR/symbol. For fixed L and M, the gap between the performance curves corresponding to coherent and noncoherent PGSC gets larger as number of combined paths ($M\times D$) increases. However, the ASER performance of noncoherent PGSC receiver asymptotically approaches that of coherent PGSC receiver (i.e., the gap between the curves gets smaller as the mean SNR/bit/branch increases). For small and moderate $M\times D$ values, noncoherent PGSC is attractive owing to its simple implementation and also because it yields comparable performance with that of the coherent PGSC receiver.

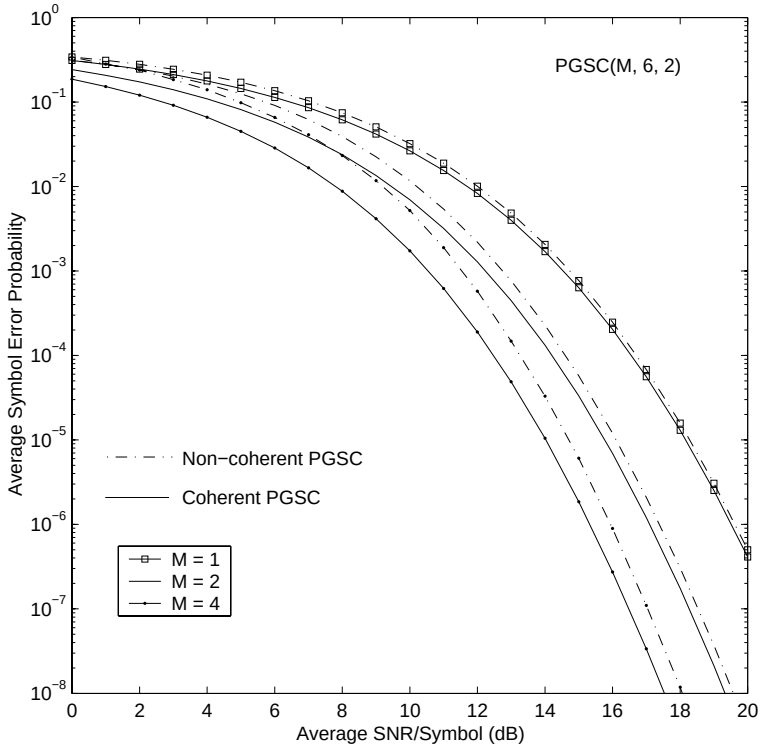

Figure 3.8 Average symbol error rate performance of π/4-DQPSK with coherent and noncoherent PGSC(M, 6, 2) receiver structures in a mixed fading channel and exponentially decaying MIP (δ = 0.1) for varying M.

3.4 Graphical User Interface to Analyze PGSC Performance

The mathematical analysis for PGSC receiver is comprehensive in the sense that it can be used to analyze the performance of various receiver structures including SC, MRC and GSC in generalized fading environment. A user friendly GUI has been developed to provide the performance metrics such as outage probability, symbol error rate etc for most of the commonly used modulation schemes. The dialog box in Figure 3.9 illustrates various parameters that a user can set using the GUI.

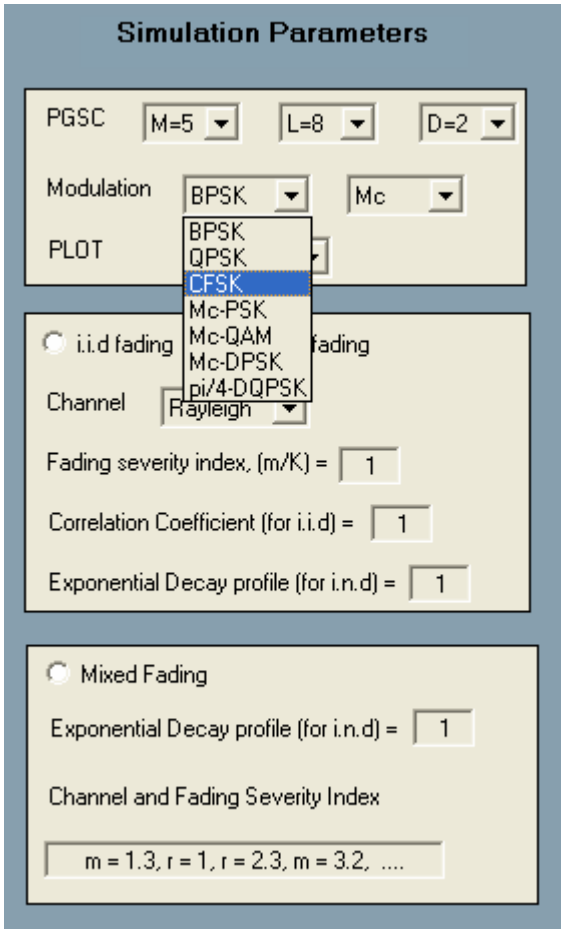

Figure 3.9 Dialog Box for specifying Simulation Parameters for PGSC

Figure 3.10 shows a screen shot of the complete GUI window depicting the ASER performance of QPSK with PGSC(2, 4, 3) in i.i.d Rayleigh fading channel.

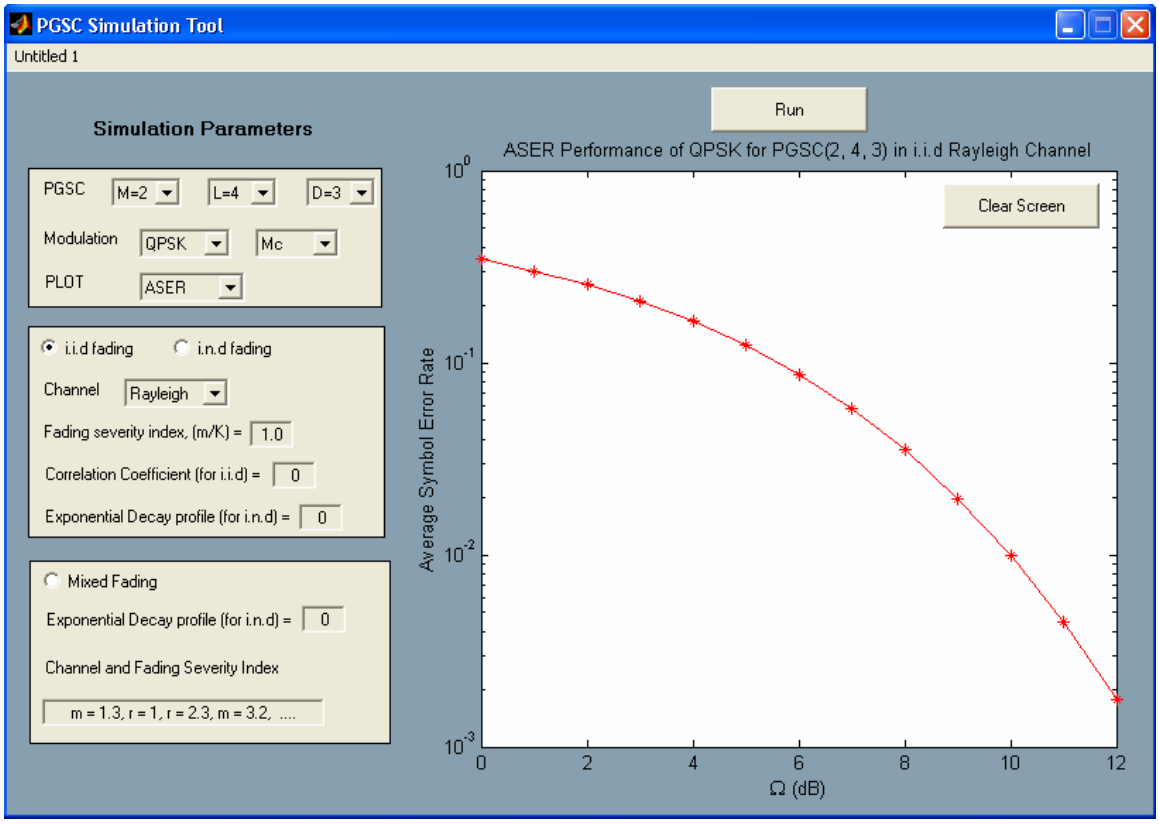

Figure 3.10 Screen Shot of the GUI showing ASER for QPSK in conjunction with PGSC(2, 4, 3) receiver

3.5 Chapter Contributions

In this chapter, we have presented a new diversity combining scheme, Partitioned General Selection Combining, for reception of signals in micro/pico-cellular environments for wideband CDMA and UWB systems having few GHz of bandwidth. The average bit error performance of various digital modulation schemes in conjunction with coherent and non-coherent PGSC receivers are analyzed for all common multipath fading channel models. The MGF and PDF of PGSC output SNR are used to facilitate ASER analysis for different modulation/detection schemes while the outage probability performance is predicted from the CDF expression. A trade-off is shown between PGSC receiver complexity and required performance. A research paper based on the work presented in this chapter is under preparation.

Table 3-1 Modulation related parameters for several noncoherent communication systems.

Modulation	***a***	***b***	η
BFSK	0	1	1
Antipodal DPSK	0	$\sqrt{2}$	1
$\pi/4$-DQPSK	$\sqrt{2-\sqrt{2}}$	$\sqrt{2+\sqrt{2}}$	1

Chapter 4

Dual-Diversity Equal Gain Combining in Correlated and Nonidentical Nakagami-m Channels

4.1 Introduction

Diversity methods have long been used in wireless systems to mitigate the detrimental effects of multipath fading and co-channel interference [26]. Moreover, portable radios that use diversity receiver have system level benefits: spatial/polarization diversity permits the use of lower transmit power to achieve a specified reliability, which in turn decreases the co-channel interference level and increases the battery life of portable terminals. Nevertheless, dual-diversity implementation with closely spaced antennas is typical for handheld wireless terminals (e.g., Panasonic's KX-TG2593B digital cordless, Qualcomm's QTP-5500 phone and Air Prime's wireless PC5230 card) owing to the cost and ergonomic considerations. Recent experimental studies [27]-[33] reveal that the envelope correlation coefficient of typical implementation of dual-antenna diversity systems may vary between 0.1 and 0.8 depending on the antenna configurations and operating environments. Consequently, any performance analysis must be revamped to account for the effects of branch correlations between the combined signals.

Reviewing the literature presented on this topic over the past few years, [27], [28], [32] and [34], performed comparative studies between selection, maximal ratio and/or equal gain diversity combining techniques using an outage probability metric (the cumulative distribution function of the combiner output statistic is plotted based on empirical data or through numerical evaluation for the special case of Rayleigh fading amplitudes). While such a measure is appropriate for analog communication systems, the average symbol error probability (ASEP) metric is more appropriate for digital communication systems. ASEP analyses that take into account of signal correlations for L^{th} order MRC and two-branch selection diversity combining (SDC) in Nakagami-m channel are provided in [35]-[36] and [37]-[39] respectively. Performance evaluation of EGC receiver, however,

is known to be a much more difficult compared to the MRC and SDC schemes. For example, [40] pointed out that ASEP analysis for EGC did not appear until the early 1990s even when the diversity paths are subject to independent fading. In fact, only [41]-[43] have treated EGC with correlations between the combined signals. The analyses in [41] and [42] are restricted to coherent binary modulation schemes for Rayleigh and Nakagami-m fading respectively. In [43], the authors derived an infinite series expression for the PDF of a sum of two correlated Nakagami-m variables with identical parameters and subsequently exploited an integral identity involving a product of Kummer functions developed in [44] and [45] to express the ASEP of *M*-ary QAM in terms of infinite sum of Lauricella hypergeometric functions. However, it is more reasonable to assume nonidentical mean signal strengths for signals received on distinct antennas since the transmitted signal will probably take different paths before arriving at the receiver. A further motivation for our analysis with nonindependent and nonidentical fading statistics is given in [40] which states that, "As digital wireless communication theory and technology become more mature, …., controlling and understanding these impairments become increasingly important to practical design."

In this *chapter*, we present a precise and computationally efficient ASEP analysis (using a moment generating function technique) for a broad range of digital modulation schemes that employ a two-branch EGC receiver in a more realistic operating environment. It turns out that our framework also facilitates the derivation of new closed-form formulas for the ASEP of DPSK with two independent inputs to the EGC combiner in Rayleigh and Nakagami-m fading without being "extremely unwieldy notationally" (see [44]) for moderate and large values of fading severity index. Explicit formulas for computing the outage probability and the higher order statistics of combiner output SNR are also derived (earlier work [41]-[43] did not present a framework for computing such metrics). In addition, a comparative study of dual-antenna diversity SDC, MRC and EGC schemes in Nakagami-m fading is also presented that takes into account the effects of branch correlation and unequal average branch SNRs.

The remainder of this chapter is organized as follows: In Section 4.2, we derive the EGC output SNR statistics for a dual-diversity system starting from the joint PDF of bivariate Nakagami-m density. Solutions to a few integrals that arise in the derivation of PDF and

CDF and/or MGF of EGC output SNR are presented in Appendix A and B respectively. Alternative infinite series expressions for the EGC output SNR statistics are derived in Appendix C while closed-form formulas for the PDF and MGF of EGC output SNR in Nakagami-m fading (assuming a half-odd integer value for the fading severity index) are provided in Appendix D. The utility of these expressions for average combined SNR analysis, outage probability analysis and ASER analysis are discussed in Section 4.3. Finally, Section 4.4 summarizes the main contributions of this chapter.

4.2 EGC Output SNR Statistics

In an EGC receiver, the output of distinct diversity branches are first co-phased, equally weighted, and then summed to give the resultant output. We are interested in computing the PDF, CDF, MGF and the higher order moments of instantaneous SNR at the dual-diversity EGC combiner output, viz.,

$$\gamma_{egc} = \frac{(X_1 + X_2)^2}{2} \equiv X^2 \tag{4.1}$$

where X_1 and X_2 are the random fading amplitudes normalized by the standard deviation of the noise. Suppose the branch amplitudes are modeled as nonindependent and nonidentical Nakagami-m random variables, the joint PDF of X_1 and X_2 can be written as [46]

$$f_{X_1X_2}(x_1,x_2) = \frac{4(x_1x_2)^m m^{m+1}}{\Gamma(m)(\Omega_1\Omega_2)^{(m+1)/2}(1-\rho)\rho^{(m-1)/2}} \exp\left[-\xi\left(\sqrt{\frac{\Omega_2}{\Omega_1}}x_1^2 + \sqrt{\frac{\Omega_1}{\Omega_2}}x_2^2\right)\right] I_{m-1}\left(2\xi\sqrt{\rho}x_1x_2\right) \tag{4.2}$$

where $m \geq ½$ denotes the fading severity index, $I_v(.)$ is the modified Bessel function of the first kind of order v, $\Gamma(.)$ is the Gamma function [47], $x_k \geq 0$ where $k \in \{1,2\}$, $\Omega_k = E\left[x_k^2\right]$ is the mean branch SNR of the k^{th} diversity path, notation E[.] denotes the statistical average of its argument, ρ ($0 < \rho < 1$) corresponds to the power correlation coefficient between the signals received on the two closely spaced antennas and $\xi = \frac{m}{(1-\rho)\sqrt{\Omega_1\Omega_2}}$.

4.2.1 A. PDF of γ_{egc}

From the definition of (4.1) and using (4.2), we can evaluate the PDF of the normalized resultant signal amplitude at the EGC combiner output as

$$p_X(x) = \sqrt{2}\int_0^{x\sqrt{2}} f_{X_1X_2}(x_1, x_2 = x\sqrt{2} - x_1)dx_1 \tag{4.3}$$

Substituting (4.2) into (4.3) and making use of the trigonometric integral representation for $I_v(.)$ [47], (4.3) may be restated as

$$p_X(x) = \frac{4\sqrt{2}(1-\rho)^m \xi^{2m}}{\sqrt{\pi}\Gamma(m-1/2)\Gamma(m)} \int_0^{\pi} \sin^{2m-2}\theta e^{-\nu(\theta)x^2}$$

$$\times\left(\int_0^{x\sqrt{2}} [x_1(x\sqrt{2} - x_1)]^{2m-1} \exp\left[-\mu(\theta)\left\{ x_1 - r_1(\theta)x \right\}^2 \right] dx_1 \right) d\theta, \quad m > ½ \tag{4.4}$$

where $h_i(\theta) = \frac{\Omega_i}{\sqrt{\Omega_1\Omega_2}} - \sqrt{\rho}\cos\theta$, $\mu(\theta) = \xi[h_1(\theta) + h_2(\theta)]$, $r_i(\theta) = \frac{\sqrt{2}h_i(\theta)}{h_1(\theta) + h_2(\theta)}$ and $\nu(\theta) = \frac{2\xi(1-\rho\cos^2\theta)}{h_1(\theta) + h_2(\theta)}$. Note that the second integral in (4.4) can be evaluated using the integral identity (A.1) (see Appendix B). Thus the PDF of γ_{egc} can be evaluated as (after applying variable transformation $\gamma = x^2$ in (4.4))

$$p_{\gamma_{egc}}(\gamma) = \frac{2\sqrt{2}(1-\rho)^m \xi^{2m}\gamma^{-1/2}}{\sqrt{\pi}\Gamma(m-1/2)\Gamma(m)} \int_0^{\pi} \sin^{2m-2}\theta e^{-\nu(\theta)\gamma}$$

$$\times I(\sqrt{2\gamma}, r_1(\theta)\sqrt{\gamma}, \mu(\theta), 2m-1)d\theta, \quad m > ½ \tag{4.5}$$

where $I(.,.,.,.)$ is defined in (A.7). Notice that, (4.5) requires the computational complexity of an infinite sum of an integral (or equivalently, involves the computational complexity of a double integral), for arbitrary real $m > ½$. However, when m is an integer or half odd-integer, (4.5) simplifies into a single integral with finite integration limits (owing to the availability of a closed-form formula for $I(.,.,.,2m\text{-}1)$), viz.,

$$p_{\gamma_{egc}}(\gamma) = \frac{(2m-1)(1-\rho)^m \xi^{2m}}{\sqrt{2}\pi} \int_0^{\pi} \sin^{2m-2}\theta e^{-\nu(\theta)\gamma} \sum_{k=0}^{2m-1} \sum_{i=0}^{2k} \binom{2k}{i}$$

$$\times \frac{(-1)^{k+i}\left(r_2(\theta)-r_1(\theta)\right)^{2k-i}\gamma^{(4m-3-i)/2}}{2^{k-i}k!\Gamma(2m-k)\mu^{(i+1)/2}(\theta)}\left[c(i,r_2(\theta))\Upsilon\left(\frac{i+1}{2},\mu(\theta)r_2^2(\theta)\gamma\right)\right.$$

$$\left.-c(i,-r_1(\theta))\Upsilon\left(\frac{i+1}{2},\mu(\theta)r_1^2(\theta)\gamma\right)\right]d\theta,\ \ m\in\left\{1,\frac{3}{2},2,...\right\} \qquad (4.6)$$

where $\Upsilon(a,x)=\int_0^x t^{a-1}e^{-t}dt$ denotes the incomplete Gamma function and the coefficients $c(.,.)$ are defined in (A.8). In Appendix C, we also provide an alternative infinite series solution for (4.6) by exploiting the power series representation for $I_{m-1}(.)$ in (4.2). Although (4.6) is valid even for half-odd integer values of m, the PDF of γ_{egc} can be derived in closed-form for this specific case. These developments are presented in Appendix D. It is also important to note that (4.6) is much more general (because it treats the case of unequal mean branch SNRs), computationally efficient and numerically stable (particularly for large ρ and m values) compared to [43].

For the special case of identical fading ($\Omega_1=\Omega_2$), the PDF of γ_{egc} can be directly obtained using (4.5) and integral identity (A.8) as

$$p_{\gamma_{egc}}(\gamma)=\frac{(2m-1)(1-\rho)^m\xi^{2m}}{\sqrt{\pi}\Gamma(2m+1/2)}\gamma^{2m-1}e^{-2\xi\gamma}\int_0^\pi \sin^{2m-2}\theta\ {}_1F_1\left(2m;2m+1/2;\xi(1+\sqrt{\rho}\cos\theta)\gamma\right)d\theta \qquad (4.7)$$

where ${}_1F_1(.;.;.)$ denotes the confluent hypergeometric function [47]. Obviously (4.7) is much more concise compared to (4.5). Moreover, if ρ = 0 (independent fading case), (4.5) can be simplified using the identity $\int_0^\pi \sin^{\mu-1}xdx=\sqrt{\pi}\Gamma(\mu/2)/\Gamma((\mu+1)/2)$ as

$$p_{\gamma_{egc}}(\gamma)=\frac{\sqrt{2}m^{2m}\Gamma(m+1/2)}{\sqrt{\pi}\Gamma(m)(\Omega_1\Omega_2)^m}\exp(-\nu\gamma)\sum_{k=0}^{T_{2m-1}}\sum_{i=0}^{2k}\binom{2k}{i}\frac{(-1)^{k+i}2^{i-k}(r_2-r_1)^{2k-i}}{k!\Gamma(2m-k)\mu^{(i+1)/2}}$$

$$\times\gamma^{(4m-3-i)/2}\left[\Upsilon\left(\frac{i+1}{2},\mu r_2^2\gamma\right)+(-1)^i\Upsilon\left(\frac{i+1}{2},\mu r_1^2\gamma\right)\right],\ \ m\geq 1/2 \qquad (4.8)$$

where $\mu=\frac{m(\Omega_1+\Omega_2)}{\Omega_1\Omega_2}$, $r_i=\frac{\sqrt{2}\Omega_i}{\Omega_1+\Omega_2}$, $\nu=\frac{2m}{\Omega_1+\Omega_2}$ and T_n is defined in (A.4). Furthermore, (4.8) reduces to a finite series when $2m$ is a positive integer. To the best of

our knowledge, the development of (4.8) is also new.

4.2.2 CDF of γ_{egc}

The knowledge of CDF of γ_{egc} is also of interest to the wireless system designers because the outage probability of EGC diversity receiver can be expressed in terms of this metric alone. The CDF of γ_{egc} can be obtained using (4.5) and (B.1) as

$$F_{\gamma_{egc}}(\gamma^*) = \int_0^{\gamma^*} p_{\gamma_{egc}}(\gamma)d\gamma$$

$$= \frac{2\sqrt{2}(1-\rho)^m \xi^{2m}}{\sqrt{\pi}\Gamma(m-1/2)\Gamma(m)} \int_0^{\pi} \sin^{2m-2}\theta J\left(\nu(\theta), \sqrt{2}, r_1(\theta), \mu(\theta), 2m-1, \gamma^*\right) d\theta, \quad m > \frac{1}{2} \qquad (4.9)$$

where the parameters $r_i(.)$, $\mu(.)$, and $\nu(.)$ are defined similar to (4.4) and $J(.,.,.,.,.,.)$ can be computed using (B.3).

4.2.3 MGF of γ_{egc}

Recognizing that MGF of the EGC combiner output SNR is the key to unified analysis of a broad range of digital modulation schemes over wireless channels, the desired MGF may be computed using (4.5) and (B.1) as

$$\phi_{\gamma_{egc}}(s) = \int_0^{\infty} e^{-s\gamma} p_{\gamma_{egc}}(\gamma)d\gamma = \frac{2\sqrt{2}(1-\rho)^m \xi^{2m}}{\sqrt{\pi}\Gamma(m-1/2)\Gamma(m)} \int_0^{\pi} \sin^{2m-2}\theta$$

$$\times J\left(s+\nu(\theta), \sqrt{2}, r_1(\theta), \mu(\theta), 2m-1, \infty\right) d\theta, \quad m > ½ \qquad (4.10)$$

where $J(.,.,.,.,.,.)$ is defined in (B.4). If m assumes an integer or a half-odd integer value, then (4.10) simplifies into a single integral with finite integration limits. In fact, for the special case of half-odd integer m values, a closed-form solution for (4.10) is also available (see (D.4)). Moreover, if the two diversity paths are statistically independent (i.e., $\rho = 0$), (4.10) reduces to numerically efficient expression:

$$\phi_{\gamma_{egc}}(s) = \frac{2\sqrt{2}m^{2m}\Gamma(2m)\Gamma(m+1/2)}{\sqrt{\pi}\Gamma(m)(\Omega_1\Omega_2)^m} \sum_{k=0}^{T_{2m-1}} \sum_{i=0}^{2k} \binom{2k}{i} \frac{(-1)^{k+i} 2^{i-k} (r_2 - r_1)^{2k-i}}{(i+1)k!\Gamma(2m-k)}$$

$$\times\left[\frac{r_2^{(i+1)}}{[s+\nu+r_2^2\mu]^{2m}}\,{}_2F_1\left(1,2m;\frac{i+3}{2};\frac{r_2^2\mu}{s+\nu+r_2^2\mu}\right)\right.$$

$$\left.+\frac{(-1)^i r_1^{i+1}}{(s+\nu+r_1^2\mu)^{n+1}}\,{}_2F_1\left(1,2m;\frac{i+3}{2};\frac{r_1^2\mu}{s+\nu+r_1^2\mu}\right)\right],\quad m>1/2 \tag{4.11}$$

where ${}_2F_1(.,.;.;.)$ denotes the Gaussian hypergeometric function [47] and the parameters r_i, μ, and ν are defined similar to (4.8). The above result is particularly interesting in view of the complicated expression for two special cases (integer or half-odd integer *m* values) derived recently in [44]. Note that the ASEP for DPSK with coherent EGC receiver is given by $\frac{1}{2}\phi_{\gamma_{egc}}(\gamma)$. Moreover, different from [19], both cases of positive integer and half-odd integer *m* values are treated in a unified sense. With the closed-form formula for the MGF of γ_{egc} thus available (*m* is a multiple of 0.5), the ASEP of *M*-ary modulation formats (e.g., MPSK) with dual-diversity EGC can be reduced into a single finite-range integral (rather than the double integral expression given by [44]).

4.2.4 Higher Order Moments of γ_{egc}

Higher-order statistics of output SNR provide another comparative performance measure of diversity systems over fading channels. The higher order statistics of γ_{egc} can be derived using the PDF depicted in (4.6) as $\Delta_n=\int_0^\infty \gamma^n p_{\gamma_{egc}}(\gamma)d\gamma$. However, a much more concise and a closed form formula for computing the n^{th} order moment of γ_{egc} can be deduced from (4.1) and making use of [46], viz.,

$$\Delta_n=E[\gamma_{egc}^n]=\left(\frac{\Omega_2}{2m}\right)^n\sum_{i=0}^{2n}\binom{2n}{i}\left(\frac{\Omega_1}{\Omega_2}\right)^{i/2}\frac{\Gamma(m+i/2)\Gamma(m+n-i/2)}{[\Gamma(m)]^2}\,{}_2F_1(-i/2,-n+i/2;m;\rho) \tag{4.12}$$

Additionally, the central moments of γ_{egc} can be computed in terms of (4.12) alone as

$$\mu_k=E[(\gamma_{egc}-\Delta_1)^k]=\sum_{i=0}^{k}\binom{k}{i}\Delta_i(-\Delta_1)^{k-i} \tag{4.13}$$

For instance, the mean and variance of the combined output SNR are given by Δ_1 and

$\mu_2 = \Delta_2 - (\Delta_1)^2$ respectively.

4.3 Performance Metrics of Diversity Receivers

In this section, we utilize the expressions derived in the preceding section to investigate several different performance metrics for an EGC receiver and provide a detailed analysis of the effects of unequal mean branch SNRs, signal correlation, channel fading severity index etc. on its receiver performance. A comprehensive comparative study of dual diversity SDC, EGC and MRC schemes is also presented.

4.3.1 Outage Probability

Figure 4.1a shows the outage probability $P_{out} = F_{\gamma_{egc}}(\gamma^*)$ performance curves for a dual-diversity EGC receiver in correlated Nakagami-m fading. It is apparent that outage performance degrades with increasing envelope correlation and/or average SNR imbalance between the two diversity branches. From this plot, it is possible to determine the average SNR/symbol/branch required to satisfy an outage requirement for a given modulation scheme. For example, if target symbol error rate of $P_e^* = 10^{-3}$ and BPSK modulation are specified, we have $\gamma^* = [erfc^{-1}(2\times 10^{-3})]^2 = 4.77$. Thus to satisfy an outage requirement of $P_{out} = 10^{-2}$, Ω_2 may be estimated as $\Omega_2 = 4.77(10^{0.32})$ = 9.94 dB when Ω_1/Ω_2 = 1 and $\Omega_2 = 4.77(10^{0.39})$ = 10.73 dB if Ω_1/Ω_2 = 0.7 (interpolated from Figure 4.1a) assuming that m = 2.5 and ρ = 0. Thus, to achieve the same outage rate of error, an average SNR ratio of 0.7 results in a meager penalty of 0.08 dB for Ω_2. However, $\Omega_2 = 4.77(10^{0.43})$ = 11.05 dB when Ω_1/Ω_2 = 1 and ρ = 0.5. Hence, signal correlation has much more detrimental effect on the outage performance than the mean branch SNR imbalance between the diversity signals. Figure 4.1b depicts the outage performances of different diversity combining techniques when Ω_1/Ω_2 = 1. It is evident that outage performance of EGC is very close to that offered by MRC and this becomes much more apparent at a higher m value. Since the difference between SDC and EGC or MRC performance curves increases as the channel experiences fewer deep fades, we can conclude that average combined SNR becomes a much more dominant factor in determining the receiver performance compared to diversity gain as channel improves.

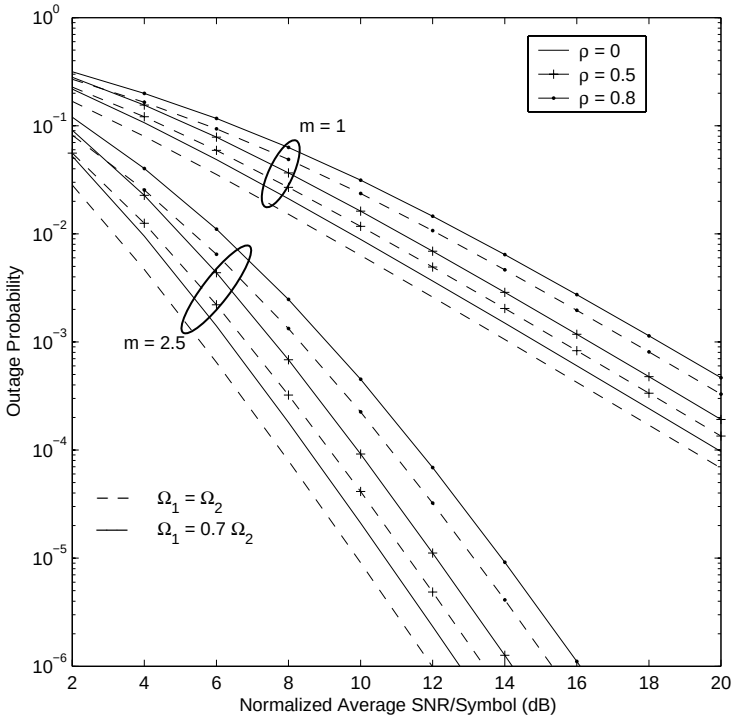

(a)

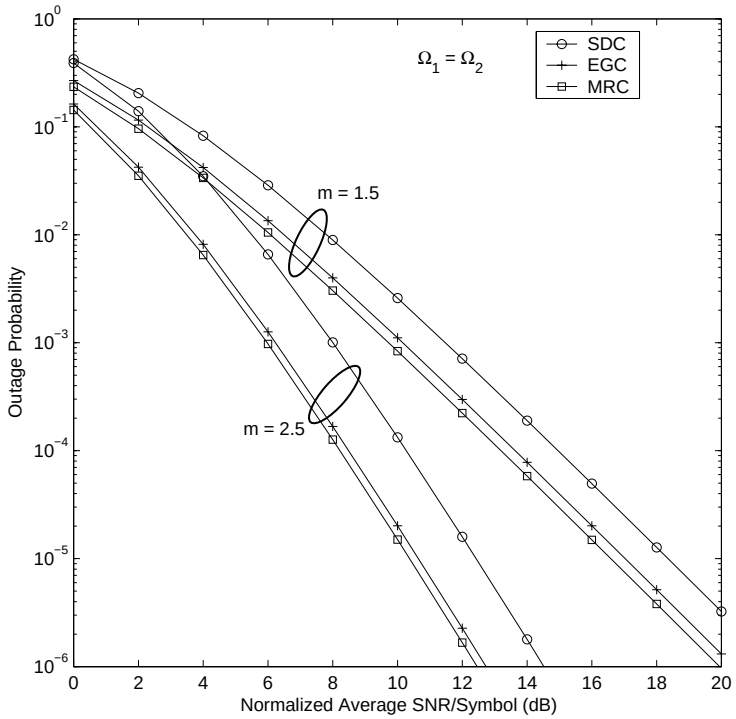

(b)

Figure 4.1 Outage probability $F_\gamma(\gamma^*)$ versus the normalized average SNR Ω_2 / γ^*: (a) dual-diversity EGC over Nakagami-m fading channels for different power correlation coefficient ρ; (b) comparative study of different diversity combining techniques at power correlation coefficient ρ = 0.3.

4.3.2 Mean and Variance of combined SNR at EGC Output

The mean combined SNR γ_{egc} can be evaluated in closed-form by setting n = 1 in (4.12), viz.,

$$\bar{\gamma}_{egc} = \frac{1}{2}\left[\Omega_1 + \Omega_2 + \frac{2\sqrt{\Omega_1\Omega_2}}{m}\left(\frac{\Gamma(m+1/2)}{\Gamma(m)}\right)^2 {}_2F_1(-1/2,-1/2;m;\rho)\right] \qquad (4.14)$$

In Figure 4.2, the normalized mean $E[\gamma_{egc}]/\bar{\Omega}$ and normalized variance $\{E[\gamma_{egc}^2]-(E[\gamma_{egc}])^2\}/(\bar{\Omega})^2$ of EGC output SNR are plotted as a function of power correlation coefficient for several values of Ω_1/Ω_2 where $\bar{\Omega} = (\Omega_1+\Omega_2)/2$. Although the normalized mean output SNR increases with increasing ρ (which is counter-intuitive), the variance of the combiner output SNR also increases with ρ. Thus a higher correlation coefficient does not directly translate into an improved receiver performance. This observation in turn suggests that the average output SNR statistic may not be an appropriate metric to perform a comparative study of different diversity combining schemes when the diversity paths are correlated. Figure 4.2 also reveals that the rate at which the normalized mean output SNR increases declines gradually as the mean branch SNR imbalance between the two branches increases. For the limiting case of ρ = 1, we have $\lim_{\rho\to 1}\bar{\gamma}_{egc} = \frac{1}{2}\left(\sqrt{\Omega_1}+\sqrt{\Omega_2}\right)^2$. These two trends are in contrast to MRC scheme where $E[\gamma_{mrc}]/\bar{\Omega} = 2$ regardless of the ratio Ω_1/Ω_2 and the value of ρ.

4.3.3 ASER Analysis

The ASEP of multilevel square QAM can be conveniently evaluated as

$$\bar{P}_S = \frac{4}{\pi}(1-1/\sqrt{M})\int_0^{\pi/2}\phi_{\gamma_{egc}}\left[\frac{1.5/(M-1)}{\sin^2\theta}\right]d\theta - \frac{4}{\pi}(1-1/\sqrt{M})^2\int_0^{\pi/4}\phi_{\gamma_{egc}}\left[\frac{1.5/(M-1)}{\sin^2\theta}\right]d\theta \qquad (4.15)$$

where M denotes the alphabet size and $\phi_{\gamma_{egc}}(\gamma)$ is defined in (C.4) (in conjunction with (B.4)) or (4.10) for real $m \geq$ ½. For the special case of half-odd integer m values, it is more appropriate to use (D.4) (in conjunction with (B.4)) respectively. Therefore, it is apparent that (4.15) is much more suitable for numerical computation compared to

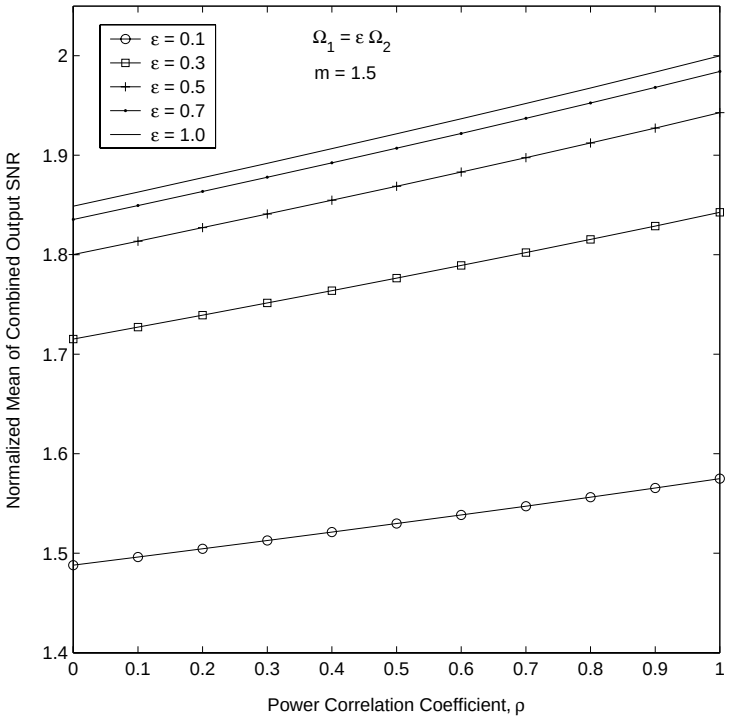

(a)

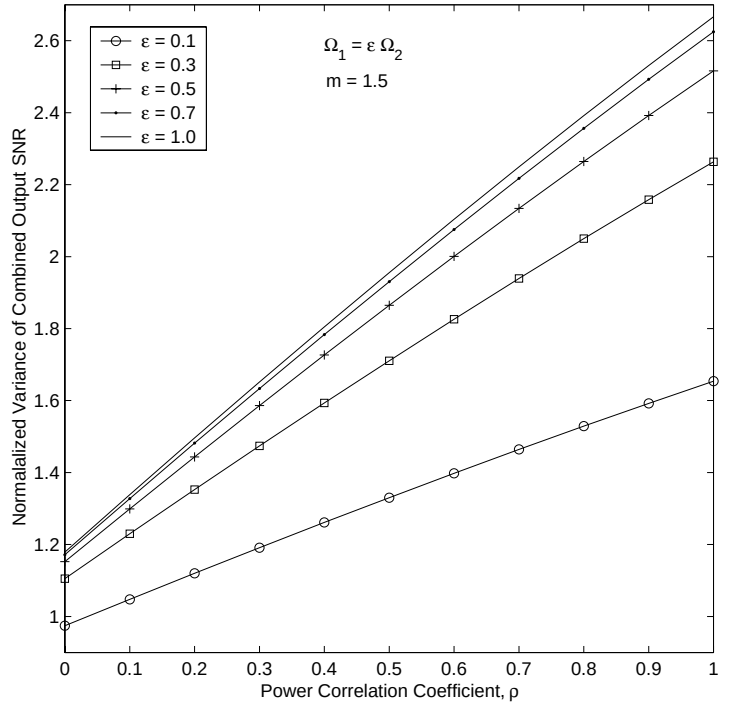

(b)

Figure 4.2 The normalized mean $E[\gamma_{egc}]/\overline{\Omega}$ and normalized variance $\{E[\gamma_{egc}^2]-(E[\gamma_{egc}])^2\}/(\overline{\Omega})^2$ of EGC output SNR versus the power correlation coefficient ρ for several values of Ω_1/Ω_2 where $\overline{\Omega}=(\Omega_1+\Omega_2)/2$.

[43] even for the special case of $\Omega_1 = \Omega_2$ because the latter involves the computational complexity of a three fold and a four-fold infinite sums[3]. Figure 4.3 illustrates the performance curves for 16-QAM with dual-diversity coherent EGC receiver in correlated Rayleigh (m = 1) and Nakagami-m (m = 3) channels with $\Omega_2 = 0.7\Omega_1$. The error performance degrades much more rapidly as power correlation factor approaches unity at large Ω_1, resulting in considerable loss of diversity gain. This observation is more pronounced as the channel experiences more severe fading.

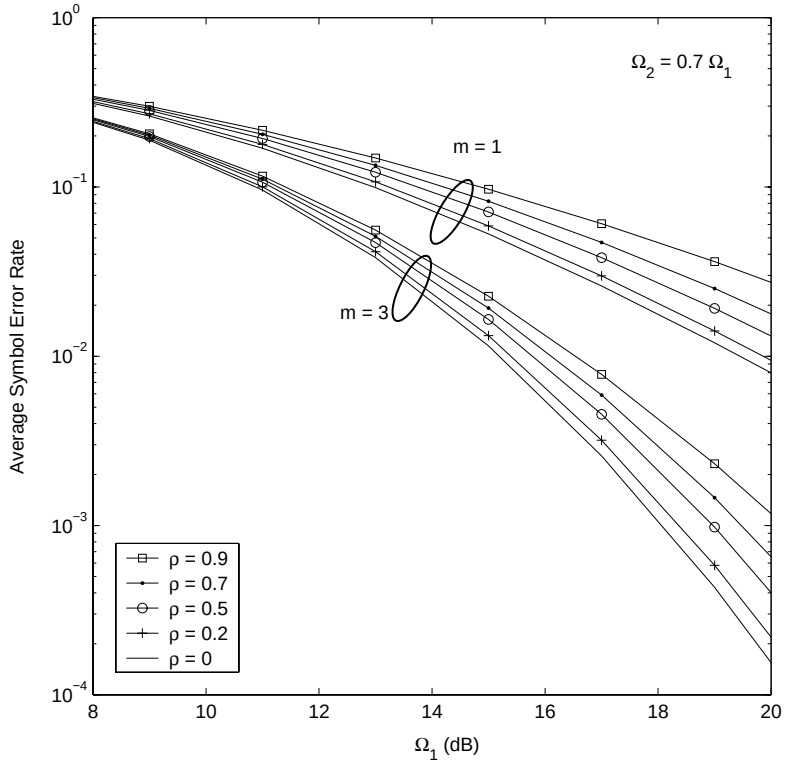

Figure 4.3 ASEP performance of 16-QAM in conjunction with a dual-diversity EGC receiver in Nakagami-m fading and $\Omega_2 / \Omega_1 = 0.7$.

Figure 4.4 compares the ASEP performance of BPSK with coherent EGC, SDC and MRC schemes as a function of signal power correlation between two closely spaced antennas. The ASEP performance of SDC and MRC can be analyzed via an MGF approach with the aid of [39] and [46] respectively:

[3] In [43], the authors expressed the conditional error probability (CEP) of *M*-ary QAM in terms of Kummer functions and then averaged it over (C.2) and utilizing [44] to get their final expression in terms of infinite sum of Lauricella hypergeometric functions.

$$\phi_{\gamma_{sdc}}(s) = \frac{2^{2m}\Gamma(2m)}{\Gamma(m)\Gamma(m+1)} \sum_{i=1, j\neq i}^{2} \left[\frac{A_{ij}}{\Omega_i B_{ij}(1+B_{ij})} \right]^m {}_2F_1(1-m, m; 1+m; (1-1/B_{ij})/2) \quad (4.16)$$

$$\phi_{\gamma_{mrc}}(s) = \left[\frac{m^2}{\Omega_1\Omega_2(1-\rho)\{(s+\alpha)^2 - \beta^2\}} \right]^m \quad (4.17)$$

where $A_{ij} = \dfrac{\Omega_j(1-\rho)/2}{[\Omega_j/\Omega_i - 1 + s\Omega_j(1-\rho)]^2}$ and $B_{ij} = \dfrac{\sqrt{[s\Omega_1\Omega_2(1-\rho) + \Omega_1 + \Omega_2]^2 - 4\rho s\Omega_1\Omega_2}}{s\Omega_1\Omega_2(1-\rho) + \Omega_j - \Omega_i}$.

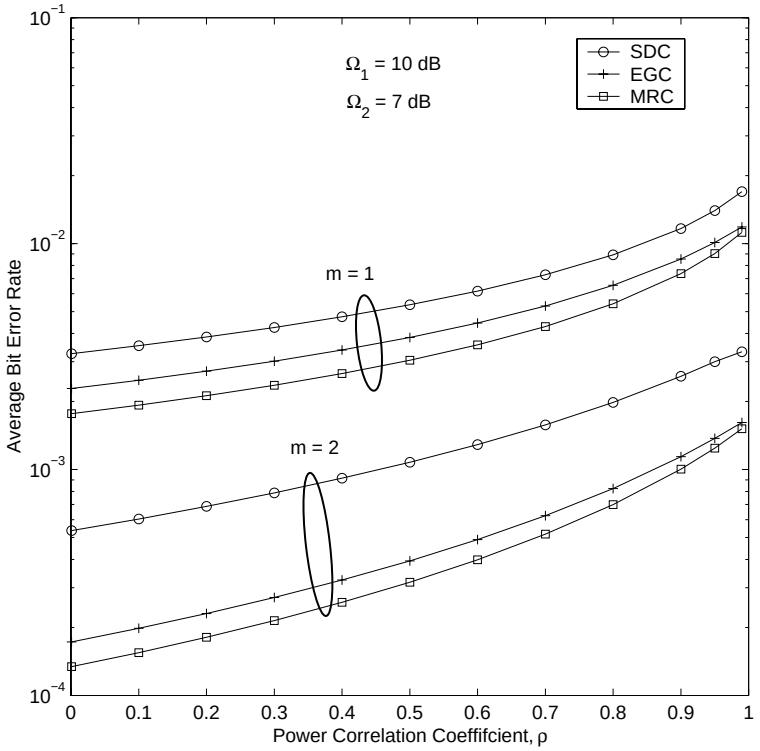

Figure 4.4 Comparative study of different diversity combining techniques for BPSK modulation in Nakagami-m fading as a function of power correlation coefficient.

It is worth mentioning here that the coefficient A_{ij} is defined slightly different from [39] to avoid numerical problems encountered when A_{ij} assumes a negative value. MRC provides the best error performance followed by EGC and SDC for a fixed m and ρ values, as expected. Figure 4.4 further reveals that diversity gain of SDC is more vulnerable to channel fading severity index compared to that of EGC and MRC (owing to

the wider spread between the SDC and EGC or MRC curves as *m* gets larger. EGC is also found to be less susceptible to branch correlation compared to MRC since the difference between their performance curves diminishes as ρ increases. In the limiting case of $\rho = 1$, EGC and MRC perform almost identically.

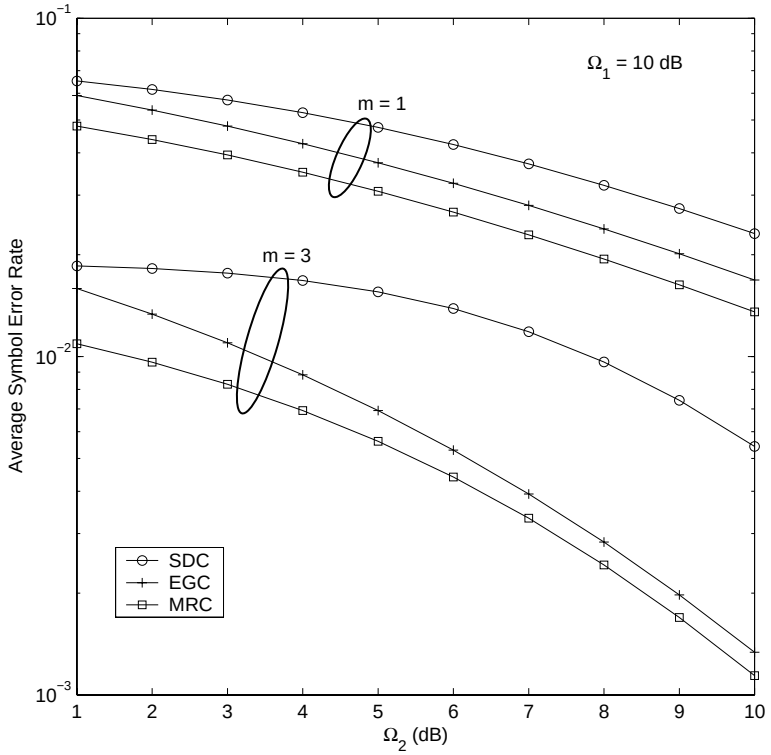

Figure 4.5 Comparative study of different dual-diversity combining techniques in Nakagami-m fading with power correlation coefficient ρ = 0.3 and QPSK modulation.

In Figure 4.5, we examine the effects of average branch SNR imbalance (Ω_2 / Ω_1) on the performance of QPSK with different dual-antenna diversity implementations. Instead of using (4.15) with $M = 4$ (recognizing that both 4-QAM and QPSK have identical signal constellation), a much more concise formula for the desired ASEP with coherent EGC receiver is given by

$$\overline{P}_s = \frac{1}{\pi} \int_0^{3\pi/4} \phi_{\gamma_{egc}} \left(\frac{1}{2\sin^2 \theta} \right) d\theta \tag{4.18}$$

Eq. (4.18) can also be used for ASEP analysis of QPSK with dual-diversity SDC and

MRC with correlated diversity paths by replacing $\phi_{\gamma_{egc}}(.)$ with (4.16) and (4.17) respectively. Numerical results reveal that the relative performance gain offered by SDC diminishes for larger values of *m* especially when $\Omega_2 \approx \Omega_1$. On the other hand, the difference between EGC and MRC performance curves gets closer as the average branch SNR imbalance decreases especially at large values of *m*. These two trends suggest that the diversity gain becomes less dominant factor (in determining the ASEP performance) compared to the average combined SNR metric in good channel conditions. To further emphasize this point, Figure 4.6 shows diversity 8-PSK performance as a function of *m* for different ρ values. Although SDC yields relatively good performance in severe fading conditions, the relative diversity improvement diminishes as *m* gets larger.

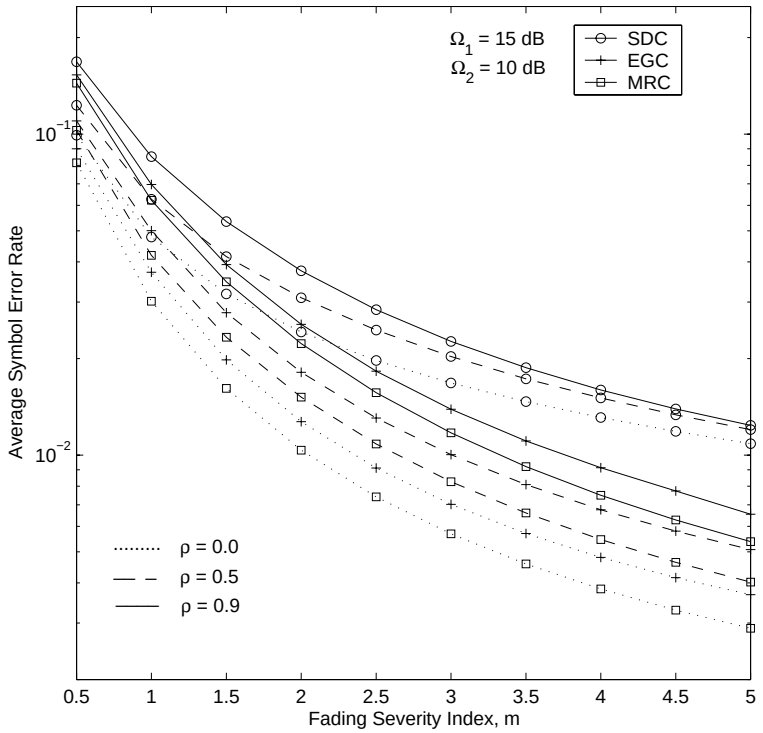

Figure 4.6 Comparative study of different diversity combining techniques for 8-PSK in Nakagami-m fading.

Moreover, it is observed that EGC is less susceptible to branch correlations compared to both SDC and MRC schemes. It is also worth mentioning that the above plots may also be used to predict ASEP performance of different digital modulation schemes for a specified antenna separation *d*. For example, Clarke [47] has derived a relationship

between ρ and antenna separation d as $\sqrt{\rho} = \left| J_0\left(\frac{2\pi d}{\lambda}\right)\right|$ where $J_0(.)$ is the Bessel function of the first kind with order zero and λ is the carrier wavelength. This result is valid for a uniform angle of arrival distribution in azimuth and identically polarized omnidirectional receiving antennas that are matched to the polarization of the incoming wave. For instance, if $\rho = 0.3$ is acceptable in a design, then d is constrained to be greater than 0.23λ.

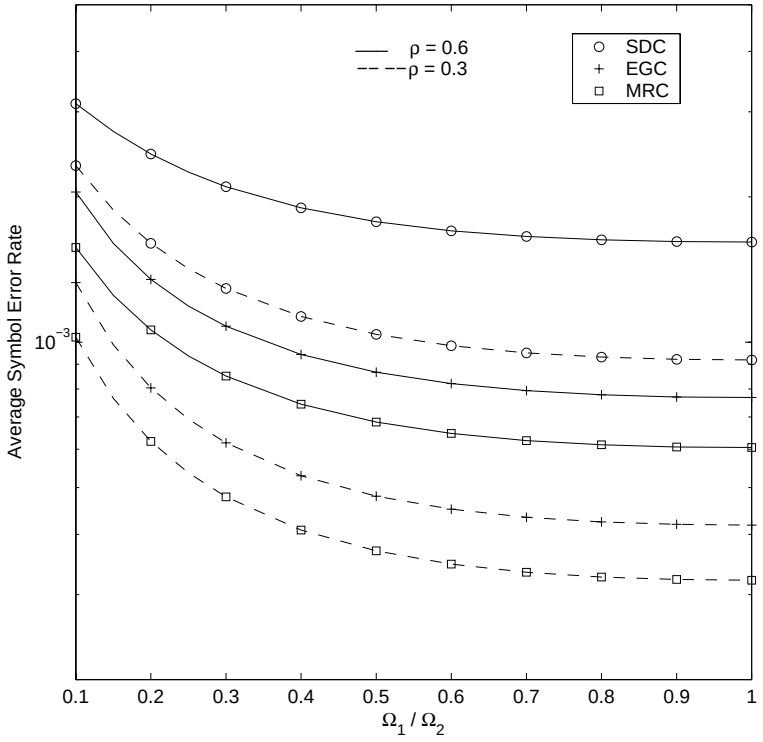

Figure 4.7 Comparative study of different diversity combining techniques for QPSK in a Nakagami-m channel (m =1.5) as a function of Ω_1 / Ω_2 while the mean SNR/branch $\overline{\Omega} = (\Omega_1 + \Omega_2)/2$ is fixed at 12 dB.

Figure 4.7 compares the ASEP performance of diversity QPSK for different Ω_1 / Ω_2 ratios but at a fixed mean SNR/branch, $\overline{\Omega} = (\Omega_1 + \Omega_2)/2$ = 12 dB. It is apparent that for an "energy sharing" communication, the ASEP performance is minimized when $\Omega_1 = \Omega_2$ regardless of the value of ρ. Also, for a fixed Ω_1 / Ω_2, the ASEP degrades as ρ increases, as anticipated. Notice also that ASEP performance curves plotted as a function of Ω_1 / Ω_2

for EGC, SDC and MRC schemes become almost flat when the average SNR/branch imbalance is less than 0.5 (i.e., $0.5 < \Omega_1 / \Omega_2 < 2$). Thus, we can conclude that the ASEP of dual-antenna diversity systems are not significantly affected by small differences in the mean branch SNRs. Consequently, the analysis of EGC or rather any dual-diversity systems in nonindependent and nonidentical Nakagami-m fading can be accurately approximated with their respective analysis under the assumption of equal branch SNR/symbol by replacing Ω_1 and Ω_2 with $(\Omega_1 + \Omega_2)/2$.

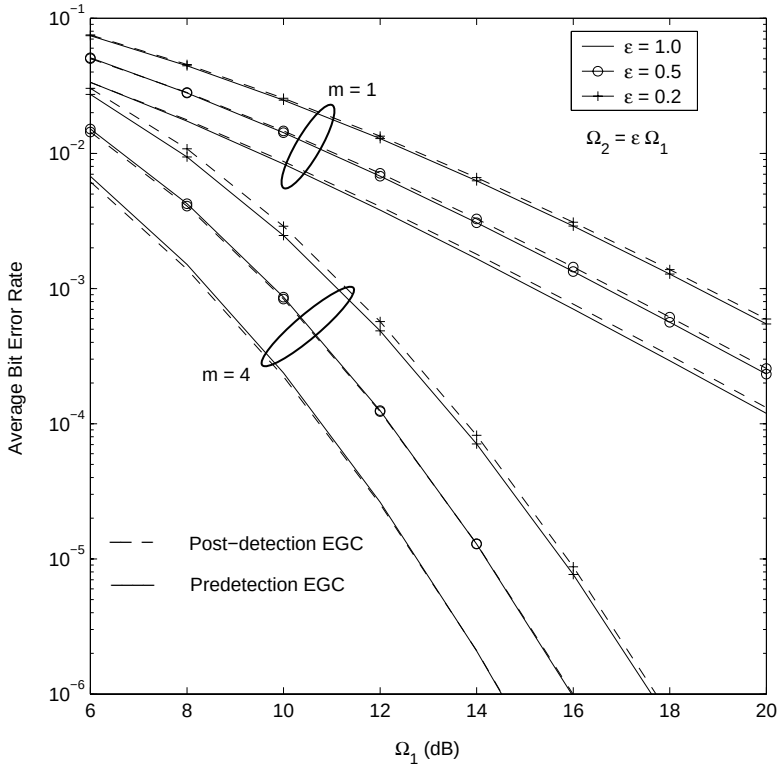

Figure 4.8 Average bit error probability performance of DQPSK with predetection (coherent) EGC and post-detection (noncoherent) EGC receiver structures in Nakagami-m fading and ρ = 0.4.

Finally, Figure 4.8 compares the average the average bit error rate probability performance of differentially detected QPSK (DQPSK) with both predetection (coherent) and post-detection (quadratic) EGC receiver in Nakagami-m fading with unbalanced inputs. We observe that dual-diversity coherent EGC and post-detection EGC perform almost identically if the mean branch SNR imbalance is less than 3 dB and for large *m* values. While the coherent EGC receiver yields slightly superior performance over the

quadratic EGC receiver when the difference between Ω_1 and Ω_2 gets larger (due to noncoherent combination loss in the quadratic receiver), it yields slightly inferior performance at higher average SNR/symbol and as *m* gets larger.

4.4 Chapter Summary

In this chapter, we have derived novel expressions for the PDF, CDF and the MGF of dual-diversity EGC output SNR in Nakagami-m fading with correlated signals, unbalanced inputs and arbitrary fading severity index. Aside from generalizing previous studies [41]-[43], the new framework facilitates efficient computation of higher order statistics of coherent EGC output SNR, outage probability (link reliability) and unified analysis of average bit or symbol error probability for a broad range of digital modulation schemes in bivariate Nakagami-m fading. Some new closed-form formulas for the EGC receiver performance are also derived for the special case of half-odd integer fading severity index. The generality and computational efficiency of the new results presented in this chapter render themselves as powerful means for both theoretical analysis and practical applications. A comprehensive comparative study of dual-antenna diversity EGC, SDC and MRC schemes that take into account of the effects of branch correlation, fade distribution and unequal average SNRs is also provided.

Two journal papers on the work presented in this chapter have been submitted to IEEE Transaction on Vehicular Technology [78] and Wireless Communications and Mobile Computing Journal [79].

Appendix A

In this appendix, we derive an infinite series and closed-form expressions for a definite integral of the form

$$I(\alpha,\beta,\mu,n)=\int_0^{\alpha}[x(\alpha-x)]^n\exp[-\mu(x-\beta)^2]dx \tag{A.1}$$

where real $n \geq 0$ and $\mu > 0$. This type of integral arises in the derivation of PDF of SNR at the output of a dual-diversity EGC receiver in correlated Rayleigh and Nakagami-m channels (see (4.4) and (C.1)) but a solution to this is not readily available in standard mathematical tables of integrals and series such as [47]. In the following, we will first consider the evaluation of (A.1) for the general case of real $n \geq 0$. Subsequently, two special cases will be treated.

Using variable substitution $t = x - \beta$, and after some algebraic manipulations, (A.1) can be rewritten as

$$\begin{aligned} I(\alpha,\beta,\mu,n) &= \int_{-\beta}^{\alpha-\beta}\left[(t+\beta)(\alpha-\beta-t)\right]^n\exp(-\mu t^2)dt \\ &= \left(\frac{\alpha}{2}\right)^{2n}\int_{-\beta}^{\alpha-\beta}\left[1-\left(\frac{4}{\alpha^2}\right)\left(t-\frac{\alpha-2\beta}{2}\right)^2\right]^n\exp(-\mu t^2)dt \end{aligned} \tag{A.2}$$

The transformation from the first line of (A.2) to the second line of (A.2) is important because we can expand the term of the form $(1-z)^n$ in the latter as a power series. The convergence of this series is guaranteed if $|z|<1$, which is satisfied in our case (will be proved shortly). Thus we have a converging series for (A.1), viz.,

$$I(\alpha,\beta,\mu,n)=\sum_{k=0}^{T_n}\frac{(-1)^k\Gamma(n+1)}{\Gamma(n-k+1)k!}\left(\frac{2}{\alpha}\right)^{2(k-n)}\int_{-\beta}^{\alpha-\beta}\left[\left(t-\frac{\alpha-2\beta}{2}\right)\right]^{2k}\exp(-\mu t^2)dt \tag{A.3}$$

where

$$T_n=\begin{cases} n & \text{if } n \text{ is non-negative integer} \\ \infty & \text{if } n \text{ is positive real} \end{cases} \tag{A.4}$$

It is evident that the infinite series (A.3) terminates and reduces to a finite series when n is a natural number. Notice also that $\left|\left(\frac{2}{\alpha}\right)\left(t-\frac{\alpha-2\beta}{2}\right)\right| \le 1$ over the interval $\{-\beta, \alpha-\beta\}$. Consequently we have proved that the series in (A.3) is absolutely convergent for arbitrary real $n \ge 0$.

Next, expanding $\left(t-\frac{\alpha-2\beta}{2}\right)^{2k}$ term in (A.3) using binomial series expansion, we obtain

$$I(\alpha,\beta,\mu,n)=\sum_{k=0}^{T_n}\frac{(-1)^k\alpha^{2(n-k)}\Gamma(n+1)}{2^{2n}k!\Gamma(n-k+1)}\sum_{i=0}^{2k}\binom{2k}{i}(-2)^i(\alpha-2\beta)^{2k-i}\int_{-\beta}^{\alpha-\beta}t^i\exp(-\mu t^2)dt \quad \text{(A.5)}$$

The integral in (A.5) can be evaluated in closed-form with the aid of [47] and by exploiting the property of even/odd functions,

$$\int_0^a t^w e^{-\mu t^2}dt=\begin{cases}\dfrac{\operatorname{sgn}(a)}{2\mu^{(w+1)/2}}\Upsilon\left(\dfrac{w+1}{2},\mu a^2\right) & \text{if } w \text{ is even}\\ \dfrac{1}{2\mu^{(w+1)/2}}\Upsilon\left(\dfrac{w+1}{2},\mu a^2\right) & \text{if } w \text{ is odd}\end{cases} \quad \text{(A.6)}$$

where sgn(.) denotes the sign of its argument and $\Upsilon(.,.)$ corresponds to the incomplete Gamma function [47]. Thus, (A.5) can be evaluated as

$$I(\alpha,\beta,\mu,n)=\sum_{k=0}^{T_n}\frac{(-1)^k\alpha^{2(n-k)}\Gamma(n+1)}{2^{2n+1}k!\Gamma(n-k+1)}\sum_{i=0}^{2k}\binom{2k}{i}\frac{(-2)^i(\alpha-2\beta)^{2k-i}}{\mu^{(i+1)/2}}$$
$$\times\left[c(i,(\alpha-\beta))\Upsilon\left(\frac{i+1}{2},\mu(\alpha-\beta)^2\right)-c(i,-\beta)\Upsilon\left(\frac{i+1}{2},\mu\beta^2\right)\right] \quad \text{(A.7)}$$

where T_n is defined in (A.4) and the coefficients $c(.,.)$ can be computed as

$$c(w,a)=\begin{cases}\operatorname{sgn}(a) & \text{if } w \text{ is even}\\ 1 & \text{if } w \text{ is odd}\end{cases} \quad \text{(A.8)}$$

(i) *Case Non-negative Integer n*

It should be noted that (A.7) reduces to a closed-form expression when n assumes a non-negative integer value since $T_n = n$ for this particular case. Next we will show that (A.1)

can also be evaluated in closed-form when $\alpha = 2\beta$ (without imposing any restriction on the choice of n).

(ii) *Case* $\alpha = 2\beta$

Letting $\alpha = 2\beta$ in the first line of (A.2), we obtain

$$I(2\beta,\beta,\mu,n) = \int_{-\beta}^{\beta} (\beta^2 - t^2)^n \exp(-\mu t^2) dt, \quad n \geq 0 \tag{A.9}$$

Observing that the integrand in (A.9) is an even function of the integration variable t, it is not difficult to show that (A.9) simplifies into (A.10) after variable substitution $y = t^2$ and making use of identity [47], viz.,

$$I(2\beta,\beta,\mu,n) = \text{sgn}(\beta) \frac{\sqrt{\pi}\Gamma(n+1)}{\Gamma(n+3/2)} \beta^{2n+1} {}_1F_1\left(1/2; n+3/2; -\mu\beta^2\right) \tag{A.10}$$

where ${}_1F_1(.;.;.)$ denotes the confluent hypergeometric function [47].

Appendix B

While computing the CDF and/or the MGF of the EGC output SNR in correlated Nakagami-m fading, we encounter the following generic integral:

$$J(\nu,\alpha,\beta,\mu,n,u)=\int_{o}^{u}\gamma^{-1/2}e^{-\nu\gamma}I\left(\alpha\sqrt{\gamma},\beta\sqrt{\gamma},\mu,n\right)d\gamma,\quad n\geq 0 \tag{B.1}$$

where $I(.,.,.,.)$ is defined in (A.1). Again, a solution to the above integral is not readily available in [47]. Making use of $\Upsilon(\alpha,x)=\frac{x^{\alpha}}{\alpha}e^{-x}{}_1F_1(1;1+\alpha;x)$ via Kummer transformation for the incomplete Gamma function in (A.1), (B.1) can be computed efficiently (circumventing the need to evaluate a double integral) as

$$\begin{aligned}J(\nu,\alpha,\beta,\mu,n,u)=&\sum_{k=0}^{T_n}\frac{(-1)^k\alpha^{2(n-k)}\Gamma(n+1)}{2^{2n+1}k!\Gamma(n-k+1)}\sum_{i=0}^{2k}\binom{2k}{i}(-2)^i\left(\alpha-2\beta\right)^{2k-i}\Gamma\left(\frac{i+1}{2}\right)\\&\times\sum_{p=0}^{\infty}\frac{\mu^p}{\Gamma((i+3)/2+p)}\left[\frac{c(i,(\alpha-\beta))[(\alpha-\beta)^2]^{(i+2p+1)/2}\Upsilon(p+n+1,u(\nu+\mu(\alpha-\beta)^2))}{[\nu+\mu(\alpha-\beta)^2]^{p+n+1}}\right.\\&\left.-\frac{c(i,-\beta)[\beta^2]^{(i+2p+1)/2}\Upsilon(p+n+1,u(\nu+\mu\beta^2))}{[\nu+\mu\beta^2]^{p+n+1}}\right]\end{aligned} \tag{B.2}$$

Note that, unlike [47], the infinite series for $\Upsilon(.,.)$ is not an alternating series. Therefore, the convergence of (B.2) is guaranteed. The above expression can be further simplified by considering the explicit cases when i takes even or odd values as

$$\begin{aligned}J(\nu,\alpha,\beta,\mu,n,u)=&\sum_{k=0}^{T_n}\frac{(-1)^k\alpha^{2(n-k)}\Gamma(n+1)}{2^{2n+1}k!\Gamma(n-k+1)}\sum_{i=0}^{2k}\binom{2k}{i}(-2)^i\left(\alpha-2\beta\right)^{2k-i}\Gamma\left(\frac{i+1}{2}\right)\\&\times\sum_{p=0}^{\infty}\frac{\mu^p}{\Gamma((i+3)/2+p)}\left[\frac{(\alpha-\beta)^{i+2p+1}\Upsilon(p+n+1,u(\nu+\mu(\alpha-\beta)^2))}{[\nu+\mu(\alpha-\beta)^2]^{p+n+1}}\right.\\&\left.+\frac{(-1)^i\beta^{i+2p+1}\Upsilon(p+n+1,u(\nu+\mu\beta^2))}{[\nu+\mu\beta^2]^{p+n+1}}\right]\end{aligned} \tag{B.3}$$

where T_n is defined in (A.4) and the coefficients $c(.,.)$ can be computed using (A.8).

Next we will show that (B.1) can be evaluated much more efficiently when $u=\infty$.

Substituting (A.7) in (B.1) and invoking the integral identity [47], we obtain

$$J(\nu,\alpha,\beta,\mu,n,\infty)=\sum_{k=0}^{T_n}\frac{(-1)^k\alpha^{2(n-k)}[\Gamma(n+1)]^2}{2^{2n}k!\Gamma(n-k+1)}\sum_{i=0}^{2k}\binom{2k}{i}\frac{(-2)^i\left(\alpha-2\beta\right)^{2k-i}}{(i+1)}$$

$$\times\left[\frac{(\alpha-\beta)^{(i+1)}}{[\nu+(\alpha-\beta)^2\mu]^{n+1}}\,{}_2F_1\left(1,n+1;\frac{i+3}{2};\frac{(\alpha-\beta)^2\mu}{\nu+(\alpha-\beta)^2\mu}\right)\right.$$

$$\left.+\frac{(-1)^i\beta^{(i+1)}}{(\nu+\beta^2\mu)^{n+1}}\,{}_2F_1\left(1,n+1;\frac{i+3}{2};\frac{\beta^2\mu}{\nu+\beta^2\mu}\right)\right] \tag{B.4}$$

where ${}_2F_1(.,.;.;.)$ denotes the Gaussian hypergeometric function [47]. It is apparent that we have a closed-form formula for $J(.,.,.,.,n,\infty)$ if n is a non-negative integer. Thus, the MGF of γ_{egc} can be evaluated in terms of a single finite range integral (if m is a positive integer) or in closed-from (if m is a half-odd integer) for specific cases.

Appendix C

In this appendix, we present alternative results for the statistics of γ_{egc} in terms of an infinite series expression (rather than an integral formula). Exploiting the power series representation for $I_v(.)$ function [47], (4.3) can be expressed as

$$p_X(x) = \frac{4\sqrt{2}m^{2m}}{\Gamma(m)(\Omega_1\Omega_2)^m(1-\rho)^m}\sum_{k=0}^{\infty}\frac{(\rho\xi^2)^k}{k!\Gamma(m+k)}\exp\left(-\frac{2\xi\sqrt{\Omega_1\Omega_2}}{\Omega_1+\Omega_2}x^2\right)$$

$$\times\int_0^{x\sqrt{2}}[x_1(x\sqrt{2}-x_1)]^{2m+2k-1}\exp\left[-\mu\left(x_1-r_1x\right)^2\right]dx_1,\quad m\geq ½ \tag{C.1}$$

where $\xi = \frac{m}{(1-\rho)\sqrt{\Omega_1\Omega_2}}$, $r_i = \frac{\sqrt{2}\Omega_i}{\Omega_1+\Omega_2}$ and $\mu = \frac{\xi(\Omega_1+\Omega_2)}{\sqrt{\Omega_1\Omega_2}}$. Similar to our development of (4.5), it is straightforward to show that the PDF of γ_{egc} is given by

$$p_{\gamma_{egc}}(\gamma) = \frac{2\sqrt{2}m^{2m}\gamma^{-1/2}}{\Gamma(m)(\Omega_1\Omega_2)^m(1-\rho)^m}\exp\left(-\frac{2\xi\sqrt{\Omega_1\Omega_2}}{\Omega_1+\Omega_2}\gamma\right)\sum_{k=0}^{\infty}\frac{(\rho\xi^2)^k}{k!\Gamma(m+k)}$$

$$\times I\left(\sqrt{2\gamma},\frac{\Omega_1}{\Omega_1+\Omega_2}\sqrt{2\gamma},\frac{\xi(\Omega_1+\Omega_2)}{\sqrt{\Omega_1\Omega_2}},2m+2k-1\right),\quad m\geq ½ \tag{C.2}$$

where $I(.,.,.,.)$ is given by (A.7). Unlike (4.5), (C.2) also holds for the limiting case of m = 0.5. Infinite series solutions for the CDF and MGF of γ_{egc} may be obtained using (B.3) and (B.4) and respectively. These results are summarized below for completeness:

$$F_{\gamma_{egc}}(\gamma^*) = \frac{2\sqrt{2}m^{2m}}{\Gamma(m)(\Omega_1\Omega_2)^m(1-\rho)^m}\sum_{k=0}^{\infty}\frac{(\rho\xi^2)^k}{k!\Gamma(m+k)}$$

$$\times J\left(\frac{2\xi\sqrt{\Omega_1\Omega_2}}{\Omega_1+\Omega_2},\sqrt{2},\frac{\sqrt{2}\Omega_1}{\Omega_1+\Omega_2},\frac{\xi(\Omega_1+\Omega_2)}{\sqrt{\Omega_1\Omega_2}},2m+2k-1,\gamma^*\right) \tag{C.3}$$

$$\phi_{\gamma_{egc}}(s) = \frac{2\sqrt{2}m^{2m}}{\Gamma(m)(\Omega_1\Omega_2)^m(1-\rho)^m}\sum_{k=0}^{\infty}\frac{(\rho\xi^2)^k}{k!\Gamma(m+k)}$$

$$\times J\left(s+\frac{2\xi\sqrt{\Omega_1\Omega_2}}{\Omega_1+\Omega_2},\sqrt{2},\frac{\sqrt{2}\Omega_1}{\Omega_1+\Omega_2},\frac{\xi(\Omega_1+\Omega_2)}{\sqrt{\Omega_1\Omega_2}},2m+2k-1,\infty \right) \qquad \text{(C.4)}$$

where $J(.,.,.,.,.,.,.)$ is defined as in Appendix B. Note that, in general, the terms of the series in (C.2)-(C.4) decrease faster with increasing summation index k for small ρ because the term ρ^k decreases rapidly. For example, the infinite series can be truncated to only the first 10 terms when $\rho = 0.3$ and $m = 2$ to achieve a good accuracy. However, when $\rho \to 1$ and/or m is large, the convergence rate is much slower. In this case, we found that (4.6), (4.9) and (4.10) (i.e., finite-range integral expressions) are much more robust than (C.2)-(C.4) since the latter is more susceptible to truncation and floating point precision errors.

Appendix D

In this appendix, we derive closed-form formulas for the PDF and MGF of γ_{egc} when m assumes a half-odd integer value. Exploiting the finite polynomial representation for $I_v(.)$ function when its order v is a half-odd integer [47], (4.3) may be restated as

$$p_X(x) = \frac{2\sqrt{2}\xi^{m+1/2}(1-\rho)^m}{\sqrt{\pi}\Gamma(m)\rho^{(2m-1)/4}} \sum_{\ell=1}^{2} e^{-\nu_\ell x^2} \sum_{k=0}^{\Lambda} U_k \eta_{\ell,k}$$

$$\times \int_0^{x\sqrt{2}} [x_1(x\sqrt{2}-x_1)]^{m-k-1/2} \exp\left(-\mu_\ell (x_1 - r_\ell x)^2\right) dx_1, \quad m \in \left\{\frac{1}{2}, \frac{3}{2}, \frac{5}{2}, \ldots\right\} \tag{D.1}$$

where the different parameters used in (D.1) are defined below:

$$\mu_\ell = \xi(\Omega_1 + \Omega_2 + (-1)^\ell 2\sqrt{\rho\Omega_1\Omega_2}) / \sqrt{\Omega_1\Omega_2} \tag{D.1a}$$

$$r_\ell = \sqrt{2}(\Omega_1 + (-1)^\ell \sqrt{\rho\Omega_1\Omega_2}) / (\mu_\ell \sqrt{\Omega_1\Omega_2}) \tag{D.1b}$$

$$\nu_\ell = 2\xi(1-\rho) / \mu_\ell \tag{D.1c}$$

$$\Lambda = \begin{cases} m - 3/2 & \text{if } m \neq 1/2 \\ 0 & \text{if } m = 1/2 \end{cases} \tag{D.1d}$$

$$U_k = \frac{(\Lambda + k)!(\xi\sqrt{\rho})^{-k}}{k!(\Lambda - k)!2^{2k}} \tag{D.1e}$$

$$\eta_{\ell,k} = \begin{cases} (-1)^k & \text{if } \ell = 1 \\ (-1)^{\Lambda+1} & \text{if } \ell = 2,\ m \neq 1/2 \\ 1 & \text{if } \ell = 2,\ m = 1/2 \end{cases} \tag{D.1f}$$

Now it is apparent that the PDF of γ_{egc} can be evaluated in closed-form using (A.7), viz.,

$$p_{\gamma_{egc}}(\gamma) = \frac{\sqrt{2}\xi^{m+1/2}(1-\rho)^m \gamma^{-1/2}}{\sqrt{\pi}\Gamma(m)\rho^{(2m-1)/4}} \sum_{\ell=1}^{2} e^{-\nu_\ell \gamma} \sum_{k=0}^{\Lambda} U_k \eta_{\ell,k}$$

$$\times I\left(\sqrt{2\gamma}, r_\ell\sqrt{\gamma}, \mu_\ell, m-k-1/2\right), \quad m \in \{0.5, 1.5, 2.5, \ldots\} \tag{D.2}$$

where $I(.,.,.,.)$ is defined in (A.7). In other words, we can simplify (4.6) and (C.2) into a

finite series for the special case of m is a multiple of 0.5. It is also straightforward to obtain the CDF and MGF of γ_{egc} using (D.2) along with (B.3) and (B.4) respectively. These results are summarized below:

$$F_{\gamma_{egc}}(\gamma^*) = \frac{\sqrt{2}\xi^{m+1/2}(1-\rho)^m}{\sqrt{\pi}\Gamma(m)\rho^{(2m-1)/4}} \sum_{\ell=1}^{2}\sum_{k=0}^{\Lambda} U_k \eta_{\ell,k} J\left(\nu_\ell, \sqrt{2}, r_\ell, \mu_\ell, m-k-1/2, \gamma^*\right) \tag{D.3}$$

$$\phi_{\gamma_{egc}}(s) = \frac{\sqrt{2}\xi^{m+1/2}(1-\rho)^m}{\sqrt{\pi}\Gamma(m)\rho^{(2m-1)/4}} \sum_{\ell=1}^{2}\sum_{k=0}^{\Lambda} U_k \eta_{\ell,k} J\left(s+\nu_\ell, \sqrt{2}, r_\ell, \mu_\ell, m-k-1/2, \infty\right) \tag{D.4}$$

Once again, our numerical experiments reveal that (D.3) and (D.4) yield a considerable computational speed advantage over (4.9) (or (C.3)) and (4.10) (or (C.4)), respectively.

Chapter 5

Some Integrals Involving Generalized Marcum Q-Function with Application to Error Probability Analysis of Diversity Receivers

5.1 Introduction

The Nakagami-m distribution is a widely accepted statistical model due to both its good fit with experimental results and its versatility [49]. Given this, the theoretical performance of communications systems in Nakagami-m fading is valuable. Particularly important are exact closed-form error probability expressions because such expressions facilitate the rapid calculation of error rates, and thereby assist design parameter optimization. In [50], the authors have derived closed-form solutions to three generic trigonometric integrals and subsequently utilize them to derive the exact closed-form ABER expressions for a broad range of coherent, differentially coherent and noncoherent digital modulation schemes in conjunction with MRC and SDC diversity receivers. However, these integrals do not facilitate the multichannel quadratic receiver analysis over Rayleigh and Nakagami-m channels or SDC with correlated diversity paths. Motivated by this need, in this chapter we derive closed-form formulas for the following two integrals which are known to arise in the ABER analysis of noncoherent digital modulation schemes with post-detection EGC and dual-branch selection diversity in correlated Nakagami-m channels:

$$I_{a,b}(p,k,m) = \int_0^\infty x^{k-1} \exp(-px) Q_m(a\sqrt{x}, b\sqrt{x}) dx \tag{5.1}$$

$$J_{a,b}(p,k,m) = \int_0^\infty x^{k-1} \exp(-px)[Q_m(a\sqrt{x}, b\sqrt{x}) - Q_m(b\sqrt{x}, a\sqrt{x})]dx, \qquad b > a \tag{5.2}$$

where Re $\{p\} > 0$, and m and k are positive integers. Previous results have been limited to cases for which $k = m$ [51] and $k = 1$ [52]. Our solution for the above integrals holds regardless of $k > m$, $k = m$ and $k < m$.

In [51], Okui obtained a concise closed-form expression for $I_{a,b}(p, m, m)$ as

$$I_{a,b}(p,m,m) = \frac{\Gamma(m)}{p^m} - \frac{(2b)^{2m}\Gamma(2m)}{\Gamma(m+1)[Y(X+Y)]^m} {}_2F_1[1-m, m; 1+m, (1-X/Y)/2], \qquad p > 0, m > 0 \tag{5.3}$$

by first expressing the generalized Marcum Q-function in terms of the generalized confluent hypergeometric function [53], viz.,

$$Q_m(a\sqrt{x}, b\sqrt{x}) = 1 - \frac{(b^2 x/2)^m}{\Gamma(m+1)} \Psi_2(m; m, m+1; -a^2 x/2, -b^2 x/2) \tag{5.4}$$

and then utilizing [53] and [54] to get (5.3). In (5.3), X and Y are defined as $X = 2p + a^2 - b^2$, $Y = [(2p + (a+b)^2)(2p + (a-b)^2)]^{1/2}$ respectively and ${}_2F_1(.,.;.;.)$ denotes the Gauss hypergeometric function. Mimicking his approach, it is possible to get a more general result for $I_{a,b}(p, k, m)$ and $J_{a,b}(p, k, m)$. These results are summarized below:

$$I_{a,b}(p,k,m) = \frac{\Gamma(k)}{p^k} - \frac{b^{2m}\Gamma(k+m)}{2^m p^{k+m}\Gamma(m+1)} F_4\left(k+m, m; m+1, m; -\frac{b^2}{2p}, -\frac{a^2}{2p}\right) \tag{5.5}$$

$$J_{a,b}(p,k,m) = \frac{\Gamma(k+m)}{2^m p^{k+m}\Gamma(m+1)}\left[a^{2m} F_4\left(k+m, m; m+1, m; -\frac{a^2}{2p}, -\frac{b^2}{2p}\right)\right.$$

$$\left. - b^{2m} F_4\left(k+m, m; m+1, m; -\frac{b^2}{2p}, -\frac{a^2}{2p}\right)\right] \tag{5.6}$$

where $F_4(.,.;.,.;.,.)$ is defined as [54]

$$F_4(\alpha, \beta; \gamma, \gamma'; x, y) = \sum_{v=0}^{\infty}\sum_{w=0}^{\infty} \frac{(\alpha)_{v+w}(\beta)_{v+w}}{(\gamma)_v(\gamma')_w v! w!} x^v y^w \tag{5.7}$$

It should be emphasized that both (5.5) and (5.6) hold even for positive real m and k values. Nevertheless, the above solution involves the computation complexity of a double infinite series. On the contrary, in this chapter, we will express (5.1) and (5.2) in terms of a finite series of algebraic functions while m and k are positive integers.

The rest of the chapter is organized as follows. In Section 5.2, we derive closed-form solutions for the integrals in (5.1) and (5.2). Alternate closed-form solutions for (5.1) and (5.2) are also presented in the Appendix. Section 5.3 deals with the application of $I_{a,b}(.,.,.)$ and $J_{a,b}(.,.,.)$ to derive error-rate expressions for many digital modulation schemes employing SDC and post-detection EGC in correlated Rayleigh and Nakagami-m fading channels. Finally, the main contributions of the chapter are provided in Section 5.4.

5.2 Closed-Form Solutions for $I_{a,b}(p, k, m)$ and $J_{a,b}(p, k, m)$

From [55], we know that the trigonometric integral representation for the generalized Marcum Q-function $Q_m(\alpha, \beta)$ varies according to $\alpha < \beta$, $\alpha = \beta$, or $\alpha > \beta$ as

$$Q_m(\alpha,\beta)=\begin{cases} H_m(\alpha,\beta) & if \quad \alpha<\beta \\ 1/2+H_m(\alpha,\beta) & if \quad \alpha=\beta \\ 1+H_m(\alpha,\beta) & if \quad \alpha>\beta \end{cases} \tag{5.8}$$

where integer $m > 0$ and the finite-range integral $H_m(\alpha, \beta)$ is defined by [55]

$$H_m(\alpha,\beta)=\left(\frac{\beta}{\alpha}\right)^m \exp\left[\frac{-(\beta-\alpha)^2}{2}\right]\frac{\alpha}{2\pi}\int_0^{2\pi}\exp\left[-\alpha\beta(1-\cos\theta)\right]\frac{\beta\cos(m-1)\theta-\alpha\cos m\theta}{\alpha^2+\beta^2-2\alpha\beta\cos\theta}d\theta \tag{5.9}$$

It is apparent that the above representation assumes an indeterminate form when $\alpha = 0$ and $m \neq 1$. Taking the limit $\alpha \to 0$ in the canonical integral representation for $Q_m(\alpha, \beta)$ and recognizing that $\lim_{\alpha\to 0}\frac{I_{m-1}(\alpha x)}{\alpha^{m-1}}=\frac{(x/2)^{m-1}}{\Gamma(m)}$, we obtain

$$Q_m(0,\beta)=\lim_{\alpha\to 0}\int_\beta^\infty x\left(\frac{x}{\alpha}\right)^{m-1}\exp\left[-(\alpha^2+\beta^2)/2\right]I_{m-1}(\alpha x)dx=\frac{\Gamma(m,\beta^2/2)}{\Gamma(m)} \tag{5.10}$$

where $\Gamma(.,.)$ denotes the complementary incomplete Gamma function and $I_v(z)$ is the modified Bessel function of the first kind. Hence the limit $\alpha \to 0$ in (5.9) converges smoothly to the exact value (5.10). As such, (5.8) and (5.9) are still useful for numerical computation if we let $\alpha = 10^{-4}$ in (5.9).

Substituting (5.10) into (5.1), using identity [54] and applying Kummer's transformation, we get

$$I_{0,b}(p,k,m)=\frac{2^k\Gamma(m+k)}{b^{2k}k\Gamma(m)}\,{}_2F_1\left(k+m,k;k+1;-\frac{2p}{b^2}\right) \tag{5.11}$$

Similarly, it can be shown that

$$J_{0,b}(p,k,m)=-\frac{b^{2m}\Gamma(m+k)}{2^m p^{k+m}\Gamma(m+1)}\,{}_2F_1\left(k+m,m;m+1;-\frac{b^2}{2p}\right) \tag{5.12}$$

The above expressions can also be derived directly from (5.5) and (5.6) by setting $a = 0$ and then simplifying the resulting expressions using [54]. Moreover, for integer values of m and k, (5.11) and (5.12) reduce to a finite series (after applying Kummer's transformation [54]), viz.,

$$I_{0,b}(p,k,m)=\frac{2^k b^{2m-2}\Gamma(k)}{(2p+b^2)^{k+m-1}}\sum_{i=0}^{m-1}\binom{m+k-1}{k+i}\left(\frac{2p}{b^2}\right)^i \tag{5.13}$$

$$J_{0,b}(p,k,m)=\left[\frac{2^k b^{2m-2}\Gamma(k)}{(2p+b^2)^{k+m-1}}\sum_{i=0}^{m-1}\binom{m+k-1}{k+i}\left(\frac{2p}{b^2}\right)^i\right]-\frac{\Gamma(k)}{p^k} \tag{5.14}$$

In the following, we will present closed-form formulas for $I_{a,b}(p, k, m)$ for the case $a \neq 0$. From (5.8), it is apparent that we need to consider three explicit cases which depend on the ratio b/a.

5.2.1 Case $0^+ < a < b$

Using (5.8) and (5.9), the integral $I_{a,b}(p, k, m)$ in (5.1) can be rewritten as (interchanging the order of integration is valid because both the integrals are convergent)

$$I_{a,b}(p,k,m)=\left(\frac{b}{a}\right)^m\frac{a}{2\pi}\int_0^{2\pi}\frac{b\cos(m-1)\theta-a\cos m\theta}{a^2+b^2-2ab\cos\theta}d\theta\times\int_0^{\infty}x^{k-1}\exp\left[-x\left\{\frac{2p+a^2+b^2-2ab\cos\theta}{2}\right\}\right]dx \tag{5.15}$$

Since the integration with respect to the random variable x can be carried out using the identity [54], (5.15) reduces to

$$I_{a,b}(p,k,m)=\frac{\Gamma(k)}{4\pi a^{k+m}b^{k+1-m}}\int_0^{2\pi}\frac{b\cos(m-1)\theta-a\cos m\theta}{(v_1-\cos\theta)(v_2-\cos\theta)^k}d\theta \tag{5.16}$$

where $v_1=\dfrac{a^2+b^2}{2ab}$, and $v_2=\dfrac{2p+a^2+b^2}{2ab}$. For our subsequent developments, it is advantageous to expand the integrand in (5.16) using partial fractions, viz.,

$$\frac{1}{(v_1-\cos\theta)(v_2-\cos\theta)^k}=\mu^k\left\{\frac{1}{(v_1-\cos\theta)}-\sum_{n=1}^{k}\frac{\mu^{1-n}}{(v_2-\cos\theta)^n}\right\} \tag{5.17}$$

where $\mu=1/(v_2-v_1)=ab/p$. Expanding (5.16) using (5.17), we obtain

$$I_{a,b}(p,k,m)=\frac{b^{m-1}\Gamma(k)}{4\pi a^m p^k}\left[\left\{\int_0^{2\pi}\frac{b\cos(m-1)\theta}{(v_1-\cos\theta)}d\theta-\int_0^{2\pi}\frac{a\cos m\theta}{(v_1-\cos\theta)}d\theta\right\}\right.$$
$$\left.-\sum_{n=1}^{k}\mu^{1-n}\left\{\int_0^{2\pi}\frac{b\cos(m-1)\theta}{(v_2-\cos\theta)^n}d\theta-\int_0^{2\pi}\frac{a\cos m\theta}{(v_2-\cos\theta)^n}d\theta\right\}\right] \tag{5.18}$$

Each of the integrals in (5.18) can be associated with the Gauss hypergeometric function using the relationship [54]:

$$\int_0^{2\pi}\frac{\cos m\theta}{(\alpha-\cos\theta)^\nu}d\theta=\frac{2^{\nu+1}\pi\Gamma(m+\nu)(\alpha-\sqrt{\alpha^2-1})^{\nu+m}}{\Gamma(m+1)\Gamma(\nu)}{}_2F_1[\nu,m+\nu;m+1;(\alpha-\sqrt{\alpha^2-1})^2],\quad \alpha>1,\mathrm{Re}\{\nu\}>0 \tag{5.19}$$

given that m is a positive integer. Furthermore, (5.19) reduces to a finite series if ν also assumes a positive integer value, viz.,

$$\int_0^{2\pi} \frac{\cos m\theta}{(\alpha - \cos\theta)^{\nu}} d\theta = \frac{2^{p+1}\,\pi\,\xi^{3\nu+m-2}}{(1-\xi^2)^{2\nu-1}} \sum_{c=0}^{\nu-1} \binom{\nu+m-1}{c} \binom{2\nu-2-c}{\nu-1} \left(\frac{1-\xi^2}{\xi^2}\right)^c \tag{5.20}$$

where $\xi = \alpha - \sqrt{\alpha^2 - 1}$. Next, substituting (5.20) into (5.18) and after considerable simplifications we obtain a closed-form solution for $I_{a,b}(p, k, m)$:

$$I_{a,b}(p,k,m) = \frac{\Gamma(k)\kappa^{m-1}}{p^k} \left[\frac{\xi_1^{\,m}(\kappa - \xi_1)}{1-\xi_1^{\,2}} - \sum_{n=1}^{k} \left(\frac{2}{\mu}\right)^{n-1} \frac{\xi_2^{\,3n+m-3}}{(1-\xi_2^{\,2})^{2n-1}} \sum_{c=0}^{n-1} \binom{2n-c-2}{n-1} \left(\frac{1-\xi_2^{\,2}}{\xi_2^{\,2}}\right)^c \right.$$
$$\left. \times \left\{ \kappa \binom{n+m-2}{c} - \xi_2 \binom{n+m-1}{c} \right\} \right] \tag{5.21}$$

where $\kappa = b/a$, $\mu = ab/p$, $\xi_1 = \nu_1 - \sqrt{\nu_1^{\,2} - 1}$, $\xi_2 = \nu_2 - \sqrt{\nu_2^{\,2} - 1}$, and the coefficients $\{\nu_1, \nu_2\}$ are defined similar to (5.16).

5.2.2 Case *a* = *b*

Using (5.8), (5.9), [54] and (5.18), the integral $I_{a,b}(p, k, m)$ can be expressed as,

$$I_{a,b}(p,k,m) = \frac{\Gamma(k)}{2p^k} + \frac{\Gamma(k)}{4\pi p^k} \left[\int_0^{2\pi} \frac{\cos(m-1)\theta - \cos m\theta}{(1-\cos\theta)} d\theta \right.$$
$$\left. - \sum_{n=1}^{k} \mu^{1-n} \left\{ \int_0^{2\pi} \frac{\cos(m-1)\theta}{(\nu_2 - \cos\theta)^n} d\theta - \int_0^{2\pi} \frac{\cos m\theta}{(\nu_2 - \cos\theta)^n} d\theta \right\} \right] \tag{5.22}$$

The first integral term in (5.22) can be simplified as

$$\int_0^{2\pi} \frac{\cos(m-1)\theta - \cos m\theta}{(1-\cos\theta)} d\theta = 2\int_0^{\pi} \frac{\sin(2m-1)\theta}{\sin\theta} d\theta = 2\pi \tag{5.23}$$

using the identity [54]. Using identities (5.20) and (5.23) in (5.22) and after standard algebraic manipulations, we get a closed-form formula for $I_{a,b}(p, k, m)$ as

$$I_{a,b}(p,k,m) = \frac{\Gamma(k)}{p^k} \left[\frac{3}{2} - \sum_{n=1}^{k} \left(\frac{2}{\mu}\right)^{n-1} \frac{\xi_2^{\,3n+m-3}}{(1-\xi_2^{\,2})^{2n-1}} \sum_{c=0}^{n-1} \binom{2n-c-2}{n-1} \left(\frac{1-\xi_2^{\,2}}{\xi_2^{\,2}}\right)^c \left\{ \binom{n+m-2}{c} - \xi_2 \binom{n+m-1}{c} \right\} \right] \tag{5.24}$$

where $\mu = ab/p$, $\xi_2 = \nu_2 - \sqrt{\nu_2^{\,2} - 1}$ and ν_2 is defined in (5.16). It may be noted that (5.21) assumes an indeterminate form when $a/b = 1$. However, the limit converges smoothly to the exact value (5.24).

5.2.3 Case *a* > *b*

Using (5.8), (5.9), [54] and (5.18), it is also not difficult to show that

$$I_{a,b}(p,k,m) = \frac{\Gamma(k)\kappa^{m-1}}{p^k}\left[\frac{1}{\kappa^{m-1}} + \frac{\xi_1^{\,m}(\kappa - \xi_1)}{1-\xi_1^{\,2}} - \sum_{n=1}^{k}\left(\frac{2}{\mu}\right)^{n-1}\frac{\xi_2^{\,3n+m-3}}{(1-\xi_2^{\,2})^{2n-1}}\sum_{c=0}^{n-1}\binom{2n-c-2}{n-1}\left(\frac{1-\xi_2^{\,2}}{\xi_2^{\,2}}\right)^c\right.$$

$$\left.\times\left\{\kappa\binom{n+m-2}{c} - \xi_2\binom{n+m-1}{c}\right\}\right] \tag{5.25}$$

where $\kappa = b/a$, $\mu = ab/p$, $\xi_1 = \nu_1 - \sqrt{\nu_1^{\,2} - 1}$, $\xi_2 = \nu_2 - \sqrt{\nu_2^{\,2} - 1}$, and the coefficients $\{\nu_1, \nu_2\}$ are defined similar to (5.16).

Next, we shall consider evaluation of the integral $J_{a,b}(.,.,.)$ defined in (5.2). Using the expressions for $I_{a,b}(.,.,.)$ in (5.21) and (5.25), a closed-form formula for $J_{a,b}(.,.,.)$ follows immediately:

$$J_{a,b}(p,k,m) = \frac{\Gamma(k)}{p^k}\left[\sum_{\substack{i=1\\ j\neq i}}^{2}\kappa_i^{\,m-1}\left\{\frac{\xi_i^{\,m}(\kappa_i - \xi_i)}{1-\xi_i^{\,2}} - \sum_{n=1}^{k}\left(\frac{2}{\mu}\right)^{n-1}\frac{\xi_j^{\,3n+m-3}}{(1-\xi_j^{\,2})^{2n-1}}\sum_{c=0}^{n-1}\binom{2n-c-2}{n-1}\left(\frac{1-\xi_j^{\,2}}{\xi_j^{\,2}}\right)^c\right.\right.$$

$$\left.\left.\times\left[\kappa_i\binom{n+m-2}{c} - \xi_j\binom{n+m-1}{c}\right]\right\} - 1\right] \tag{5.26}$$

where $\kappa_1 = b/a$, $\kappa_2 = a/b$, $\mu = ab/p$, $\xi_1 = \nu_1 - \sqrt{\nu_1^{\,2} - 1}$, $\xi_2 = \nu_2 - \sqrt{\nu_2^{\,2} - 1}$, and $\{\nu_1, \nu_2\}$ are defined in (5.16). The applications of (5.13), (5.14), (5.21), (5.24), (5.25) and (5.26) for the ABER analysis of diversity systems (including generalized selection combining receiver) over fading channels will be discussed in the following section.

5.3 Applications

The conditional bit error probability of a variety of differentially coherent and noncoherent digital modulation schemes in conjunction with a multichannel quadratic receiver is given by [56]

$$P_b(\gamma, N) = \frac{1}{2} + \frac{1}{2^{2N-1}} \sum_{\ell=1}^{N} \binom{2N-1}{N-\ell} [Q_\ell(a\sqrt{\gamma}, b\sqrt{\gamma}) - Q_\ell(b\sqrt{\gamma}, a\sqrt{\gamma})] \tag{5.27}$$

where N denotes the number of diversity paths combined, and the coefficients $\{a, b\}$ for four different modulation schemes are summarized in Table 5-1.

Table 5-1 Modulation related parameters for several differentially coherent and noncoherent digital communication systems with a multichannel quadratic receiver.

Modulation	***a***	***b***
Binary Orthogonal FSK	0	1
Binary DPSK	0	$\sqrt{2}$
DQPSK with Gray coding	$\sqrt{2-\sqrt{2}}$	$\sqrt{2+\sqrt{2}}$
Noncoherent detected binary correlated signals (correlation coefficient $0 < \lvert\rho\rvert < 1$)	$\sqrt{\frac{1-\sqrt{1-\lvert\rho\rvert^2}}{2}}$	$\sqrt{\frac{1+\sqrt{1-\lvert\rho\rvert^2}}{2}}$

5.3.1 Post-Detection EGC

5.3.1.1 *L*-th order Diversity in Rayleigh Fading Environment

The PDF of the L-th order post-detection EGC output SNR in a Rayleigh fading environment with correlated diversity branches is given by [50]

$$f_\gamma(\gamma) = \sum_{i=1}^{L} \frac{\pi_i}{\lambda_i} \exp(-\gamma/\lambda_i) \tag{5.28}$$

where $\gamma > 0$, $\pi_i = \prod_{j=1, j\neq i}^{L} \lambda_i/(\lambda_i - \lambda_j)$ and λ_i is the i-th eigenvalue of the matrix $R\Lambda$ where R is a diagonal matrix defined as $R = diag(\Omega_1, \Omega_2, \ldots, \Omega_L)$, Ω_i denotes the mean SNR of the i-th branch and Λ is a positive definite matrix of dimension L (determined by the branch covariance matrix). Thus, the ABER of different modulation schemes summarized in Table 5-1 may be computed in closed-form as

$$\overline{P_b} = \int_0^\infty P_b(\gamma, L) f_\gamma(\gamma) d\gamma = \frac{1}{2} + \frac{1}{2^{2L-1}} \sum_{\ell=1}^{L} \binom{2L-1}{L-\ell} \sum_{i=1}^{L} \frac{\pi_i}{\lambda_i} J_{a,b}(\lambda_i^{-1}, 1, \ell) \tag{5.29}$$

using (5.2), (5.14) or (5.26). The calculated ABER performance of DPSK using Eq. (29) and Table 1 matches exactly with the results in [57]. As an example, Figure 5.1 illustrates the effect of diversity order on the error probability performance of DQPSK in conjunction a post-detection EGC receiver in a correlated Rayleigh fading environment, branch covariance matrix is given in [57].

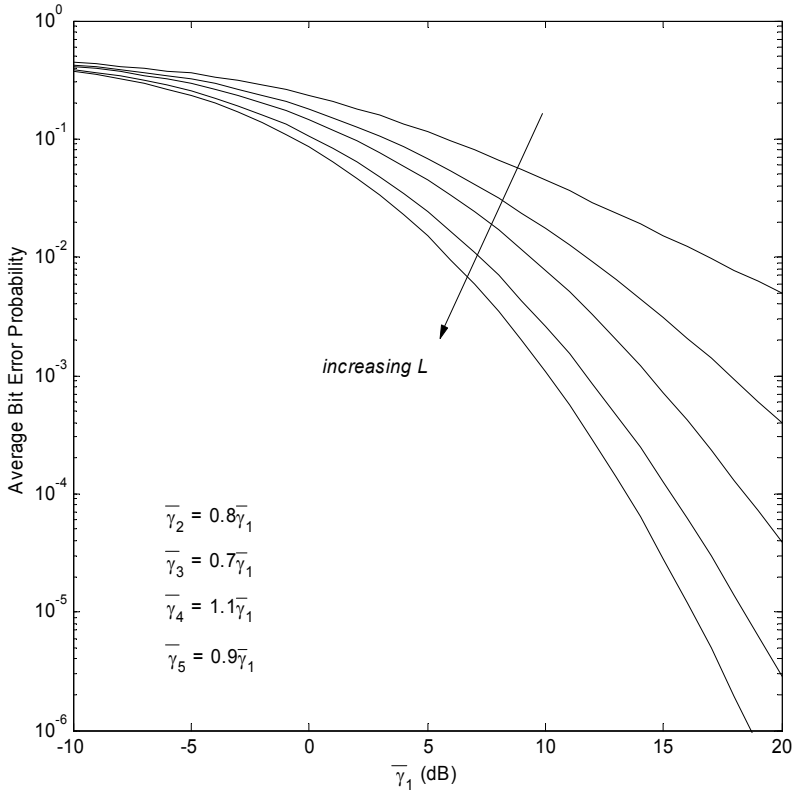

Figure 5.1: Error rates for DQPSK with Gray coding employing post-detection EGC diversity over a correlated Rayleigh channel with variation of diversity order $L \in \{1, 2, 3, 4, 5\}$.

5.3.1.2 *L*-th order Diversity in a Nakagami-m Channel

Since the PDF of post-detection EGC output SNR in a Nakagami-m fading with independent, identically distributed (i.i.d) diversity path follows a Gamma distribution; the ABER performance for this can be readily evaluated in closed-form for positive integer *mL* as

$$\overline{P_b} = \frac{1}{2} + \frac{1}{2^{2L-1}\Gamma(mL)}\left(\frac{m}{\Omega}\right)^{mL}\sum_{\ell=1}^{L}\binom{2L-1}{L-\ell}J_{a,b}\left(\frac{m}{\Omega}, mL, \ell\right) \tag{5.30}$$

where Ω denotes the average received SNR per branch, L is the diversity order, m is Nakagami-m fading severity index. As an example, Figure 5.2 illustrates the effect of fade distributions on the error probability performance of DQPSK in conjunction with 3rd and 6th order post-detection EGC in a Nakagami-m fading environment.

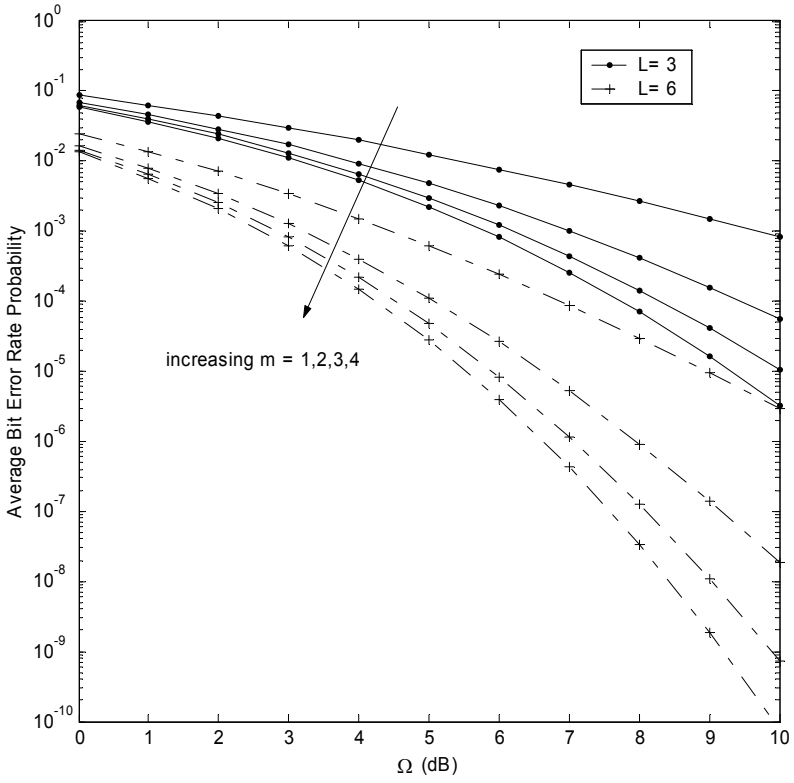

Figure 5.2: Error rates for DQPSK with Gray coding employing 3rd-and 6th-order post-detection EGC diversity over Nakagami-m channel.

It should be emphasized that previous ABER formulas obtained via the MGF approach have been restricted to a single finite-range integral expression or as a tight upper bound [58] for the ABER except for the special cases of binary DPSK and binary orthogonal signaling. Note that it is also possible to express $\overline{P_b}$ in closed-form when the diversity branches are correlated and/or with unequal mean signal strengths because the PDF of the

quadratic combiner output SNR can be expressed as weighted sum of Gamma PDFs. These results are omitted here for brevity.

5.3.2 Selection Diversity Combiner (SDC)

5.3.2.1 Dual-Diversity SDC over Rayleigh and Nakagami-m Channel with Correlated Diversity Branches

The CDF of dual-diversity SDC with correlated diversity branches in a Rayleigh fading environment is given by [59]

$$F_\gamma(\gamma) = 1 - \exp(-\gamma/\Omega_1)Q(a_2\sqrt{\gamma}, b_1\sqrt{\gamma}) - \exp(-\gamma/\Omega_2)[1 - Q(b_2\sqrt{\gamma}, a_1\sqrt{\gamma})] \quad (5.31)$$

where $a_i = \sqrt{\frac{2}{\Omega_i(1-\rho)}}$, $b_i = \sqrt{\frac{2\rho}{\Omega_i(1-\rho)}}$, Ω_i is average received SNR per branch $i \in \{1,2\}$ and ρ is correlation coefficient between the diversity branches ($\rho \neq 0,1$). The CDF expression in (5.31) can be used to obtain average bit error probability as (using integration by parts)

$$\overline{P_b} = \int_0^\infty P_b(\gamma) f_\gamma(\gamma) d\gamma = -\int_0^\infty F_\gamma(\gamma)\left[\frac{d}{d\gamma} P_b(\gamma)\right] d\gamma \quad (5.32)$$

To illustrate the use of (5.32) for deriving the ABER formulas in closed-form, let us consider the binary DPSK and NCFSK for which the conditional error probability can be expressed as $P_b(\gamma) = \tfrac{1}{2}e^{-q\gamma}$ (q = 1 for DPSK and q = ½ for NCFSK). Since $\frac{d}{d\gamma} P_b(\gamma) = -\frac{q}{2} e^{-q\gamma}$, the ABER for these modulation schemes in conjunction with dual-diversity SDC receiver over Rayleigh fading channels is given by

$$\overline{P_b} = \frac{q}{2}\left[\frac{1}{q(1+q\Omega_2)} + I_{b_2,a_1}(q+\Omega_2^{-1},1,1) - I_{a_2,b_1}(q+\Omega_1^{-1},1,1)\right] \quad (5.33)$$

where a_i, b_i , and Ω_i are defined in (30). Similarly recognizing that $\frac{d}{d\gamma} P_b(\gamma) = -\sqrt{\frac{c}{4\pi\gamma}} \exp(-c\gamma)$ for binary phase-shift keying (c = 1) and coherent binary frequency-shift keying (c = ½), one can immediately derive a closed-form ABER expression for the above modulation schemes as

$$\overline{P_b} = \sqrt{\frac{c}{4\pi}}\left[\frac{1}{c(1+c\Omega_2)} + I_{b_2,a_1}(c+\Omega_2^{-1},\tfrac{1}{2},1) - I_{a_2,b_1}(c+\Omega_1^{-1},\tfrac{1}{2},1)\right] \quad (5.34)$$

where a_i, b_i, and Ω_i are defined in (5.31). Eq. (5.34) is obtained with the aid of (5.1), (5.5) and (5.31). For the special case of identical mean signal strengths, (5.34) simplifies to

$$\overline{P_b} = \sqrt{\frac{c}{4\pi}}\left[\frac{1}{c(1+c\Omega_2)} + J_{b_1,a_1}(c+\Omega^{-1}, ½, 1)\right] \tag{5.35}$$

where $a_2 = a_1 = \sqrt{\frac{2}{\Omega(1-\rho)}}$, $b_2 = b_1 = \sqrt{\frac{2\rho}{\Omega(1-\rho)}}$ and $J_{a,b}(.,.,.)$ is defined in (5.6). To the best of the authors' knowledge, the closed-form ABER formulas presented in (5.34) and (5.35) are new. Although it does not appear possible to obtain closed-form ABER formula for higher order alphabets using the above approach, one may resort to the MGF approach to derive the desired ASER in terms of a single integral with finite integration limits. A closed-form expression for the MGF of the SDC output SNR in Nakagami-m channel with correlated diversity branches can be obtained by taking the Laplace transform of the PDF given in [61] and using (5.1):

$$\phi_\gamma(s) = \sum_{i=1, j\neq 1}^{2} \frac{1}{(1+s\Omega_j)^m} - \frac{1}{\Gamma(m)\Omega_j{}^m} I_{a_j,b_i}(s+\Omega_j^{-1}, m, m) \tag{5.36}$$

where a_i, b_i , Ω_i, and ρ are defined in (5.31) and m is the Nakagami-m fading severity index (positive integer). Using this MGF, ASER performance of a broad class of modulation formats can be immediately obtained. For example, the ASER performance of M-ary PSK is given by

$$\overline{P_s} = \frac{1}{\pi}\int_0^{\pi-\pi/M} \phi_\gamma\left(\frac{\sin^2(\pi/M)}{\sin^2\theta}\right) d\theta \tag{5.37}$$

where M denotes the alphabet size. Note that (5.37) is slightly more general and much more concise than [62].

5.3.2.2 L-th Order SDC in a Nakagami-m Channel

The ABER performance of noncoherent modulation schemes tabulated in Table 5-1 in conjunction with SDC over Nakagami-m channel with the i.i.d diversity branches may be readily computed in closed-form using the PDF given in [50] and (5.27) with $N = 1$ as

$$\overline{P_b} = \frac{1}{2}\left[1 + \frac{1}{\Gamma(m)}\sum_{c=0}^{L-1}(-1)^c \binom{L-1}{c} \sum_{z=0}^{c(m-1)} \beta(z,c,m)\left(\frac{m}{\Omega}\right)^{m+z} J_{a,b}\left(\frac{m(1+c)}{\Omega}, m+z, 1\right)\right] \tag{5.38}$$

where Ω is average received SNR per branch, L denotes the diversity order, and the fading severity index m assumes a positive integer value. The coefficients $\beta(.,.,.)$ in (5.38) may be computed recursively as

$$\beta(z,k,c) = \sum_{i=z-c+1}^{z} \frac{\beta(i,k-1,c)}{(z-i)!} U_{[0,(k-1)(c-1)]}(i) \tag{5.39}$$

where $U_{[\upsilon,\omega]}(i) = \begin{cases} 1 & \upsilon \le i \le \omega \\ 0 & otherwise \end{cases}$, $\beta(0, 0, c) = \beta(0, k, c) = 1$, $\beta(z, 1, c) = \frac{1}{z!}$ and $\beta(1, k, c) = k$.

5.3.3 Hybrid Generalized Selection Combining in Rayleigh Fading Channels

In a generalized selection diversity combining receiver, GSC(N, L), a subset of N paths with the highest SNR out of L available paths are combined. It is obvious that GSC(1, L) and GSC(L, L) are simply the classical SDC and post-detection EGC receiver, respectively.

5.3.3.1 GSC(N, L) with Identical Fading Statistics

Closed-form ABER formulas for a variety of noncoherent and differentially coherent modulation schemes that employ post-detection GSC(N, L) may be immediately obtained by using the PDF in [63] and (5.27) as

$$\overline{P_b} = \frac{1}{2} + \frac{1}{2^{2N-1}} \sum_{\ell=1}^{N} \binom{2N-1}{N-\ell} \left[\sum_{i=0}^{N-1} \frac{d_i}{\Omega^{i+1}\Gamma(i+1)} J_{a,b}(1/\Omega, i-1, \ell) + \sum_{j=1}^{L-N} g_j J_{a,b}\left(\frac{1+j/N}{\Omega}, 1, \ell \right) \right] \tag{5.40}$$

where Ω is average received SNR per branch, $\{a, b\}$ for the various modulation schemes are listed in Table 5-1 and the coefficients d_i and g_i in (5.40) are defined as

$$d_{N-1-i} = \binom{L}{N} \sum_{c=1}^{L-N} \binom{L-N}{c} \frac{(-1)^{i+c+1} N^i}{c^i} \tag{5.41}$$

$$g_j = \binom{L}{N} \binom{L-N}{j} \frac{(-1)^{N+j} N^{N-1}}{j^{N-1}} \tag{5.42}$$

5.3.3.2 GSC(N, L) with Non-identical Fading Statistics

The PDF of GSC(N, L) output SNR in a Rayleigh channel with nonidentical diversity branches can be obtained by taking the inverse Laplace transform of the corresponding MGF given in [63] as

$$f_\gamma(\gamma) = \frac{1}{N} \sum_{\sigma \in T_{L,N}} \left[\prod_{k=L-N+1}^{L} \Omega_{\sigma(k)}^{-1} \right] \left[\sum_{i=0}^{L-N} (-1)^i \sum_{\theta \in W_{L-N,i}} \sum_{j=L-N+1}^{L} C_j \exp(-\hbar_j x) \right] \tag{5.43}$$

where Ω_n denotes the average SNR of n-th diversity branch, $\sum_{\sigma \in T_{L,N}} = \sum_{\substack{\sigma \in S_L, \sigma(1)<\sigma(2)<\ldots<\sigma(L-N) \\ \sigma(L-N+2)<\ldots<\sigma(L)}}$,

S_n is the set of all permutations of integers $\{1,2,...,n\}$, $\sigma \in \mathrm{S_n}$ denotes the specific function $\sigma = \{\sigma(1),\sigma(2),...,\sigma(n)\}$ which permutes the integers $\{1,2,...,n\}$, $W_{n,i}$ is the set of all combinations of integers $\{1,2,...,n\}$ taken i at a time and the coefficients C_j in (5.43) are defined as

$$C_j = \prod_{n=L-N+1; n \neq j}^{L} (\Delta_n - \Delta_j)^{-1} \tag{5.44}$$

where $$\Delta_j = \begin{cases} \frac{1}{N} \left(\sum_{t \in \theta} \Omega_{\sigma(t)}^{-1} + \sum_{q=L-N+1}^{L} \Omega_{\sigma(q)}^{-1} \right) & \text{if } j = L-N+1 \\ \Omega_{\sigma(j)}^{-1} & \text{otherwise} \end{cases}$$

The constructions of $T_{L,N}$ and $W_{n,i}$ can be implemented within a few command lines in MATLAB. Using (5.43), (5.27), (5.14) or (5.26), we get the desired ABER in closed-form, viz.,

$$\overline{P_b} = \frac{1}{2} + \frac{1}{2^{2N-1} N} \sum_{\sigma \in T_{L,N}} \left[\prod_{k=L-N+1}^{L} \Omega_{\sigma(k)}^{-1} \right] \sum_{\ell=1}^{N} \binom{2N-1}{N-\ell} \sum_{i=0}^{L-N} (-1)^i \sum_{\theta \in W_{L-N,i}} \sum_{j=L-N+1}^{L} C_j J_{a,b}(\Delta_j, 1, \ell) \tag{5.45}$$

where the coefficients C_j and Δ_j are defined in (5.44). Figure 5.3 illustrates the ABER performance curves for DQPSK with a non-coherent GSC(N, 5) rake receiver in a Rayleigh environment with exponentially decaying multipath intensity profile (δ = 0.2). The average SNR of the n-th diversity path is $\overline{\gamma_n} = \Theta e^{-n\delta} \overline{\gamma_b}$ where $\overline{\gamma_b}$ denotes the average SNR/bit and the parameter Θ is chosen such that the constraint $\sum_{n=1}^{L} \overline{\gamma_n} = \overline{\gamma_b}$ is satisfied, solving for Θ yields $\overline{\gamma_n} = \frac{(1-e^{-\delta}) e^{-\delta(n-1)}}{1-e^{-L\delta}} \overline{\gamma_b}$. It is apparent from Figure 5.3 that GSC(4, 5) or even GSC(3, 5) has performance virtually identical to the post-detection EGC receiver.

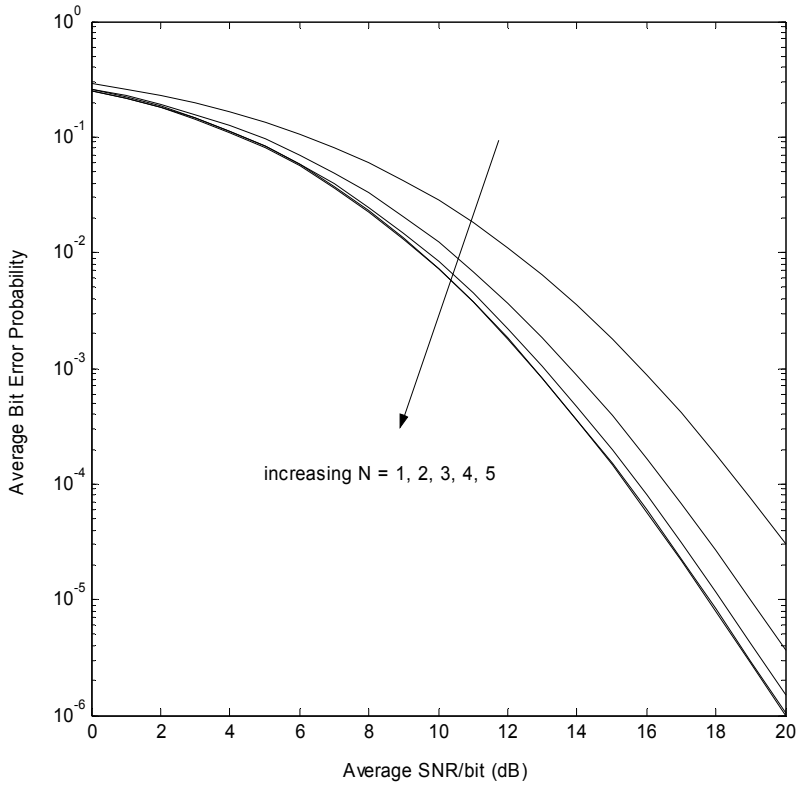

Figure 5.3: ABER performance of DQPSK in conjunction with a noncoherent GSC(*N*, 5) rake receiver in a Rayleigh channel with nonidentical fading statistics and $\delta = 0.2$.

5.4 Chapter Summary

In this chapter, we have derived closed-form formulas for two integrals involving the generalized Marcum Q-function. Many new closed-form ABER expressions have been derived including the cases such as coherent BPSK and BFSK in conjunction with dual-diversity SDC in correlated Rayleigh fading channels. Applications of the results for the performance evaluation of SDC, post-detection EGC and hybrid GSC(*N, L*) receivers in Rayleigh and Nakagami-m fading environment are also presented.

The work presented in this chapter is appearing in IEEE Transaction on Vehicular Technology, Oct'03 [80] and another journal paper based on the related work presented in the following Appendix has been submitted to IEEE Transaction on Wireless Communications [81].

Appendix

In this section, we will derive alternate closed-form solutions to (5.1) and (5.2) exploiting the contour integral representation for $Q_m(a\sqrt{x}, b\sqrt{x})$. From [60, pp.885], we know that the generalized Marcum Q-Function can be expressed in terms of a contour integral as

$$Q_m(\alpha,\beta) = \frac{1}{2\pi j}\oint_{\Gamma} \frac{e^{g(z)}}{z^m(1-z)}dz \tag{A.1}$$

where $g(z) = [\alpha^2(1/z-1)/2 + \beta^2(z-1)/2]$ and Γ is a circular contour of radius less than unity that encloses the origin. Unlike the trigonometric integral representations for $Q_m(a\sqrt{x}, b\sqrt{x})$ [39, Eq. (C-26)], this representation holds regardless of $\alpha < \beta$, $\alpha = \beta$, or $\alpha > \beta$ in $Q_m(\alpha, \beta)$. Substituting (A.1) into (4.1) and performing the integration with respect to x first (interchanging the order of integration is valid because both the integrals are convergent), we obtain

$$I_{a,b}(p,k,m) = \Gamma(k)\left(-\frac{2}{b^2}\right)^k \left[\frac{1}{2\pi j}\oint_{\Gamma} \frac{dz}{(1-z)z^{m-k}(z^2-\nu_0 z+\nu_1)^k}\right] \tag{A.2}$$

where $\nu_0 = (2p + a^2 + b^2)/b^2$ and $\nu_1 = (a/b)^2$. For the special case of $b = 0$, it can be shown that

$$I_{a,0}(p,k,m) = \frac{\Gamma(k)}{p^k} \tag{A.3}$$

If $b > 0$, then (A.2) can be rewritten as

$$I_{a,b}(p,k,m) = \Gamma(k)\left(-\frac{2}{b^2}\right)^k \left[\frac{1}{2\pi j}\oint_{\Gamma} \frac{1}{(1-z)z^{m-k}(z-r_1)^k(z-r_2)^k}dz\right] \tag{A.4}$$

where the denominator of the integrand has two positive roots $\begin{bmatrix} r_1 \\ r_2 \end{bmatrix} = \frac{1}{2}\left[\nu_0 \mp \sqrt{\nu_o^{\,2} - 4\nu_1}\right]$.

It can be easily shown that $0 \le r_1 < 1$ and $r_2 > 1$ for any value of the ratio $0 \le a/b < \infty$. To derive closed-form expressions for $I_{a,b}(p, k, m)$ depicted in (A.4) by applying residue theorem, we need to first consider two explicit cases of $a = 0$ and $a \neq 0$. Furthermore, when $a \neq 0$ we need to consider two special cases for which $k \ge m$ and $k < m$. Details are provided in the following subsections.

A. Case $a = 0$

When $a = 0$, the integrand in (A.4) has only one pole inside the unit circle ($z = 0$). By applying residue theorem to (A.4), we get

$$I_{0,b}(p,k,m) = \Gamma(k)\left(-\frac{2}{b^2}\right)^k \frac{1}{(m-1)!}\frac{d^{(m-1)}}{dz^{(m-1)}}\left\{\frac{1}{(1-z)(z-r_2)^k}\right\}\Bigg|_{z=0} \tag{A.5}$$

Using the Leibnitz's differentiation rule [59, Eq. (0.42)], and after standard algebraic manipulations, we obtain a closed-form formula for $I_{0,b}(p, k, m)$

$$I_{0,b}(p,k,m) = \Gamma(k)\left[\frac{2}{2p+b^2}\right]^k \sum_{n=0}^{m-1}\binom{k+n-1}{n}\left[\frac{b^2}{2p+b^2}\right]^n \tag{A.6}$$

B. Case $a \neq 0$

(i) Case $k \geq m$

When $k \geq m$, the denominator of the integrand in (A.4) has one positive root inside the unit circle and one outside the unit circle. In this case, applying the residue theorem, we get

$$I_{a,b}(p,k,m) = \Gamma(k)\left(-\frac{2}{b^2}\right)^k \frac{1}{(k-1)!}\frac{d^{(k-1)}}{dz^{(k-1)}}\left\{\frac{z^{k-m}}{(1-z)(z-r_2)^k}\right\}\Bigg|_{z=r_1} \tag{A.7}$$

Now invoking the Leibnitz's differentiation rule [59, Eq. (0.42)], and much after simplifications, we obtain a closed-form expression for $I_{a,b}(p, k, m)$

$$I_{a,b}(p,k,m) = \Gamma(k)\left[\frac{2}{b^2(1-r_1)(r_2-r_1)}\right]^k r_1^{k-m}\sum_{n=0}^{k-1}\binom{k-1+n}{n}\left(\frac{1-r_1}{r_2-r_1}\right)^n \sum_{\ell=0}^{U(n)}\binom{k-m}{\ell}\left(\frac{1-r_1}{r_1}\right)^\ell \tag{A.8}$$

where $\{r_1, r_2\}$ are defined similar to (A.4) and $U(n) = \begin{cases} k-m, & \text{if } m \geq n+1 \\ k-n-1, & \text{otherwise} \end{cases}$. As a check on the result, consider the case $k = m$. For this choice of parameters, (A.8) reduces to

$$I_{a,b}(p,m,m) = \Gamma(m)\left[\frac{2}{b^2(1-r_1)(r_2-r_1)}\right]^m \sum_{n=0}^{m-1}\binom{m-1+n}{n}\left(\frac{1-r_1}{r_2-r_1}\right)^n \tag{A.9}$$

We would like to point out that (A.9) is equivalent to [22, Eq. (6)] but slightly simpler than the latter.

(ii) Case $k < m$

If $k < m$, the denominator of the integrand in (A.4) has two roots inside the unit circle and one outside the unit circle. Therefore, applying the residue theorem, we get

$$I_{a,b}(p,k,m) = \Gamma(k)\left(-\frac{2}{b^2}\right)^k \left[\frac{1}{(k-1)!}\frac{d^{(k-1)}}{dz^{(k-1)}}\left\{\frac{1}{(1-z)z^{M-k}(z-r_2)^k}\right\}\Bigg|_{z=r_1} \right.$$

$$\left. + \frac{1}{(m-k-1)!}\frac{d^{(m-k-1)}}{dz^{(m-k-1)}}\left\{\frac{1}{(1-z)(z-r_1)^k(z-r_2)^k}\right\}\Bigg|_{z=0} \right] \tag{A.10}$$

Once again utilizing the Leibnitz's differentiation rule [59, Eq. (0.42)] in (A.10), and after much simplifications, we get a closed-form formula for $I_{a,b}(p, k, m)$, viz.,

$$I_{a,b}(p,k,m) = \Gamma(k)\left(\frac{2}{b^2}\right)^k \left[\left(\frac{-1}{r_1 r_2}\right)^k \sum_{c=0}^{m-k-1} \frac{1}{r_2^{\,c}} \sum_{\mu=0}^{c} \binom{k-1+\mu}{\mu}\binom{k-1+c-\mu}{c-\mu}\left(\frac{r_2}{r_1}\right)^{\mu} \right.$$

$$\left. + \frac{1}{r_1^{m-k}}\left(\frac{1}{(1-r_1)(r_2-r_1)}\right)^k \sum_{n=0}^{k-1}\binom{k-1+n}{n}\left(\frac{1-r_1}{r_2-r_1}\right)^n \sum_{\ell=0}^{k-1-n}\binom{m-k-1+\ell}{\ell}\left(\frac{r_1-1}{r_1}\right)^{\ell} \right] \tag{A.11}$$

where $\{r_1, r_2\}$ are defined in (A.4). It should be emphasized that (A.8) and (A.9) hold regardless of $a > b$, $a = b$ and $a < b$.

Using the expressions for $I_{a,b}(p, k, m)$ in (A.3), (A.6), (A.8) or (A.11), a closed-form formula for $J_{a,b}(p, k, m)$ can be immediately obtained for positive integer values of m and k as

$$J_{a,b}(p,k,m) = \begin{cases} I_{a,b}(p,k,m) - I_{a,b}(p,k,m) & \text{if } a > 0 \\ I_{0,b}(p,k,m) - \Gamma(k)/\,p^k & \text{if } a = 0 \end{cases} \tag{A.12}$$

where Re $\{p\} > 0$.

Chapter 6

Improving the Range of Ultra-wideband Transmission using Rake Receivers

6.1 Introduction

Although practical UWB systems have been in existence since 1960s, it is only becoming commercially available now owing to decreased costs and recent developments in chip development (i.e., CMOS technology scaling down from .25 to .13 micron), the evolution of the marketplace, and the Federal Communications Commission (FCC) recognition. In 1998, the FCC began the process of regulatory review and subsequently adopted a First Report and Order towards the commercialization of this technology for short-range communications on February 14, 2002 [65]. The range of a UWB communication system is primarily limited by the spectral mask (maximum power output of -41 dB/MHz from 3.1 GHz to 10.6 GHz) set by the FCC. The fine time resolution of multipaths induced by the channel for a UWB system (typically in the order of 100 – 300 picoseconds) can be exploited using a rake receiver to capture significant amount of energy found in the multipath components and to benefit from multipath diversity gain. However, the total number of detectable multipaths could be as large as one hundred [66] since the UWB signals occupy bandwidth greater than 500 MHz or has a fractional bandwidth greater than 0.2. Consequently, classical rake receiver designs such as MRC or SC are no longer appropriate, from the viewpoint of complexity and performance trade-off.

In this chapter, we examine the throughput-range trade-off UWB communication systems that employ two different receiver structures (see Figure 6.1) in multipath fading channels: (a) GSC(N, L) that combines a subset of N multipaths with the highest instantaneous SNR out of L resolvable multipaths in a similar fashion to MRC; and (b) partial MRC (hereafter, referred to as PMRC(N, L)) which combines N multipaths with the largest mean SNR. Clearly, PMRC is simpler to implement compared to GSC owing to the reduced selection circuitry complexity (i.e., the need to select N paths with the

largest instantaneous SNR in the latter). The motivation for performance analyses of the above two suboptimal receiver structures is based on the propagation measurements of UWB signals at Virginia Tech [67] which indicates that significant amount of energy are found in a few dominant multipaths particularly for the LOS case. For example, approximately 80% of the receiver energy could be captured by combining only 12 dominant multipaths. However, for the non-line-of-sight (NLOS) situation, approximately 75% of energy is captured by combining 30 dominant multipaths.

Previous related work in this subject is as follows: In [68], the performance comparisons between GSC and PMRC over Nakagami-m channels have been studied in the context of spread-spectrum signals, however, with only a few multipaths. In [69], the authors resorted to a semi-analytical approach for analyzing the ABER performance of GSC and PMRC at a fixed distance. In contrast, in this chapter, we examine the throughput-range performance of UWB for the two different reduced complexity receiver structures over generalized fading channels via exact and approximate ABER expressions (rather than a semi-analytical approach).

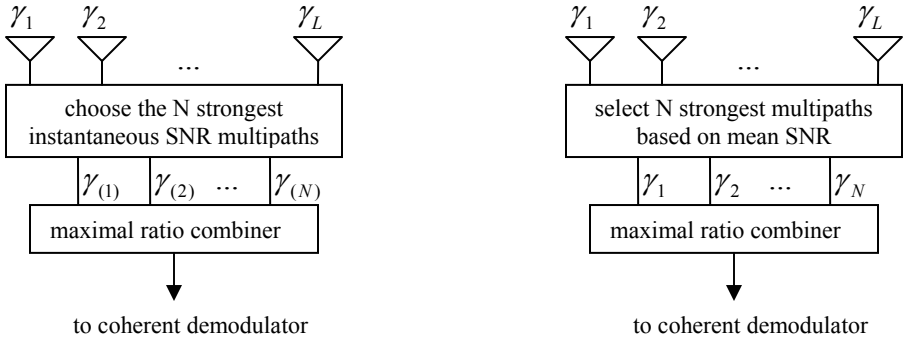

Figure 6.1 (a) GSC(N, L) receiver that adaptively combines N paths with strongest instantaneous SNRs. (b) PMRC(N, L) rake receiver that combines N paths with strongest mean SNRs.

The organization of the remaining of this chapter is as follows. In Section 6.2, we derive the throughput-range relationship over wireless channels with L statistically independent multipaths. In Section 6.3, we present exact and approximate formulae for predicting the

performance of GSC and PMRC with independent but non-identically distributed (i.n.d) multipaths and subsequently present a comparative study on the range extension realized using GSC and PMRC receivers. Section 6.4 investigates the effect of envelope correlations between multipaths on the performance of GSC and PMRC receivers. Section 6.5 presents some numerical results. Finally, in section 6.6 we summarize the major contributions of the chapter.

6.2 Throughput-Range Trade-off

In this section we will present analytical expressions for the throughput as a function of the distance for the GSC and PMRC receiver structures. For this purpose, we assume a pulse amplitude modulated (PAM) UWB system operating in a Rayleigh or a Nakagami-m fading environment.

The bit error probability for a coherent *M*-ary PAM system is given by

$$P_b = \frac{M-1}{M} erfc\left(\sqrt{\frac{3c\gamma}{M^2-1}}\right) \tag{6.1}$$

where M is the alphabet size and $c = \log_2 M$ denotes the number of information bits carried by each symbol. The instantaneous SNR/bit is $\gamma = (E_b / N_o)\alpha^2$ where E_b denotes received energy per bit, *No* is noise spectral density and α denotes random fading amplitude. The average SNR/bit at the receiver input can be computed as $\gamma = (P_r T_p / kN_o)$ where P_r is average received signal strength and T_p denotes the time between transmitted pulses. If we neglect the effect of shadowing, the received power at a distance *d* from the transmitter can be modeled as

$$P_r = \frac{P_t G_t G_r}{L_s}\left(\frac{\lambda}{4\pi d}\right)^n \tag{6.2}$$

where n denotes the path-loss exponent, L_s is the system loss factor not related to propagation ($L_s \geq 1$), λ is the carrier frequency used for computing distance loss and $\{G_t, G_r\}$ denotes the transmitter and receiver antenna gain respectively. Using above developments, it can be shown that the maximum achievable throughput, R_b, at distance d is given by

$$R_b = c/T_p = \frac{P_t G_t G_r}{N_o \gamma L_s}\left(\frac{\lambda}{4\pi d}\right)^n \tag{6.3}$$

The noise spectral density is $N_o = kTF$ where k is Boltzmann's constant, T is temperature and F denotes the noise figure. From (6.3) it is apparent that for fixed transmit power, throughput is a function of d^n. The average SNR/bit required to evaluate (6.3) for a given bit-error-rate performance can be found by averaging (6.1) over the PDF of GSC or PMRC output SNR in a realistic UWB environment. Details are provided in Section 6.3.

6.3 Suboptimal Rake Receivers

6.3.1 GSC in i.i.d and Mixed Fading Channels

6.3.1.1 Exact Analysis of GSC(N, L)

To analyze the ABER performance of M-ary PAM, it is desirable to rewrite (6.1) as

$$P_b = \frac{2(M-1)}{\pi k M}\int_0^{\pi/2} \exp\left(-\frac{3c/(M^2-1)}{\cos^2\theta}\gamma\right)d\theta \tag{6.4}$$

by exploiting a trigonometric integral representation for erfc(.) function [70]. Using (6.4), the ABER of M-ary PAM can be easily computed via the moment generating function (MGF) approach, viz.,

$$\overline{P_b} = \frac{2(M-1)}{\pi k M}\int_0^{\pi/2} \phi_\gamma\left(\frac{3c/(M^2-1)}{\cos^2\theta}\right)d\theta \tag{6.5}$$

where $\phi_\gamma(.)$ denotes the MGF of the GSC output SNR γ_{gsc}. The MGF expressions for the GSC output SNR over an i.i.d and mixed fading environment can be found in [71]-[72]. These are summarized in (6.6) and (6.7) respectively,

$$\phi_{\gamma_{gsc}}(s) = N\binom{L}{N}\int_0^\infty e^{-sx}p(x)[F(x)]^{L-N}[\phi(s,x)]^{N-1}dx \tag{6.6}$$

$$\phi_{\gamma_{gsc}}(s) = \sum_{\sigma\in T_{L,N}}\int_0^\infty e^{-sx}f_{\sigma(L-N+1)}(x)\left[\prod_{t=1}^{L-N}F_{\sigma(t)}(x)\right]\left[\prod_{k=L-N+2}^{L}\phi_{\sigma(k)}(s,x)\right]dx,\ \ 1\le N\le L \tag{6.7}$$

where $p(x)$, $F(x)$ and $\phi(s, x)$ denote the PDF, CDF and the marginal MGF respectively and $\sum_{\sigma\in T_{L,N}} = \sum_{\substack{\sigma\in S_L,\sigma(1)<\sigma(2)<\ldots<\sigma(L-N)\\ \sigma(L-N+2)<\ldots<\sigma(L)}}$.

It is also possible to obtain closed form ABER expression for GSC receiver with i.n.d diversity paths operating in Rayleigh fading channels, by using the PDF given in [73] along with (6.1) as

$$\overline{P_b} = \frac{(M-1)^2(M+1)}{6Mc}\left[N!N^{L-N}\prod_{z=1}^{L}\Omega_z\right]^{-1}\sum_{\sigma\in S_L}\sum_{i=1}^{L}{}_2F_1\left(1,\frac{3}{2};2;-\frac{\beta_i(M^2-1)}{3c}\right)p_i \qquad (6.8)$$

where Ω_i denotes the average SNR/bit of the i-th path, $\beta_i = \frac{1}{N}\sum_{z=0}^{i-1}\Omega_{\sigma(L-z)}^{-1}$, $p_i = \left[\prod_{j=1,j\neq i}^{L}(\beta_j-\beta_i)\right]^{-1}$, S_L is the set of all permutations of integers $[1,2,...,L]$, $\sigma \in S_L$ denotes the specific function $\sigma = [\sigma(1),\sigma(2),...,\sigma(L)]$ which permutes the integers $[1,2,...,L]$ and ${}_2F_1(.,.;.;.)$ denotes the Gauss hypergeometric function .

6.3.1.2 Approximate Analysis of GSC(N, L)

The throughput-range performance of UWB systems employing GSC receivers can be analyzed using (6.3), (6.5) and (6.6), (6.7) or (6.8). However, as the number of detectable multipaths increases, (6.7)-(6.8) become computationally intensive and turn out to be impractical for the case $L \geq 15$. As such, an approximate ABER formula is needed to predict the performance of GSC(N, L) with i.n.d multipaths. It seems that a very good approximation can be achieved by setting $\Omega = \frac{1}{L}\sum_{i=1}^{L}\gamma_i$, $m \approx (K+1)^2/(2K+1)$ and $m = \frac{1}{L}\sum_{i=1}^{L}m_i$ in (6.6). This hypothesis is further validated by the results presented under Section V.

6.3.2 PMRC(N, L)

The MGF of PRMC(N, L) output SNR may be computed as

$$\phi_{\gamma_{pmrc}}(s) = \prod_{k=1}^{N}\phi_{\gamma_k}(s) \qquad (6.9)$$

where $\phi_{\gamma_k}(.)$ denotes the MGF of the k-th strongest (mean SNR) diversity path. Hence, the ABER performance of PMRC may be analyzed using (6.5) and (6.9). Now the desired throughput can be easily computed using (6.3), (6.5) and (6.9).

6.4 Effect of Multipath Correlations

In order to gain significantly from the use of diversity, there must be sufficient level of

statistical independence in the fading of the received signal in each of the diversity branches. In UWB communication systems with closely packed antenna elements, an assumption of decorrelated multipath signals may lead to grossly overestimated diversity gains. As such study of the effect of multipath correlation on the performance of UWB communication systems becomes important. In this section, we will provide analytical expressions to evaluate the ABER performance of GSC receiver structure over evenly correlated Nakagami-m fading channels.

Let $\gamma_{(1)},...,\gamma_{(L)}$ denote the instantaneous SNRs in ascending order, viz., $\gamma_{(1)} < \gamma_{(2)} < ... < \gamma_{(L)}$. Using the property of *exchangeability*, the joint PDF of the ordered set of instantaneous SNR can be expressed as

$$f_{\gamma_{(1)},...,\gamma_{(2)}}(x_1,...,x_L) = \sum_{\sigma \in S_L} f_{\gamma_1,...,\gamma_L}(x_1,...,x_L) \tag{6.10}$$

where S_L is defined similar to (6.8). The joint PDF of the ordered instantaneous SNRs can be obtained using [74] and (6.10),

$$f_{\gamma_{(1)},...,\gamma_{(2)}}(x_1,...,x_L) = \xi^m \sum_{p=0}^{\infty} \frac{\Gamma(m+p)}{\Gamma(m)p!} \xi^p \sum_{\substack{0 \le \ell_1,...,\ell_L \le p \\ \ell_1+...+\ell_L = p}} \frac{p!}{\ell_1!...\ell_L!} \sum_{\sigma \in S_L} \prod_{k=1}^{L} g_{\sigma(k)}(x_k, v_k, \Lambda) \tag{6.11}$$

where $m \geq ½$ denotes the fading severity index, Ω is the average received SNR/bit per branch, ρ denotes the power correlation coefficient ($0 < \rho < 1$), $\xi = \left(\frac{1-\rho}{1+(L-1)\rho} \right)$, $v_k = \ell_k + m$, $\Lambda = \frac{m}{\Omega(1-\rho)}$ and $g_k(.,.,.)$ is defined as

$$g_k(x_k, v_k, \Lambda) = \frac{\Lambda^{v_k} x^{v_k - 1} e^{-\Lambda x}}{\Gamma(v_k)} \tag{6.12}$$

It is apparent from (6.11) that we can compute the MGF $\phi_{\gamma_{gsc}}(.)$ in a similar fashion to GSC with i.n.d fading statistics [72], viz.,

$$\phi_{\gamma_{gsc}}(s) = E\left[\exp\left(-s \sum_{i=L-N+1}^{L} \gamma_i \right) \right] = \xi^m \sum_{p=0}^{\infty} \frac{\Gamma(m+p)}{\Gamma(m)p!} \xi^p \sum_{\substack{0 \le \ell_1,...,\ell_L \le p \\ \ell_1+...+\ell_L = p}} \frac{p!}{\ell_1!...\ell_L!} I(N,L) \tag{6.13}$$

where, I(., .) is defined as

$$I(N,L)=\sum_{\sigma\in T_{L,N}}\int_0^{\infty}e^{-sx}g_{\sigma(L-N+1)}(x)\left[\prod_{t=1}^{L-N}G_{\sigma(t)}(x)\right]\left[\prod_{k=L-N+2}^{L}\phi_{\sigma(k)}(s,x)\right]dx,\quad 1\le N\le L \qquad (6.14)$$

where $G_k(y)=\int_0^y g_k(x)dx$, $\phi_k(s,x)=\int_x^{\infty}e^{-st}g_k(t)dt$. Using the identity [75], functions $G_k(.)$ and $\phi_k(.,.)$ may be computed in closed form as

$$G_k(y)=1-\frac{\Gamma(v_k,\Lambda x)}{\Gamma(v_k)} \qquad (6.15)$$

$$\phi_k(s,x)=\left(\frac{\Lambda}{s+\Lambda}\right)^{v_k}\frac{\Gamma(v_k,(s+\Lambda)x)}{\Gamma(v_k)} \qquad (6.16)$$

where $\Gamma(a,x)=\int_x^{\infty}t^{a-1}e^{-at}dt$ denotes the complementary incomplete Gamma function [75].

It may be noted that (6.13) is much more concise yet more general and numerically efficient than [74]. Now, the throughput performance can be easily analyzed using (6.13) along with (6.3).

6.5 Numerical Results

The results discussed in this section use the following assumptions:

Table 6-1 Simulation Parameters

Transmit Power spectral density	-41 dBm/Mhz
Transmitter Antenna Gain, G_t	0 dBi
Receiver Antenna Gain, G_r	0 dBi
System Loss, L_s	5 dB
Noise Figure, F	6 dB
Path-loss exponent, n	1.6 (LOS) 2.7 (NLOS)
Operating Bandwidth, B_s	2.5 GHz
Center Frequency, f_c	3.75 GHz

Figure 6.2 compares the accuracy of "approximate ABER analysis" presented in Section-6.3 against the "exact ABER analysis" using (6.7) for GSC(N, 12) receiver with i.n.d

diversity branches in a Rayleigh fading channels. It is evident that the throughput curves corresponding to approximate ABER match closely with the exact throughput curves. It may be noted that the approximate analysis in conjunction with (6.6) serves as a lower bound of the exact performance while (6.9) serves as an upper bound

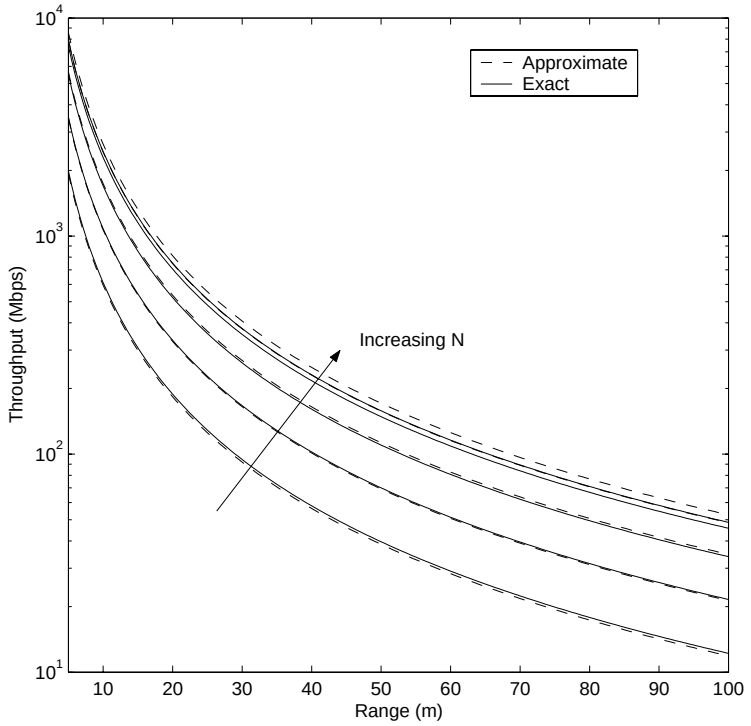

Figure 6.2 Throughput performance of GSC(*N*, 12) receiver that adaptively combines $N \in \{1, 2, 4, 8, 12\}$ paths in a Rayleigh channel with nonidentical fading statistics, δ = 0.2 and path-loss exponent, n = 1.7.

Figure 6.3 draws comparison between the throughput performance of GSC(*N*, 30) and PMRC(*N*, 30) receiver structures in a Rayleigh environment with exponentially decaying multipath intensity profile (δ = 0.2). The average SNR of the n-th diversity path is $\overline{\gamma_n} = Ce^{-n\delta}\overline{\gamma_b}$ where $\overline{\gamma_b}$ denotes the average SNR/bit and the parameter Θ is chosen such that the constraint $\sum_{n=1}^{L} \overline{\gamma_n} = \overline{\gamma_b}$ is satisfied, solving for C yields $\overline{\gamma_n} = \frac{(1-e^{-\delta})e^{-\delta(n-1)}}{1-e^{-L\delta}}\overline{\gamma_b}$. As expected, GSC receiver outperforms PMRC for fixed number of combined paths N. For instance, GSC(10, 30) and PMRC(20, 30) have identical throughput performances. From Figure 6.3, it is also apparent that as the number of combined paths-N are increased;

throughput performance of PMRC becomes virtually identical with GSC. Based on these observations, we can conclude that deployment of GSC(N, L) receiver is desirable for the cases when $N << L$. Whereas, for $N \geq L/2$ an PMRC rake receiver is preferable because of its low complexity and virtually identical throughput performance when compared to GSC(N, L).

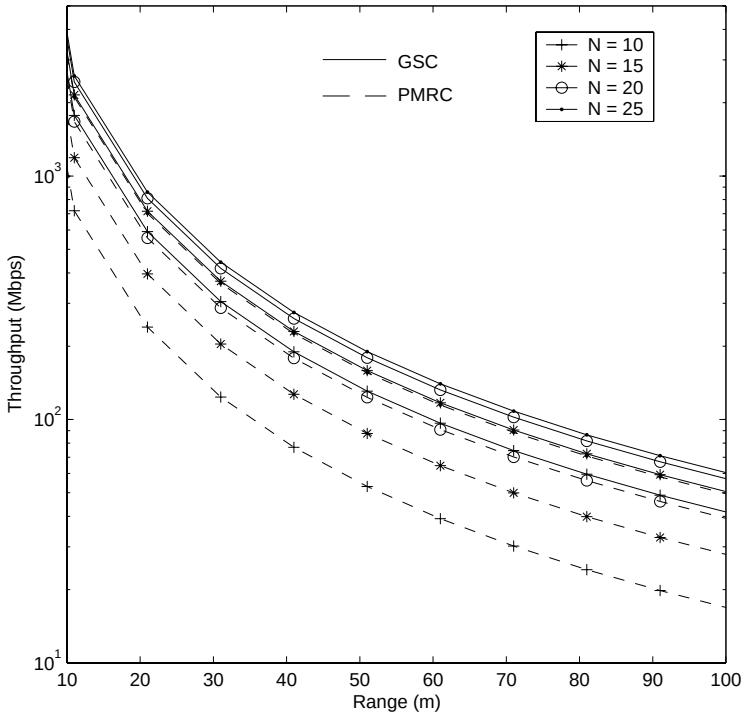

Figure 6.3 Comparison between the Throughput performances of 2-ary PAM that employs either GSC (N, 30) receiver or a PMRC receiver that combines first N paths in an i.n.d Rayleigh channel and path-loss exponent, n = 1.7.

Figure 6.4 depicts the performance of the 5-tap PMRC(5, 20) rake receiver in Nakagami-m fading channel for varying fade distributions. It is evident that improving channel condition translates into a considerable improvement in the receiver throughput. Figure 6.5 presents throughput analysis for GSC(N, 20) receiver for path-loss exponent, n = 3.5. A comparative study of Figure 6.4 and Figure 6.5 suggests major fallback in throughput with even a slightest increase in the path-loss exponent n. The rate, at which the throughput falls, declines gradually as range increases.

Finally, Figure 6.6 illustrates the effect of multipath correlations on the throughput

performance of GSC receiver for different number of combined paths *N*. The throughput performance degrades with increase of multipath correlation, as expected. Throughput falls by almost 50% for $\rho = 0.8$.

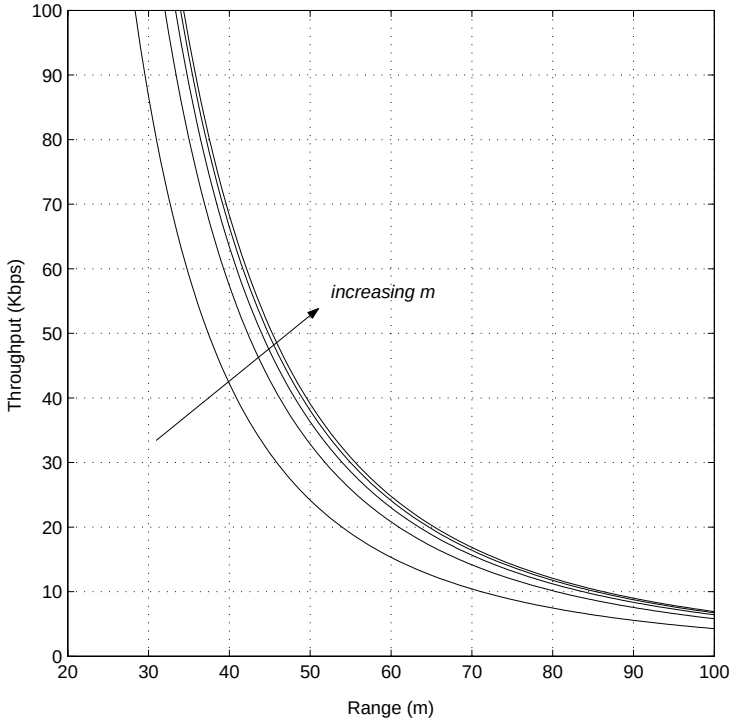

Figure 6.4 Throughput performance of 2-ary PAM in conjunction with a PMRC (5, 20) rake receiver that combines first 5 paths in a Nakagami-m fading channel, $m \in \{1, 2, 3, 4, 5\}$, and path-loss exponent, n = 2.7.

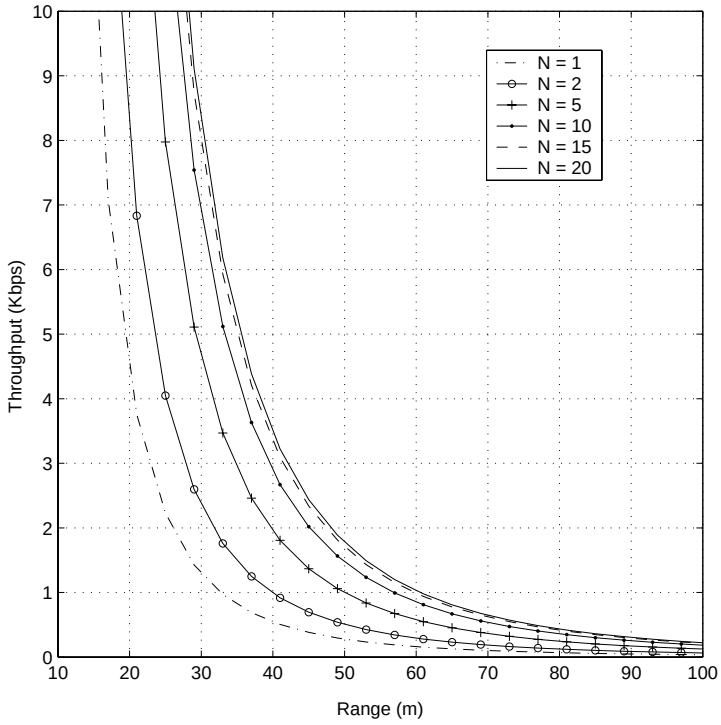

Figure 6.5 Throughput performance of 2-ary PAM in conjunction with a GSC(*N*, 20) receiver in a Rayleigh fading channel and path-loss exponent, $n = 3.5$.

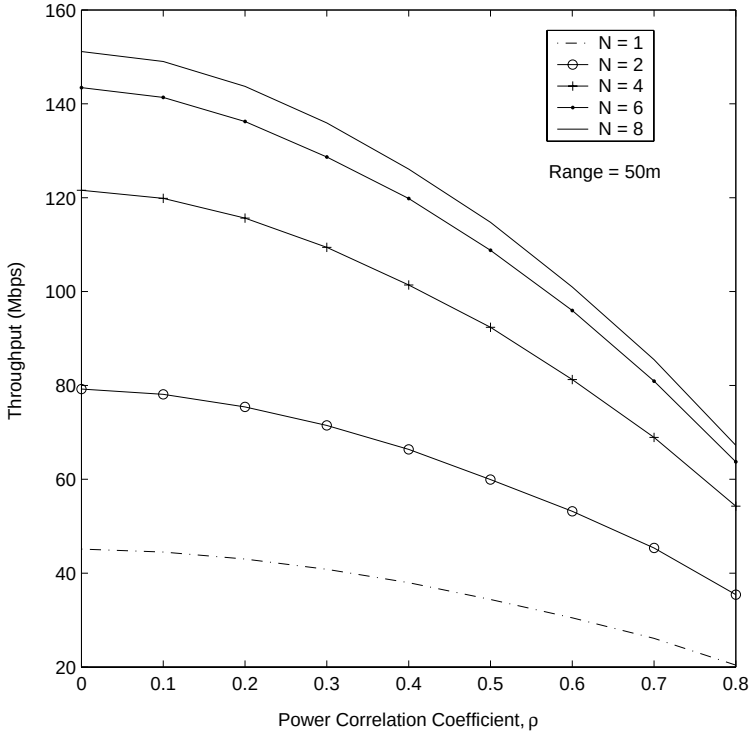

Figure 6.6 Effect of multipath correlation on the throughput performance of 2-ary PAM in conjunction with a GSC(*N*, 8) receiver in a Rayleigh fading channel and path-loss exponent, $n = 1.7$.

6.6 Chapter Summary

In this chapter, we have presented the throughput-range performance of UWB systems in conjunction with suboptimal rake receivers over i.i.d as well as mixed fading channels. An approximate formula for predicting the performance of GSC receiver with i.n.d multipaths is also presented. The throughput performance is also considered under the effect of multipath correlation. The range improvement of UWB systems using suboptimal rake receivers is the topic of a paper appearing in 2003 Fall Vehicular Technology Conference, Florida [82].

Chapter 7

Conclusions and Future Work

7.1 Summary of Contributions and Publications

This thesis has presented a unified analytical framework to study the performance of hybrid general selection combining receivers for ultra-wideband, spread-spectrum and millimeter-wave communication systems. A detailed study on the performance effects of using these sub-optimal but reduced complexity receivers has also been presented. As a part of this research work, a graphical-user-interface simulation tool has also been developed which can be used to predict the performance related parameters of a wireless communication system. In Chapter 6, we also explored the possibility of improving the range of UWB communications with the aid of suboptimal rake receivers in correlated channels.

Another major contribution of this research effort is the development of exact mathematical framework to analyze the performance of dual-branch EGC receivers operating in correlated Nakagami-m channels. The results presented on this topic are completely new and facilitate efficient evaluation of mean and variance of coherent EGC output SNR, outage probability and average bit or symbol error rate for a wide range of digital modulation schemes. A comprehensive study vis-à-vis performance of various dual-diversity receivers in fading channels is also presented.

Last but not the least, we have also presented closed-form solutions for some very important integrals involving generalized Marcum Q-function which often arise in the analysis of multichannel diversity reception of differentially coherent and noncoherent digital communications in Rayleigh and Nakagami-m channels.

The work summarized in this thesis has resulted in some published papers, and transactions manuscripts currently under review or preparation. A list follows:

- Sudhanshu Gaur, A. Annamalai, "Some Integrals Involving the $Q_m(a\sqrt{x}, b\sqrt{x})$ with Application to Error Probability Analysis of Diversity Receivers," Appearing

in IEEE Transaction on Vehicular Technology, October, 2003.

- Sudhanshu Gaur, A. Annamalai, "Contour Integral Representation for the Generalized Marcum Q-Function and its Application to Diversity Problems," IEEE Transaction on Wireless Communications, in review.
- Sudhanshu Gaur, A. Annamalai, "Moment Generating Function Based Performance Evaluation of Two-Branch Equal Gain Combining Diversity Receivers over Correlated Nakagami-m Fading Channels," IEEE Transaction on Vehicular Technology, in review.
- Sudhanshu Gaur, A. Annamalai, "Analysis of Dual-Diversity Coherent Equal Gain Combining in Nonindependent and Nonidentical Nakagami-m Channels," Wireless Communications and Mobile Computing, in review.
- Sudhanshu Gaur, A. Annamalai, "Improving the Range of Ultrawideband Transmission using Rake Receivers," Appearing in Vehicular Technology Conference – VTC Fall'03, Orlando, Florida.
- Sudhanshu Gaur, A. Annamalai, "A General Framework for Performance Evaluation of Hybrid Partitioned Diversity Combining Scheme," manuscript under preparation

7.2 Further Research Directions

The following are some ideas and potential problems that might be interesting areas to pursue in future.

7.2.1 Reduced Complexity Rake Receivers

The results obtained for reduced complexity rake receivers are restricted to equally correlated fading channels. Wherein practical situations this might not be the case. It would be an interesting research problem to extend the existing framework to arbitrary correlated channels.

7.2.2 EGC Receivers

With regards to EGC receivers, extending mathematical framework to arbitrary diversity

order seems an obvious research problem. The research domain can be further extended by considering arbitrarily correlated Rician channels.

7.2.3 Application of Order Statistics to Multi-user Diversity

Most of the analysis for suboptimal rake receivers utilizes known results from order statistics literature. Order statistics also renders itself useful for analyzing the multi-user diversity problem. In the following Appendix, we present a brief discussion along with some results on multi-user scheduling problem.

Appendix

In this appendix, we show how known results from order statistics can be applied to solve multi-user scheduling problems. We are interested in analyzing the performance of a wireless network consisting of N_r active users that contend for resources using random access (Slotted Aloha) mechanism. Each mobile transmits request with a probability p. At the end of contention phase, resources are allocated using greedy scheduling i.e. preference is given to the nodes with best channel condition (perfect power control is assumed). Since the allocation is made at some point, it is assumed that the channel condition doesn't vary much for the entire duration of (current) data transfer.

Probability of exactly k requests can be expressed using binomial distribution, viz.

$$\Pr(k) = \binom{N_r}{k} p^k (1-p)^{Nr-k} \tag{A.1}$$

It is assumed that each node requests a fraction R of the total system capacity, C_T . Thus the maximum number of users that can be supported simultaneously, $L = C_T / R$. Now, the effective packet error probability of the system can be expressed as

$$\overline{P_E} = \sum_{k=1}^{Nr} \binom{Nr}{k} p^k (1-p)^{Nr-k} \frac{1}{U(k)} \sum_{n=1}^{U(k)} \overline{P_{E(n)}} \tag{A.2}$$

where $U(k) = \min(L, k)$ and $\overline{P_{E(n)}}$ denotes the average packet error rate of the n-th strongest link (i.e., n-th order statistics $\gamma_{(1)} \geq ... \gamma_{(n)} \geq ... \gamma_{(N)}$). Suppose we assume that the instantaneous SNRs can be modeled as i.i.d Rayleigh random variables with average SNR, Ω. From the order statistics, the PDF of the k-th statistic $\gamma_{(k)}$ of the ordered instantaneous SNRs $\gamma_{(1)} \geq ... \gamma_{(k)} \geq ... \gamma_{(N)}$ is given by

$$f_k(\gamma) = k \binom{N}{k} F_\gamma^{N-k}(\gamma)[1 - F_\gamma(\gamma)]^{k-1} f_\gamma(\gamma) \tag{A.3}$$

For i.i.d Nakagami-m channel, (A.4) may be computed as

$$f_k(\gamma) = \frac{k}{\Gamma(m)} \binom{N}{k} \sum_{i=0}^{k-1} (-1)^i \binom{k-1}{i} \sum_{n=0}^{N-k+i} (-1)^n \binom{N-k+i}{n}$$

$$\times \sum_{z=0}^{n(m-1)} \beta(z,n,m)\left(\frac{m}{\Omega}\right)^{z+m} \gamma^{m+z-1} \exp\left(-\frac{(n+1)m}{\Omega}\gamma\right) \tag{A.4}$$

where m denotes the fading index. The coefficients $\beta(.,.,.)$ in (A.4) may be computed recursively as

$$\beta(z,k,c) = \sum_{i=z-c+1}^{z} \frac{\beta(i,k-1,c)}{(z-i)!} I_{[0,(k-1)(c-1)]}(i) \tag{A.5}$$

where $I_{[\upsilon,\omega]}(i) = \begin{cases} 1 & \upsilon \le i \le \omega \\ 0 & otherwise \end{cases}$, $\beta(0, 0, c) = \beta(0, k, c) = 1$, $\beta(z, 1, c) = \frac{1}{z!}$ and $\beta(1, k, c) = k$. For i.i.d Rayleigh fading channel, (A.4) quickly reduces to

$$f_k(\gamma) = \frac{k}{\Omega}\binom{N}{k}\sum_{i=0}^{N-k}(-1)^i\binom{N-k}{i}\exp\left(-(k+i)\frac{\gamma}{\Omega}\right) \tag{A.6}$$

To compute the average packet error rate $\overline{P_{E(k)}}$ of the k-th link, we assume that the SNR for all bits in the packet is the same. So, the average packet error probability is given by

$$\overline{P_{E(k)}} = \int_0^\infty \{1-[1-P_b(\gamma)]^B\} f_k(\gamma) d\gamma = 1 - \sum_{j=0}^{B}(-1)^j\binom{B}{j}\int_0^\infty [P_b(\gamma)]^j f_k(\gamma) d\gamma \tag{A.7}$$

where B denotes number of bits in a packet. For DPSK modulation, $P_b(\gamma) = \frac{1}{2}e^{-\gamma}$, average packet error rate of the kth link can be obtained by using (A.7) as

$$\overline{P_{E(k)}} = 1 - \frac{k}{\Gamma(m)}\binom{N}{k}\sum_{i=0}^{k-1}(-1)^i\binom{k-1}{i}\sum_{n=0}^{N-k+i}(-1)^n\binom{N-k+i}{n}\sum_{z=0}^{n(m-1)}\beta(z,n,m)$$

$$\times\sum_{j=0}^{B}\left(-\frac{1}{2}\right)^j\binom{B}{j}\left[\frac{m}{(n+1)m+j\Omega}\right]^{z+m}\Gamma(z+m) \tag{A.8}$$

Again, for i.i.d Rayleigh channel, average packet error of the k-th strongest link can be expressed as

$$\overline{P_{E(k)}} = 1 - k\binom{N}{k}\sum_{i=0}^{N-k}(-1)^i\binom{N-k}{i}\sum_{j=0}^{B}(-1)^j\binom{B}{j}\frac{1}{2^j(k+i+j\Omega)} \tag{A.9}$$

It may be noted that the ABER of the k-th link can be obtained by setting $B = 1$ in (A.8)

or (A.9). The effective packet error rate (or the bit error rate) of the system can be computed using (A.2) and (A.8). For the special case of m = 1 (Rayleigh channel), a compact expression can be obtained, viz.,

$$\overline{P_E} = 1 - \sum_{k=1}^{Nr} \binom{Nr}{k} p^k (1-p)^{Nr-k} \sum_{n=1}^{U(k)} \frac{n}{U(k)} \binom{k}{n} \sum_{i=0}^{k-n} (-1)^i \binom{k-n}{i} \sum_{j=0}^{B} \binom{B}{j} \frac{(-1)^j}{2^j (n+i+j\Omega)} \quad \text{(A.10)}$$

The expression (A.2) with minor modifications can also be used to compute the effective packet error rate when the resources are allocated in a more traditional manor, viz. Round Robin. The average packet error rate expression for all the links is same for the Round Robin scenario and is given by

$$\overline{P_{E(k)}} = \int_0^\infty \{1 - [1 - P_b(\gamma)]^B\} f_\gamma(\gamma) d\gamma = 1 - \sum_{j=0}^{B} \binom{B}{j} (-1)^j \int_0^\infty [P_b(\gamma)]^j f_\gamma(\gamma) d\gamma$$

$$= 1 - \sum_{j=0}^{B} \binom{B}{j} \left(-\frac{1}{2}\right)^j \left(\frac{m}{m+j\Omega}\right)^m \quad \text{(A.11)}$$

Eq. (A.11) can be used along with (A.2) to compute the effective packet (bit) error rate of the Round Robin scheduler. Figure A.1 compares the effective packet error rates of Round Robin and Greedy algorithms.

To compare the throughput performance of Round Robin and Greedy Scheduler, we define "*good throughput*" metric as

$$\overline{\rho} = \sum_{k=1}^{Nr} \binom{Nr}{k} p^k (1-p)^{Nr-k} \frac{1}{U(k)} \sum_{n=1}^{U(k)} R(1 - \overline{P_{E(n)}}) \quad \text{(A.12)}$$

Figure A.2 illustrates the "good throughput" of the two scheduling algorithms based on above developments.

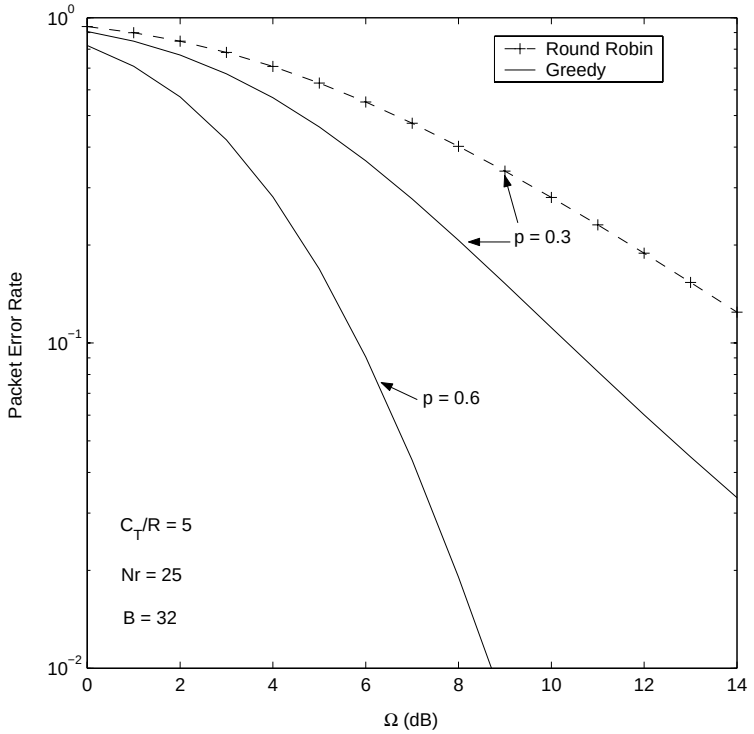

Figure A.1 The effective packet error rates of the two scheduling schemes as a function of SNR in a Rayleigh fading channel.

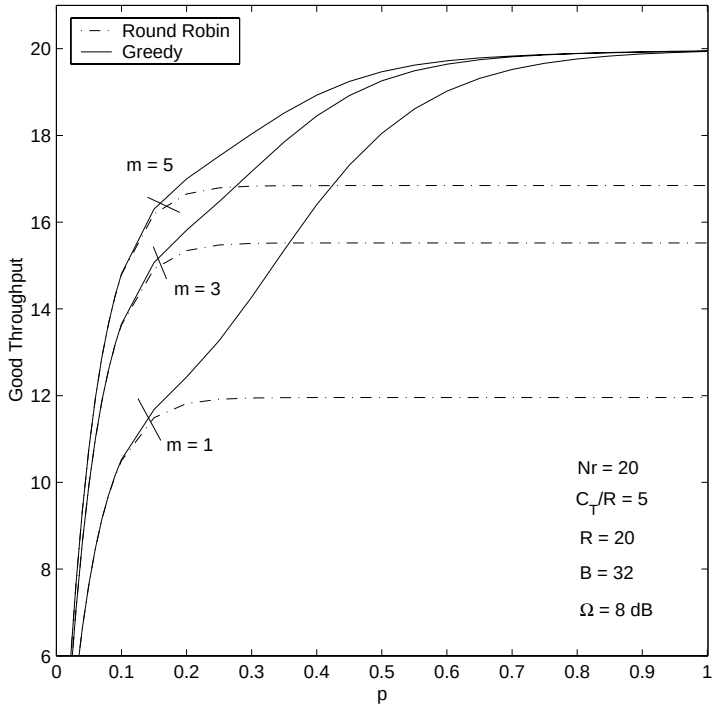

Figure A.2 Good Throughput performance of Greedy and Round Robin Scheduler for varying values of fading severity index m.

Bibliography

[1] 3G Home, Press Release, http://www.3g.co.uk/PR/August2003/5709.htm, Aug. 7, 2003,

[2] Cahner's "Wireless Week", http://www.instat.com/rh/wirelessweek/gw0006hs_summary.htm, May 2000.

[3] M. Zeng, A. Annamalai, and V. Bhargava, "Recent Advances in Cellular Wireless Communications," IEEE Communications Magazine, Vol. 37, Sept. 1999, pp. 128-138.

[4] M. Zeng, A. Annamalai, and V. Bhargava, "Harmonization of Global Third Generation Mobile Systems," IEEE Communications Magazine, Vol. 38, Dec. 2000, pp. 94-104.

[5] A. Hamilton, "Forget dotcoms. Wireless Is Where It's At," ZDNet Asia worldwide website, http://www.zdnetasia.com/news/dailynews/story/0,2000010021,10052998,99.htm, Feb. 03, 2000.

[6] H. Suzuki, "A Statistical Model for Urban Radio Propagation" *IEEE Transactions on Communications,* Vol. 27, July 1977, pp.673-680.

[7] W. R. Braun and U. Dersch, "A Physical Mobile Radio Channel Model" *IEEE Transactions on Vehicular Technology*, Vol. 40, Feb. 1991, pp. 472-482.

[8] M. Nakagami, "The m-distribution - A General Formula of Intensity Distribution of Rapid Fading" *Statistical Methods of Radio Wave Propagation*, Pergamon, 1960, pp. 3-36.

[9] M. Z. Win, G. Chrisikos and N. R. Sollenberger, "Performance of Rake Reception in Dense Multipath Channels. Implications of Spreading Bandwidth and Selection Diversity Order," *IEEE Journal on Selected Areas in Communications*, Vol. 18, No. 8, August 2000.

[10] W. C. Lau, M. S. Alouini and M. K. Simon, "Optimum Spreading Bandwidth for Selective RAKE Reception over Rayleigh Fading Channels," *IEEE Journal on Selected Areas in Communications*, Vol. 19, No. 6, May 2001.

[11] R. J. Cramer, M. Z. Win and R. A. Scholtz, "Impulse Radio Multipath Characteristics and Diversity Reception," *International Conference on Communications*, Vol. 3, 1998.

[12] N. Kong; T. Eng and L. B. Milstein, "A Selection Combining Scheme for RAKE Receivers," *Proc. 1995 Fourth IEEE International Conference on Universal Personal Communications*, pp. 426 -430.

[13] N. Kong and L. B. Milstein, "Average SNR of a Generalized Diversity Selection Combining Scheme," *IEEE Communications Letters*, Vol. 3, No. 3, pp. 57 -59, Mar. 1999.

[14] N. Kong and L. B. Milstein, "SNR of Generalized Diversity Selection Combining with Nonidentical Rayleigh Fading Statistics," *IEEE Transactions on Communications*, Vol. 48, pp. 1266 -1271, Aug. 2000.

[15] M. Win and J. Winters, "Analysis of Hybrid Selection/Maximal-Ratio Combining in Rayleigh Fading," *IEEE Transactions on Communications*, Vol. 47, pp. 1773-1776, Dec. 1999.

[16] M.-S. Alouini and M. K. Simon, "An MGF-Based Performance Analysis of Generalized Selection Combining over Rayleigh Fading Channels," *IEEE Transactions on Communications*, Vol. 48, pp. 401-414, Mar. 2000.

[17] M. Alouini and M. Simon, "Performance of Coherent Receivers with Hybrid SC/MRC over Nakagami-m Fading Channels," *IEEE Transactions on Vehicular Technology*, Vol. 48, pp. 1155-1164, July 1999.

[18] Annamalai and Tellambura, "Error Rates of Hybrid SC/MRC Diversity Systems on Nakagami-m Channels," *Proc. IEEE Wireless Communications and Networking Conference*, pp. 227-231, Sept. 2000.

[19] Y. Ma and C. Chai, "Unified Error Probability Analysis for Generalized Selection Combining in Nakagami Fading Channels," *IEEE J. Selected Areas Commun.*, Vol. 18, pp. 2198-2210, Nov. 2000.

[20] A. Annamalai and C. Tellambura, "Performance Evaluation of Generalized Selection Diversity Systems over Nakagami-m Fading Channels," to appear in the *International Journal on Wireless Communicationsand Mobile Computing*, Wiley, 2002.

[21] A. Annamalai, G. Deora and C. Tellambura, "Unified Error Probability Analysis for Generalized Selection Diversity in Rician Fading Channels," *Proc. IEEE Vehicular Technology Conference*, May 2002, pp. 2042-2046.

[22] G. Deora, "Simulation and Mathematical Tools for Performance Analysis of Low-Complexity Receivers," Thesis submitted to ECE Dept., Virginia Tech, Jan, 2003.

[23] Y. Roy, J. Yves and S. A. Mahmoud, "Selection Diversity Combining with Multiple Antennas for MM-Wave Indoor Wireless Channels," *IEEE Journal on Selected Areas in Communications*, Vol. 14, No. 4, May 1996.

[24] J. Abate, W. Whitt "Numerical Inversion of Laplace Transforms of Probability Distribution" ORSA Journal in Computing, Vol. 7, no. 1 1995, pp. 36-43.

[25] A. Annamalai and C. Tellambura, "Error Rates for Nakagami-m Fading Multichannel Reception of Binary and M-ary Signals," *IEEE Transactions on Communications*, Vol. 49, pp. 58-68, Jan. 2001.

[26] G. L. Stuber, *Principles of Mobile Communications*, Norwell, MA: Kluwer Academic Publishers, 1996.

[27] C. B. Dietrich, K. Dietze, J. R. Nealy, W. L. Stutzman, "Spatial, Polarization, and Pattern Diversity for Wireless Handheld Terminals", *IEEE Trans. on Antennas and Propagation*, Vol. 49, No. 9, Sep. 2001, pp. 1271-1281.

[28] L. Lukama, K. Konstantinou, D. J. Edwards, "Polarization Diversity Performance for UMTS," *IEE International Conf. on Antennas and Propagation*, April 2001, pp. 193-197.

[29] J. S. Colburn, Y. Rahmat-Samii, M. A. Jensen, and G. J. Pottie, "Evaluation of Personal Communications Dual-Antenna Handset Diversity Performance," *IEEE Trans. on Vehicular Technology*, Vol. 47, pp. 737–746, Aug. 1998.

[30] C. Braun, G. Engblom, and C. Beckman, "Antenna Diversity for Mobile Telephones," *Proc. IEEE APS Symp.*, June 1998, pp. 2220–2223.

[31] K. Ogawa and T. Uwano, "A Diversity Antenna for Very Small 800 MHz Band Portable Telephones," *IEEE Trans. on Antennas Propagation*, pp.1342–1345, Sept. 1994.

[32] A. M. D. Turkmani, A. A. Arowojolu, P. A. Jefford, and C. J. Kellet, "An Experimental Evaluation of the Performance of Two-Branch Space and Polarization Diversity Schemes at 1800 MHz," *IEEE Trans. on Vehicular Technology*, Vol. 44,

pp. 318–326, May 1995.

[33] K. Dietze, C. Dietrich, W. L. Stutzman, “Analysis of a Two-Branch Maximal Ratio and Selection Diversity System with Unequal SNRs and Correlated Inputs for a Rayleigh Fading Channel,” *IEEE Trans. on Wireless Communications*, Vol. 1, April 2002, pp. 274-281.

[34] D. G. Brennan, "Linear Diversity Combining Techniques", *Proc. IRE*, Vol. 47, pp. 1075-1102, June 1959.

[35] V. Aalo, “Performance of Maximal-Ratio Diversity Systems in a Correlated Nakagami-Fading Environment,” *IEEE Transactions on Communications*, Vol. 43, Aug. 1995, pp. 2360 -2369.

[36] Q. T. Zhang, “Maximal-Ratio Combining over Nakagami Fading Channels with an Arbitrary Branch Covariance Matrix,” *IEEE Trans. on Vehicular Technology*, Vol. 48, July 1999, pp. 1141 -1150.

[37] S. Okui, “Effects of CIR Selection Diversity with Two Correlated Branches in the m-Fading Channel,” *IEEE Trans. on Communications*, Vol. 48, Oct. 2000, pp. 1631 - 1633.

[38] S. Okui, “Probability of Co-channel Interference for Selection Diversity Reception in the Nakagami-m Fading Channel,” *IEE Proceedings on Communications, Speech and Vision*, Vol. 139, Feb. 1992, pp. 91-94.

[39] C. Tellambura, A. Annamalai, V. K. Bhargava, “Closed Form and Infinite Series Solutions for the MGF of a Dual-Diversity Selection Combiner Output in Bivariate Nakagami Fading,” *IEEE Trans. on Communications*, Vol. 51, April 2003, pp. 539-542.

[40] N. C. Beaulieu, “Introduction to ‘Linear Diversity Combining Techniques’,” *Proc. IEEE,* Vol. 91, No. 2, Feb. 2003, pp. 328-330.

[41] R. Mallik, M. Win and J. Winters, “Performance of Predetection Dual Diversity in Correlated Rayleigh Fading: EGC and SD,” *Proc. IEEE GLOBECOM*’00, pp. 932-936. Also appeared in the *IEEE Trans. on Communications*, Vol. 50, July 2002.

[42] A. Annamalai, V. Ramanathan and C. Tellambura, "Analysis of Equal Gain Diversity Receiver in Correlated Fading Channels," *Proc. IEEE Vehicular Technology Conference*, Fall 2002, pp. 2038-2041.

[43] C. Iskander and P. Mathiopoulos, "Performance of M-QAM with Coherent Equal Gain Combining in Correlated Nakagami-m fading," *Electronic Letters*, Vol. 39, No. 1, Jan. 2003, pp. 141-142.

[44] A. Annamalai, C. Tellambura and V. Bhargava, "Equal-Gain Diversity Receiver Performance in Wireless Channels," *IEEE Trans. on Communications*, Vol. 48, Oct. 2000, pp. 1732-1745.

[45] A. Annamalai, Jing Su and C. Tellambura, "Exact Analysis of Equal Gain Diversity Systems over Fading Channels," *Proc. IEEE Vehicular Tech. Conference*, May 2000, pp. 1031-1034.

[46] M. Nakagami, "The m-distribution – A General Formula of Intensity Distribution of Rapid Fading" in W. G. Hoffman, "*Statistical Methods in Radio Wave Propagation*" New York: Pergamon Press, 1960, pp. 3-36.

[47] I. Gradshteyn and I. Ryzhik, *Table of Integrals, Series and Products*, Academic Press, 1995.

[48] R. H. Clarke, "A Statistical Theory of Mobile-Radio Reception," *Bell Systems Technical Journal*, July-Aug. 1968, pp. 957-1000.

[49] J.G. Proakis, *Digital Communications*, Fourth Edition, McGraw-Hill, New York, 2001.

[50] A. Annamalai and C. Tellambura, "Error Rates for Nakagami-m Fading Multichannel Reception of Binary and M-ary Signals," *IEEE Transaction on Communications*, Vol. 49, No. 1, January 2001.

[51] S. Okui, "Probability of Co-Channel Interference for Selection Diversity Reception in the Nakagami-m Fading Channel," *IEE Proceedings-I*, Vol.139, No.1, February 1992, pp. 91-94.

[52] A. Annamalai, C. Tellambura and V. K. Bhargava, "A General Method for Calculating Error Probabilities over Fading Channels," *Proc. IEEE International Conference on Communication*, June 2000, pp. 36-40.

[53] H. Bateman, Tables of Integral Transforms, Vol. 1 and 2, McGraw-Hill, 1954.

[54] I.S. Gradshteyn and I.M. Ryzhik, *Table of Integrals, Series and Products*, Academic Press, 1995.

[55] C.W Helstrom, *Elements of Signal Detection and Estimation*, Prentice-Hall, New Jersey, 1995.

[56] M.K. Simon and M.S. Alouini, "A Unified Approach to the Probability of Error for Noncoherent and Differentially Coherent Modulations Over Generalized Fading Channels," *IEEE Transaction on Communications*, Vol. 46, No. 12, December 1998.

[57] Q. T. Zhang, "Exact Analysis of Postdetection Combining for DPSK and NFSK Systems Over Arbitrarily Correlated Nakagami Channels," IEEE Trans. Communications, Vol. 46, No. 11, Nov. 1998.

[58] A. Annamalai and C. Tellambura, "Cauchy-Schwartz Bound on the Generalized Marcum Q-Function with Applications," *Journal on Wireless Communications and Mobile Computing*, Vol. 1, March 2001, pp. 243-253.

[59] M. Schwartz, W. R. Bennett and S. Stein, *Communication Systems and Techniques*, New York: McGraw-Hill, 1966.

[60] C. Tellambura, A.J. Mueller, and V.K. Bhargava, "Analysis of M-ary phase-shift-keying with diversity reception for land-mobile satellite channels," *IEEE Trans. Veh. Technology*, Vol. 46, pp. 910-922, Nov. 1997.

[61] C. Tellambura, A. Annamalai and V.K. Bhargava, "Contour Integral Representation for Generalized Marcum Q-Function with its Application to Unified Analysis of Dual Branch Selection Diversity over Correlated Nakagami-m Channels," *Proc. IEEE Vehicular Technology Conference*, May 2000, Tokyo, pp. 1031-1034.

[62] M.K. Simon and M.S. Alouini, "A Unified Performance Analysis of Digital Communication with Dual Selection Diversity over Correlated Rayleigh and Nakagami-m Fading Channels," *IEEE Trans. on Communications*, Vol. 47, Jan 1999, pp. 33-43.

[63] Y. Roy, J. Yves and S. A. Mahmoud, "Selection Diversity Combining with Multiple Antennas for MM-Wave Indoor Wireless Channels," *IEEE Journal on Selected Areas in Communications*, Vol. 14, No. 4, May 1996.

[64] A. Annamalai, "Theoretical Diversity Improvement in GSC(N, L) and T-GSC(μ, L) over Generalized Fading Channels," *Proc. IEEE ISWC'2002*, Victoria, Sept, 2002.

[65] FCC Notice of Proposed Rule Making, "Revision of Part 15 of the Commission's Rules Regarding Ultrawideband Transmission Systems," *ET-Docket* 98-153.

[66] D. Cassioli, M. Z. Win, and A. F. Molisch, "A Statistical Model for the UWB Indoor Channel," *Proc. Of IEEE Vehicular Tech. Conf.*, Rhodos, Greece, May 2001, vol. 2, pp. 1159-1163.

[67] A. Safaai-Jazi, A. Muqaibel, A. Attiya, A. Bayram, and S. Riad, "Ultra-Wideband Time-Domain Indoor Channel Measurements," Virginia Tech., Feb. 7, 2003.

[68] R. Wong, A. Annamalai, and V. K. Bhargava, "Evaluation of Predetection Diversity Techniques for Rake Receivers," *Proc IEEE PACRIM*, 1997, pp. 227-230.

[69] D. Cassioli, M. Z. Win, F. Vatalaro and A. Molisch, "Performance of Low-Complexity Rake Reception in a Realistic UWB Channel," *IEEE International Conf. on Communications*, 2002, Vol. 2, pp. 763-767.

[70] C. Tellambura, A. J. Mueller, and V. K. Bhargava, "Analysis of M-ary phase-shift keying with diversity reception for land-mobile satellite channels," *IEEE Trans. Veh. Tech.*, Vol. 46, pp. 910-922, Nov. 1997.

[71] A. Annamalai, G. Deora and C. Tellambura, "Unified Error Probability Analysis for Generalized Selection Diversity in Rician Fading Channels," *Proc. IEEE Vehicular Technology Conference,* Birmingham, May 2002, pp. 2042 -2046.

[72] G. Deora, "Simulation and Mathematical Tools for Performance Analysis of Low-Complexity Receivers," Thesis submitted to ECE Dept., Virginia Tech, Jan, 2003.

[73] A. Annamalai, "Theoretical Diversity Improvement in GSC(N, L) and T-GSC(μ, L) over Generalized Fading Channels," *Proc. IEEE ISWC'2002*, Victoria, Sept, 2002.

[74] R. K. Mallik and M. Z. Win, "Analysis of Hybrid Selection/Maximal-Ratio

Combining in Correlated Nakagami Fading," *IEEE Trans. On Comm*., Vol. 50, No. 8, August 2002

[75] I.S Gradshteyn and I.M. Ryzhik, *Table of Integrals, Series and Products*, Academic Press, 1995.

[76] J.G. Proakis, *Digital Communications*, Third Edition, McGraw-Hill, New York, 1995.

[77] Sudhanshu Gaur, A. Annamalai, "A General Framework for Performance Evaluation of Hybrid Partitioned Diversity Combining Scheme," manuscript under preparation

[78] Sudhanshu Gaur, A. Annamalai, "Moment Generating Function Based Performance Evaluation of Two-Branch Equal Gain Combining Diversity Receivers over Correlated Nakagami-m Fading Channels," IEEE Transaction on Vehicular Technology, in review.

[79] Sudhanshu Gaur, A. Annamalai, "Analysis of Dual-Diversity Coherent Equal Gain Combining in Nonindependent and Nonidentical Nakagami-m Channels," Wireless Communications and Mobile Computing, in review.

[80] Sudhanshu Gaur, A. Annamalai, "Some Integrals Involving the $Q_m(a\sqrt{x}, b\sqrt{x})$ with Application to Error Probability Analysis of Diversity Receivers," Appearing in IEEE Transaction on Vehicular Technology, October, 2003.

[81] Sudhanshu Gaur, A. Annamalai, "Contour Integral Representation for the Generalized Marcum Q-Function and its Application to Diversity Problems," IEEE Transaction on Wireless Communications, in review.

[82] Sudhanshu Gaur, A. Annamalai, "Improving the Range of Ultrawideband Transmission using Rake Receivers," Appearing in Vehicular Technology Conference – VTC Fall'03, Orlando, Florida.

Vita

Sudhanshu Gaur was born on July 24, 1979 in Meerut, an ancient city in the northern Indian state of Uttar Pradesh. He attended Indian Institute of Technology, Kharagpur, and received a Bachelor's in Instrumentation Engineering in May 2000. After graduation, he worked with Sasken Communication Technologies, in his capacity as Protocol Design Engineer in the 2.5G Communications Group. In Fall 2001, he joined Virginia Tech for graduate studies with an emphasis on Wireless Communications. While at Virginia Tech, Sudhanshu was actively involved with the Mobile and Portable Radio Research Group (MPRG). After completing his M.S. in Electrical Engineering in Fall 2003, he moved to Atlanta, GA to attend Georgia Tech for PhD. He is currently a research assistant at the Smart Antenna Research Lab, a part of Georgia Centers for Advanced Telecommunications Technology (GCATT), Atlanta.